Stress and Deformation Analysis of the Master Leaf of an Automobile Leaf Spring

Thesis submitted in partial fulfillment of
the requirements for the degree of

Master of Mechanical Engineering

By

SUSHANTA GHUKU

Examination Roll No.: M4MEC1618
Registration No.: 111915 of 2010 - 2011

Under the guidance of

Prof. Kashi Nath Saha

DEPARTMENT OF MECHANICAL ENGINEERING
FACULTY OF ENGINEERING & TECHNOLOGY
JADAVPUR UNIVERSITY
KOLKATA – 700032

MAY 2016

FACULTY OF ENGINEERING AND TECHNOLOGY

JADAVPUR UNIVERSITY

CERTIFICATE OF APPROVAL*

This foregoing thesis is hereby approved as a credible study of an engineering subject carried out and presented in a manner satisfactory to warrant its acceptance as a prerequisite to the degree for which it has been submitted. It is understood that by this approval the undersigned do not endorse or approve any statement made, opinion expressed or conclusion drawn therein but approve the thesis only for the purpose for which it has been submitted.

Committee
On Final Examination for
Evaluation of the Thesis

_____

_____

*Only in case the thesis is approved.

FACULTY OF ENGINEERING AND TECHNOLOGY

JADAVPUR UNIVERSITY

We hereby recommend that the thesis presented under our supervision by ***Mr. Sushanta Ghuku*** *entitled* ***"Stress and Deformation Analysis of the Master Leaf of an Automobile Leaf Spring"*** *be accepted in partial fulfillment of the requirements for the degree of Master of Mechanical Engineering.*

Countersigned ----------

Thesis Advisor

Head of the Department
Mechanical Engineering
Jadavpur University

Dean of Faculty of
Engineering and Technology
Jadavpur University

ACKNOWLEDGEMENT

At the very outset, I acknowledge, with sincere appreciation and gratitude, the generous and arduous guidance and inspiration provided to me by my honorable guide, Prof. Kashi Nath Saha without which my thesis could not have reached this stage. Words of thanks fall short to express my gratitude to him in proper dimensions for his kind co-operation and methodical guiding in course of the thesis work.

I would also like to convey my thanks to the Head of the Department, all academic and technical staffs of Mechanical Engineering Department, Jadavpur University, especially faculty members and laboratory-in-charge of Machine Elements Laboratory who helped me to complete the thesis work.

I would like to express my deepest sense of gratitude to Sri Sunil Karmakar, former Sr. Supdt. (Tech), and Sri Aurobindo Jana, Laboratory attendant, of Machine Elements Laboratory, Mechanical Engineering Department, Jadavpur University for their kind cooperation and help during the course of the thesis work, especially during the experimentations. In this connection, I am also obliged to my juniors of Machine Design specialization, Amrita Sengupta, Ujjwal Kumar, Sayantan Mondal, Vaibhav Gangwar and Aarohi Gupta, for their help in conducting the experimental work.

I am highly grateful to Ms. Priyambada Nayak, a research scholar of Mechanical Engineering Department, Jadavpur University, who, inspite of her busy academic schedule, extended her valuable support throughout the course of the thesis work.

I would also like to express my sincere gratitude to my seniors of Machine Elements laboratory whose support, suggestions and helping attitudes helped my way out to the timely completion of the thesis. I tender special thanks to Sri Amit Banerjee and Sri Arkadeb Mukhopadhyay for their continuous help throughout the course of thesis writing. Special mention of my classmates, Sri Jayanta Sarkar and Sri Tamonash Jana is called for the stimulating discussions, support and fun which were always constructive and refreshing.

In this respect, I would also like to grab this opportunity to express my heart-felt gratitude to my brother, sister and friends, without whose suggestions and hospitality it could have been difficult to carry out the project work and complete the thesis in time.

Last but not the least, the constant support and encouragement extended by my beloved parents is deeply and appreciatively acknowledged.

Date: (Sushanta Ghuku)

Contents

List of Nomenclatures

b	Width of the beam / master leaf spring
F	Vertical conservative load applied at the tip of cantilever beam
h	Thickness of the beam / master leaf spring
I	Moment of area of the beam / master leaf spring
l	Projected length of the beam ($L - \delta_x$)
s, n	Curvilinear coordinate system, in normalized form
x, y	Cartesian coordinate system
$O_{x\,y\,z}$	Origin of Cartesian coordinate system
L	Length of the beam / span of master leaf
M	Bending moment
N_f, N_g	Number of precision points used to represent physical and computational domain in the solution algorithm
N_L	Number of load steps
P	A constant transverse load coming from distributed loading ($= qL$) /horizontal restraining force coming from asymmetric geometry of master leaf spring
$q(s), \bar{q}(s)$	Intensity of distributed load in dimensional and non-dimensional form
$q_n(s)$	Vertical component of q
S_g / S_c	Sensitivity of strain gauge / bridge circuit
x_{tip}^0, y_{tip}^0	x, y coordinates of the tip at no load condition
$x_{tip}^{N_L}, y_{tip}^{N_L}$	x, y coordinates of the tip at load step N_L
α	Normalized load parameter corresponding to F
δ_x, δ_ξ	Shortening / stretching of the beam in dimensional and normalized

	form
δ_y, δ_η	Beam deflection in dimensional and normalized form
ε_{err}	Error limit in calculation of arc length
ξ, η	Cartesian coordinate system in normalized form
φ	The slope dy/dx at location s
$\varphi_{tip}^{0}, \varphi_{tip}^{N_L}$	The slope dy/dx at the free end of the beam at location $s = L$ at initial configuration (i.e., at no load condition) and for load step N_L
$\varphi_0^0, \varphi_0^{N_L}$	Slope at the fixed end ($s = 0$) corresponding to no load and load step N_L (It should be noted that $\varphi_0^0 = \varphi_0^{N_L} = 0$)
ρ	Radius of curvature of elastic curve
W	Vertical load applied to master leaf spring
L_W	Distance of load (W) line from $O_{x\,y\,z}$
r_n	Radius of curvature of neutral axis of master leaf spring
R_L, R_R	Reaction forces at left and right roller supports
α_L, α_R	Reaction force angles at left and right roller supports
$P_{x\,L}, P_{x\,R}, P_{y\,L}, P_{y\,R}$	Horizontal and vertical components of reaction forces at left and right roller supports
H_W	y coordinate of master leaf profile at $x = L_W$
V_x	Shear force at location x ($0 \leq x \leq L$)
M_x	Bending moment at location x ($0 \leq x \leq L$)
$\sigma_{b\,x}$	Bending stress at location x ($0 \leq x \leq L$)
$\sigma_{t\,x}$	In plane tensile stress at location x ($0 \leq x \leq L$)
σ_{exp}	Experimental bending stress at strain gauge locations

List of Figures

Page no.

List of Tables

Page no.

Chapter 1

INTRODUCTION

Leaf spring is the simplest form of spring, commonly made of spring steel and widely used in vehicle suspension system. This type of spring is typically constructed from one or more flat, thin, flexible arc shaped steel strips that are joined together in order to work as a single unit. Leaf spring can either be attached directly to the frame at both ends or attached directly at one end, usually at the front, while the other end is attached through a shackle (a short swinging arm). The shackle takes up the tendency of the leaf spring to elongate when compressed and thus makes for softer springiness. In order to conserve natural resources and economize energy, weight reduction has been the main focus of automobile manufacturer in the present scenario. So in recent times, various non-metallic materials like polymers, functionally graded materials (FGM), composites, etc. are being used as leaf spring material due to their high strength to weight ratio. Due to its numerous applications, analysis of leaf springs has been of great interest to several researchers. The main cause of failure of leaf spring is due to large bending but there are several other types of loading such as braking torque, driving torque, fatigue loads, shock load due to road irregularities, sudden loads due to the wheel travelling over the bumps, etc., which may also impose failure. However, analysis of failure of leaf spring under those other than bending types of loading is another class of study, and not undertaken in this thesis.

Experimental stress and deflection analysis of leaf spring under bending type of loading include several techniques. Generally load-deflection behavior of leaf springs are studied through three point bending test in leaf spring testing rig and the developed stresses in leaf spring is measured by using strain gauge technique. In corresponding theoretical analysis, leaf springs are generally modeled as a bundle of prismatic beams under bending. Traditionally analysis is carried out with small deflection theory to simplify the analysis. But several researchers have pointed out that for better characterization of such problems analysis should be carried out through non-linear model. In static analysis of beams, two types of nonlinearities are most commonly encountered, geometric and material. Material nonlinearity is associated with nonlinear stress-strain relations whereas nonlinear curvature-slope and strain-displacement relations give rise to geometric nonlinearity. Depending on the nature of

problem any one or both of the nonlinearities are included in the analysis. Although elasticity theory has vast application in engineering problems over the last few centuries, there still exist these nonlinear problems where a rigorous solution cannot be obtained and approximate methods have to be applied. However, improvement in the field of computational powers of the modern computers has changed the scenario. At present various nonlinear mathematical models and solution algorithms, available to researchers, are employed to arrive at realistic predictions regarding the behavior of mechanical systems.

1.1 Objective of the thesis

A thorough literature review in the subject area reveals that static analysis of leaf springs is ever interesting and a huge number of studies are reported in literature. However, it is observed that theoretical and numerical works on leaf spring models are abundant but on the other hand pure experimental works are few. In addition, there is insufficiency in modeling of roller supports, through which the eye end of leaf spring is mounted. Asymmetry in the geometry and discontinuity in the material due to presence of clamping bolt hole in master leaf spring have not also been considered properly.

In the present thesis, stress and deflection analysis of the master leaf of a leaf spring bundle is carried out experimentally. The experimental works are performed in two parts. In the first part of the experimental work, master leaf spring is modeled as curved cantilever beam considering only one half of the master leaf subjected to tip concentrated load. To validate the experimental model, load-deflection behavior of master leaf spring is also studied theoretically. The physical system is modeled as a curved cantilever beam, subjected to a tip concentrated load undergoing large deflection, in this study. Nonlinear differential equations are obtained for large deflection analysis of such a cantilever beam and these equations are solved numerically to get deflection profiles of the concerned problem. The theoretical study is further extended to predict load-deflection behavior of initially curved cantilever beams under different types of loads. From comparison between experimental and theoretical results, several observations are made.

To overcome insufficiencies of the present model, in second part of the experimental work, a leaf spring testing rig is designed and set-up in our laboratory. In this new experimental set-up, stress and deflection behavior of master leaf spring is studied, modeling

it as a curved beam under three point bending. Moreover, asymmetry in the geometry of master leaf is considered and stress concentration effect due to presence of clamping bolt hole in master leaf spring is studied. In corresponding theoretical analysis, master leaf is modeled as a curved beam under combined bending and stretching stress field. Shear force, bending moment, etc., developed in the loaded master leaf is evaluated and finally the deflection profile is obtained. The theoretical results are validated with experimental ones and observations are reported.

1.2 Basics of leaf spring design

Leaf spring is generally made from several leaves stacked on top of each other in several layers, with progressively shorter leaves, usually of semi-elliptical shape, as shown in Fig. 1.1. In the most common configuration, the region near the centre of arc length provides location for the axle mounting, while tie holes are provided at either end for attachment to the vehicle body. Basics of leaf spring design can be found in several text books of Machine design (Khurmi and Gupta (2005), Bhandari (2010)).

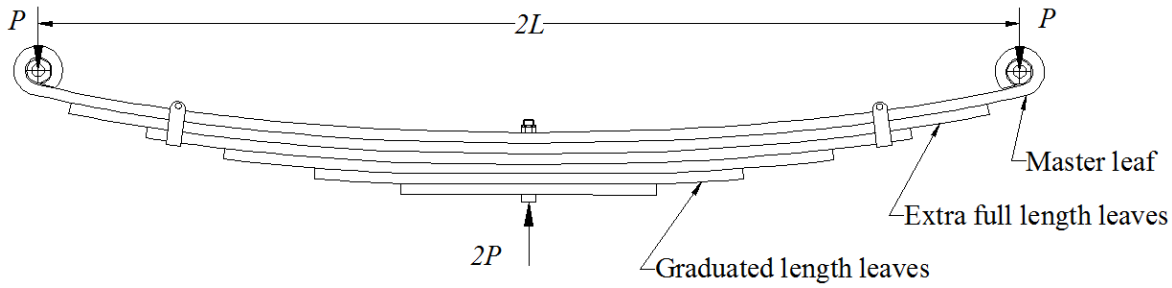

Fig. 1.1 Schematic diagram of leaf spring.

The leaf at the top, known as master leaf, has maximum length and then the lengths gradually decrease from the top leaf to bottom leaf. The master leaf is bent at both ends to form the spring eyes. Two bolts are inserted through these eyes to fix the leaf spring to the automobile body. Multi-leaf springs are provided with one or two extra full length leaves in addition to master leaf. The extra full length leaves are stacked between the master leaf and the graduated length leaves. The extra full length leaves are provided to support the transverse shear force. For the purpose of analysis, the leaves are divided into two groups namely master leaf along with graduated-length leaves forming one group and extra full-length leaves forming the other. Only one half of this spring is considered for analysis, the

equivalent model being a centrally clamped cantilever beam as shown in Fig. 1.2. The group of graduated-length leaves along with the master leaf can be treated as a triangular plate, as shown in Fig. 1.2. In this case, it is assumed that the individual leaves are separated and the master leaf is placed at the centre. Then the second leaf is cut longitudinally into two halves, each of width $(b/2)$ and placed on each side of the master leaf. A similar procedure is repeated for other leaves. The resultant shape is approximately a triangular plate of thickness t and a maximum width at the support as $(n_g\ b)$. The bending stress in the plate at the support is given by,

$$(\sigma_b)_g = \frac{M_b y}{I} = \frac{(P_g\ L)\ (t/2)}{\left[\frac{1}{12}(n_g\ b)(t^3)\right]}$$

$$\Longrightarrow (\sigma_b)_g = \frac{6P_g L}{n_g\ b\ t^2}. \tag{1.1}$$

In Eq. (1.1), b is width of each leaf, n_g is number of graduate-length leaves including master leaf, t is thickness of each leaf, P_g is portion of P taken by the graduated-length leaves, P is the force applied at the end of the spring, L is length of the cantilever or half of the length of leaf spring.

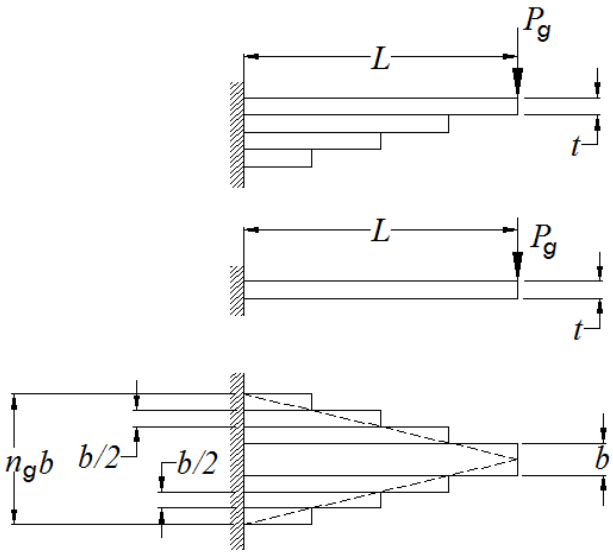

Fig. 1.2 Graduated-length leaves as triangular plate.

It can be proved that the deflection (δ_g) at the load point of the triangular plate is given by,

$$\delta_g = \frac{P_g\ L^3}{2\ E\ I_{max}} = \frac{P_g\ L^3}{2\ E\left[\frac{1}{12}(n_g\ b)(t^3)\right]}$$

$$\Longrightarrow \delta_g = \frac{6\,P_g\,L^3}{E\,n_g\,b\,t^3}. \tag{1.2}$$

Similarly, the extra full length leaves can be treated as a rectangular plate of thickness t and uniform width $(n_f\ b)$, as shown in Fig. 1.3. The bending stress at the support is given by,

$$(\sigma_b)_f = \frac{M_b y}{I} = \frac{(P_f\,L)\,(t/2)}{\left[\frac{1}{12}(n_f\,b)(t^3)\right]}$$

$$\Longrightarrow (\sigma_b)_f = \frac{6P_f L}{n_f\,b\,t^2}. \tag{1.3}$$

The deflection at the load point is given by,

$$\delta_f = \frac{P_f\,L^3}{3\,E\,I} = \frac{P_f\,L^3}{3\,E\left[\frac{1}{12}(n_f\,b)(t^3)\right]}$$

$$\Longrightarrow \delta_f = \frac{4\,P_f\,L^3}{E\,n_f\,b\,t^3}. \tag{1.4}$$

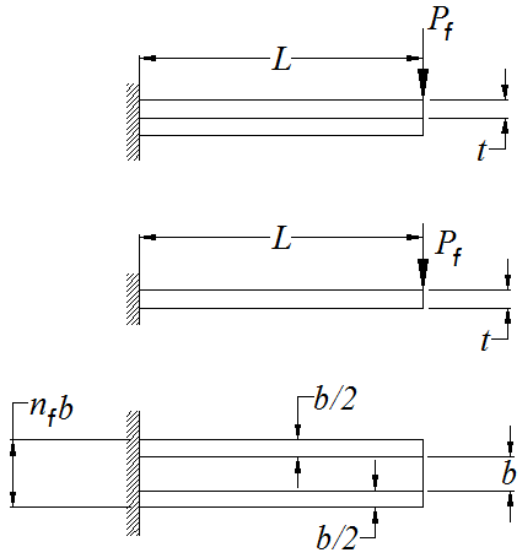

Fig. 1.3 Extra full-length leaves as rectangular plate.

In Eq. (1.4), n_f is the number of extra full-length leaves and P_f is portion of P taken by the extra full-length leaves. Since the deflection of full-length leaves is equal to the deflection of graduated-length leaves,

$$\delta_g = \delta_f$$

$$\Longrightarrow \frac{6\,P_g\,L^3}{E\,n_g\,b\,t^3} = \frac{4\,P_f\,L^3}{E\,n_f\,b\,t^3}$$

$$\Longrightarrow \frac{P_g}{P_f} = \frac{2\,n_g}{3\,n_f}, \text{ and} \tag{1.5}$$

$$P_g + P_f = P. \tag{1.6}$$

From Eqs. (1.5) and (1.6),

$$P_f = \frac{3\, n_f\, P}{3\, n_f + 2\, n_g}. \tag{1.7}$$

$$P_g = \frac{2\, n_g\, P}{3\, n_f + 2\, n_g}. \tag{1.8}$$

Substituting the above values in Eqs. (1.1) and (1.3),

$$(\sigma_b)_g = \frac{12\, PL}{(3\, n_f + 2\, n_g) b\, t^2}. \tag{1.9}$$

$$(\sigma_b)_f = \frac{18\, PL}{(3\, n_f + 2\, n_g) b\, t^2}. \tag{1.10}$$

It is obvious from the above equations that bending stresses in full-length leaves are 50% more than those in graduated-length leaves. The deflection at the end of the spring is determined from Eqs. (1.2) and (1.8). It is given by,

$$\delta = \frac{12\, P\, L^3}{E\, b\, t^3 (3\, n_f + 2\, n_g)}. \tag{1.11}$$

Leaf springs are designed using these load-stress and load-deflection equations for trivial applications only because the actual behavior under large deflection is quite different.

1.3 Method of experimentation

In the present work, stress and deflection behavior of a master leaf spring under bending type of loading conditions is studied experimentally. The load-deflection study includes two different techniques, a direct measurement technique and an indirect measurement technique. In direct measurement technique, deflection profile of master leaf spring is obtained by measuring coordinates of some marked points on it, using height gauge, scale and plumb. On the other hand, in indirect measurement of deflection profiles, image processing technique is adopted. Whereas, development of stresses in master leaf spring is studied by using strain gauge technique. These techniques are briefly described in the following two sub-sections.

1.3.1 Image processing techniques

Image processing technique is widely used in experimental mechanics, in which result of an experiment is obtained by processing an image. Digital image is a two dimensional representation of a scene where luminance of objects in that scene are assigned in each picture element or pixel. Thus digital image is stored as a matrix and digital image processing

is a collection of algorithms applied on that image or image matrix to extract useful information of the captured scene. The foundation of digital image processing is well developed and has already become classical. Digital image processing eliminates tedious manual work and makes the process of data analysis more accurate and objective. In image processing technique, camera and illumination system are the two key elements. Due to inhomogeneous illumination or lighting system, many spurious points and/or false edges are formed as wrong informations, when captured images are processed through commercial softwares. Thus image acquisition and post-processing should be done carefully, for extracting accurate information from digital image.

There are some established displacement measurement methods based on the phenomenon of light interference, like various moire techniques, holographic interferometry or speckle, etc. In these methods a pattern of fringes appears on the specimen surface when image is captured in the camera. The fringes are contour lines of some specific deformation characteristics like in-plane displacements or off-plane displacements.

There are also image processing methods based on the phenomenon of birefringence – various versions of photoelasticity. Photoelasticity is an experimental method to determine the stress distribution in a material. It is usually a contour map of the differences of principal stresses. The method is based on the property of birefringence, as exhibited by certain transparent materials. Birefringence is the phenomenon in which a ray of light passing through a birefringent material experiences two refractive indices. The property of birefringence is observed in many optical crystals. Upon the application of stresses, photoelastic materials exhibit the property of birefringence, and the magnitude of the refractive indices at each point in the material is directly related to the state of stresses at that point. For materials do not show photoelastic behavior, models made of special transparent materials are tested which has geometry similar to the real structure under investigation.

Digital image processing is an important tool of machine vision technique which is used to extract information from real physical objects. It helps to take a decision from the sensed images in a non-invasive way with minimal human intervention. A wide application of machine vision system is addressed in the field of manufacturing industry for non-invasive inspection of manufactured products. In these methods, usually specimens made of real structural materials are tested.

1.3.2 Strain gauge technique

Development of stresses in structural members under load is obtained through strain gauge technique. The most widely used gauge, however, is the bonded metallic resistance strain gauge. The metallic strain gauge consists of a very fine wire or, more commonly, metallic foil arranged in a grid pattern. The grid pattern maximizes the amount of metallic wire or foil subject to strain in the parallel direction. The grid is bonded to a thin backing, called the carrier, which is attached directly to the test specimen. It is very important that the strain gauge be properly mounted onto the test specimen so that the strain is accurately transferred from the test specimen, through the adhesive and strain gauge backing, to the foil itself. Manufacturers of strain gauges are the best source of information for proper mounting of strain gauges.

A fundamental parameter of the strain gauge is its sensitivity to strain, expressed quantitatively as the gauge factor (S_g). Gauge factor is defined as the ratio of fractional change in electrical resistance to the fractional change in length (strain) and given by $S_g = \frac{\Delta R}{R}/\frac{\Delta L}{L} = 1 + 2\nu + \frac{\Delta \rho}{\rho}/\frac{\Delta L}{L}$, where R is resistance of the conductor, ΔR is change in resistance, L is length of the conductor, ΔL is change in length of the conductor, ν is Poisson's ratio of the material, ρ is specific resistance and $\Delta \rho$ is change in specific resistance (Doebelin and Manik (2011)).

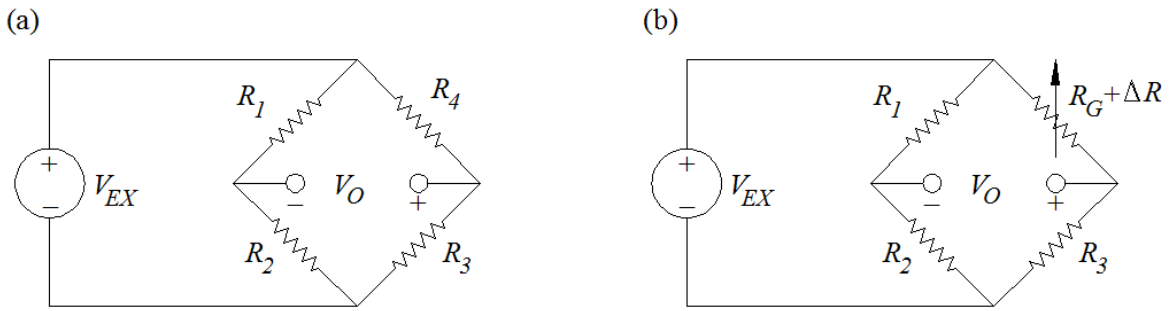

Fig. 1.4 (a) Wheatstone bridge and (b) quarter bridge circuits.

Strain measurement requires accurate measurement of very small changes in resistance. To measure such small changes in resistance, strain gauges are almost always used in a bridge configuration with a voltage or current excitation source. The general Wheatstone

bridge, shown in Fig. 1.4 (a), consists of four resistive arms with an excitation voltage, V_{EX}, that is applied across the bridge. The corresponding output voltage of the bridge is $V_O = \left[\frac{R_3}{R_3+R_4} - \frac{R_2}{R_1+R_2}\right] V_{EX}$. The bridge is said to be balanced when the output voltage V_O is zero. Any change in resistance in any arm of the bridge will result in a nonzero output voltage. Therefore, if any one of four resistive arms is replaced with an active strain gauge as shown in Fig. 1.4 (b), changes in the strain gauge resistance will unbalance the bridge and produce a nonzero output voltage. If the nominal resistance of the strain gauge is designated as R_G, then the strain-induced change in resistance, ΔR, can be expressed as $\Delta R = R_G\, S_g\, \varepsilon$. Assuming that $R_1 = R_2$ and $R_3 = R_G$, the equation for bridge sensitivity (S_c) of quarter bridge circuit can be rewritten as $S_c = \frac{V_O}{V_{EX}} = -\frac{S_g\, \varepsilon}{4}\left\{1/(1 + S_g\, \frac{\varepsilon}{2})\right\}$. Presence of the term $\left\{1/(1 + S_g\, \frac{\varepsilon}{2})\right\}$ in sensitivity expression makes the output of quarter bridge circuit nonlinear with respect to strain.

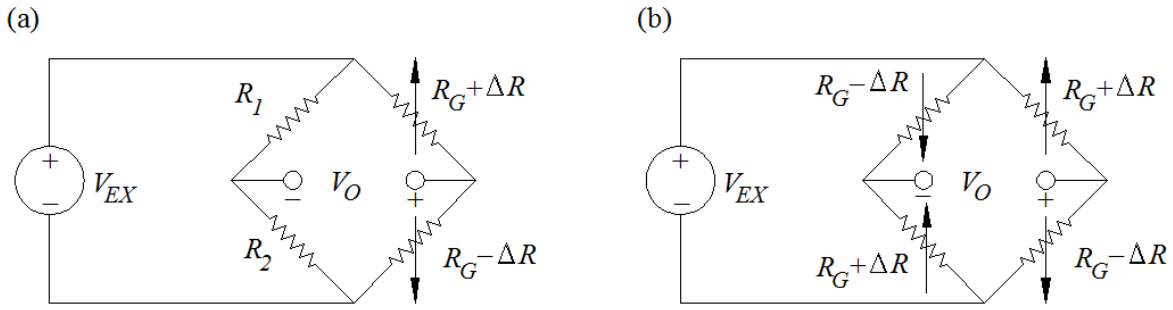

Fig. 1.5 (a) Half bridge and (b) full bridge circuits.

Sensitivity of the bridge to strain is doubled by making two gauges active, although in opposite directions. As shown in Fig. 1.5 (a), one gauge is mounted in tension and the other one is mounted in compression stress fields to attain resistance values of $(R_G + \Delta R)$ and $(R_G - \Delta R)$ respectively. This half-bridge configuration yields circuit sensitivity as $S_c = \frac{V_O}{V_{EX}} = -\frac{S_g\, \varepsilon}{2}$, which is linear and approximately double of the sensitivity for quarter bridge circuit. Finally the sensitivity of the circuit can further be increased by making all four of the arms of the bridge active, and mounting two gauges in tension and two gauges in compression as shown in Fig. 1.5 (b). Sensitivity of such a full-bridge circuit is given by $S_c = \frac{V_O}{V_{EX}} = -S_g\, \varepsilon$. Sometimes strain gauges are mounted in transverse direction also to account for Poisson's ratio effect.

1.4 Theoretical analysis

In theoretical analysis, load-deflection behavior of master leaf spring is obtained by modeling it as cantilever beam following large deflection theory. The governing differential equation is derived based on Euler-Bernoulli theory and integrated directly which leads to solution in terms of elliptic integrals. The elliptic integrals are evaluated numerically in MATLAB® computational platform using Gaussian quadrature integration scheme, without using elliptic function explicitly. On the other hand, in analysis of master leaf spring as curved beam under three point bending, Winkler-Bach analytical curved beam theory is used for comparison of bending moment, bending stress, etc. developed in it with experimental results. In addition, effect of stress concentration in developed stress field due to the presence of drill hole in master leaf is addressed using analytical equations of stress distribution around a geometric discontinuity of a structure. Brief descriptions of static analysis of beam, elliptic integrals and stress concentration due to presence of geometric discontinuity in structural members are presented in the following sub-sections.

1.4.1 Static analysis of beam

When a beam is subjected to pure bending moment M, Euler-Bernoulli beam theory states that the bending moment is proportional to the change in curvature of the beam and may be written mathematically as $\frac{1}{\rho} = \frac{M}{EI}$, where I is the area moment of inertia of the beam cross-section about neutral axis and ρ denotes the radius of curvature of the neutral surface. Several aspects of beam bending analysis under static loading can be found in several text books on strength of materials (Timoshenko and Young (2009), Nag and Chanda (2010), etc.). In curvilinear coordinate system (s, n) curvature is given by $1/\rho = d\varphi/ds$, where φ is the slope dy/dx at location s and it is also a measure of normal direction n. When the analysis is carried out in Cartesian coordinate system (x, y), the curvature is given by $\frac{1}{\rho} = \frac{d^2y}{dx^2} \Big/ \left[1 + \left(\frac{dy}{dx}\right)^2\right]^{3/2}$. In case of axially varying transverse load or bending moment, the neutral surface of the bent beam does not necessarily bend in the form of circular arc. In such non-uniform bending it is generally assumed that the Euler-Bernoulli moment-curvature relation holds at each cross-section, for both small and large deflection of beams. But the slope-curvature relation is calculated differently in those cases.

1.4.1.1 Small deflection

In case of small deflection analysis of beam, it is assumed that slope $\frac{dy}{dx}$ of the elastic curve is very small and its square can be neglected in the curvature formula. So, in small deflection analysis, curvature $(1/\rho)$ is approximated as $\frac{d^2y}{dx^2}$ and the differential equation of the elastic line of the beam becomes $\frac{d^2y}{dx^2} = \frac{M}{EI}$. Solution of this equation, $y = f(x)$ defines the shape of the elastic line or the deflection curve (as it is frequently called).

1.4.1.2 Large deflection

Several structural members can undergo large displacements without exceeding their specified elastic yield stress limit. For better characterization of such bending problems, analysis is carried out using large deflection theory. The first reported work regarding the large deformation of flexible members was given by Leonhard Euler in 1744. Main features of large deflection analysis are constant beam length at any configuration during bending, moment arm shortening and presence of slope of the deflection curve in the expression of curvature. In Cartesian coordinate system (x, y), curvature-moment relationship is given by $\frac{d^2y}{d\,x^2}\Big/\left[1 + \left(\frac{dy}{dx}\right)^2\right]^{3/2} = \frac{M}{E\,I}$ (Fertis (2006)). This equation shows that the deflection is no longer a linear function of the bending moment. These types of problems are known to involve geometric nonlinearity. A simple analytical solution to such bending problems is not possible, because of the presence of nonlinear terms in governing equation. Since Euler, many mathematicians, scientists, and engineers researched this subject and proposed many methodologies to solve large deflection problems of beams. The more widely used analytical methods include power series, elliptic integrals, etc. Numerical methods include numerical integration approach with iterative shooting technique, Newton-Rhapson iteration technique, the incremental finite element or finite difference method, etc.

1.4.1.3 Curved beam

Numerous mechanical parts subjected to bending, like crane hooks, leaf springs, arches, etc., are not initially straight and they are called initially curved beams. If x direction is considered along the span of the beam and y direction is along the applied loads, the centroidal axis of a curved beam has an initial curvature in xy plane. Relations between

stress, moment and deflection in loaded curved beams are well known from Winkler-Bach theory. According to this theory, when a curved beam is subjected to pure bending M, the bending stress at any layer with radius of curvature r is given by $\sigma = \frac{M\,(r_n - r)}{A\,r\,(r_n - r_c)}$, where r_n is radius of curvature of the neutral surface, r_c is radius of curvature of the centroidal surface and A is cross-sectional area of the beam (Nag and Chanda (2010)). For rectangular cross-section of width b and thickness h, radius of curvature of the neutral surface is given by $r_n = \frac{h}{\ln(r_2/r_1)}$, where $r_1 = r_c - \frac{h}{2}$ and $r_2 = r_c + \frac{h}{2}$.

1.4.2 Elliptic integrals

The first reported study of elliptic integrals was in 1655 when John Wallis began to study the arc length of an ellipse. Both John Wallis (1616-1703) and Isaac Newton (1643-1727) published an infinite series expansion for the arc length of ellipse. But it was not until the late 1700's, when Legendre began to use elliptic functions for problems such as the movement of a simple pendulum and the deflection of a thin elastic bar, that elliptic integrals could be defined in terms of simple functions. Basic mathematics involved in evaluation of elliptic integrals and elliptic functions are available in many text books (Spiegel et al. (2009)). Brief introductions of elliptic integrals and elliptic functions are presented in the following two sub-sections.

1.4.2.1 Evaluation of elliptic integrals

An integral of the form $\int R(x, y)dx$, where $R(x, y)$ is a rational function of x and y, and $y^2 = P(x)$ where P is a polynomial of degree 3 or 4, is called an elliptic integral. There are three basic forms of Legendre elliptic integrals, called first, second and third kinds. In their most general form, elliptic integrals are presented in a form referred to as incomplete integrals. The incomplete elliptic integrals of first, second and third kinds are denoted by F, E and Π respectively and they are given by $F = \int_0^{\varphi} \frac{d\theta}{\sqrt{1-k^2 sin^2\theta}}$, $E = \int_0^{\varphi} \sqrt{1 - k^2 sin^2\theta}\, d\theta$ and $\Pi = \int_0^{\varphi} \frac{1}{1-n\, sin^2\theta} \frac{d\theta}{\sqrt{1-(sin\alpha\, sin\theta)^2}}$ (Spiegel et al. (2009)). In these expressions, the parameter k ($0 \le k^2 \le 1$) is called the modulus of the elliptic integral, φ ($0 \le \varphi \le \frac{\pi}{2}$) is the amplitude angle, α is the modular angle and n is called the characteristic and can take on any value,

independently of the other arguments. Elliptic integrals are said to be 'complete' when the amplitude $\varphi = \frac{\pi}{2}$.

1.4.2.2 Types of elliptic functions

The theory of elliptic integrals was exceedingly complicated due to presence of infinitely many values for each elliptic integral. In 1827, Abel simplified the subject immensely by inverting elliptic integrals to get elliptic functions. There are several types of elliptic functions including Weierstrass elliptic functions as well as related theta functions but the most common elliptic functions are the Jacobian elliptic functions, based on the inverses of the three types of elliptic integrals. The Jacobi elliptic functions are described briefly in the following paragraph.

The three standard forms of Jacobi elliptic integrals are the sine, cosine and delta amplitude elliptic functions and they are denoted by $sn\,(u,k)$, $cn\,(u,k)$ and $dn\,(u,k)$ respectively. Here, $u = F(\varphi,k) = \int_0^{\varphi} \frac{d\theta}{\sqrt{1-k^2 sin^2\theta}}$, k is referred to as the elliptic modulus of u and φ, the upper bound on the elliptic integral is referred to as the Jacobi amplitude (amp). The inversion of the elliptic integral gives $\varphi = F^{-1}(u,k) = amp(u,k)$ and from this relation we can write $\sin\varphi = \sin(amp(u,k)) = sn\,(u,k)$, $\cos\varphi = \cos(amp(u,k)) = cn\,(u,k)$ and $\sqrt{1-k^2 sin^2\varphi} = \sqrt{1-k^2 sin^2(amp(u,k))} = dn\,(u,k)$ (Spiegel et al. (2009)). These functions are doubly periodic generalizations of the trigonometric functions satisfying $sn\,(u,0) = \sin u$, $cn\,(u,o) = \cos u$ and $dn\,(u,o) = 1$.

1.4.3 Stress concentration

Localized high stresses due to presence of geometric discontinuities in a loaded solid give rise to stress concentration which is primarily responsible for local yielding, fatigue and fracture. Figure 1.6 represents a large, thin flat plate subjected to a uniform tensile stress σ in x direction. A hole is present in the middle of the plate which causes stress redistribution in the plate. Generally the size of hole is assumed to be very small compared to plate width, thus the change in stress distribution will be localized in neighborhood of the hole. Hence, the stresses acting far away from the hole, i.e., at a distance several times the hole diameter, remain unchanged as in the plate with no hole.

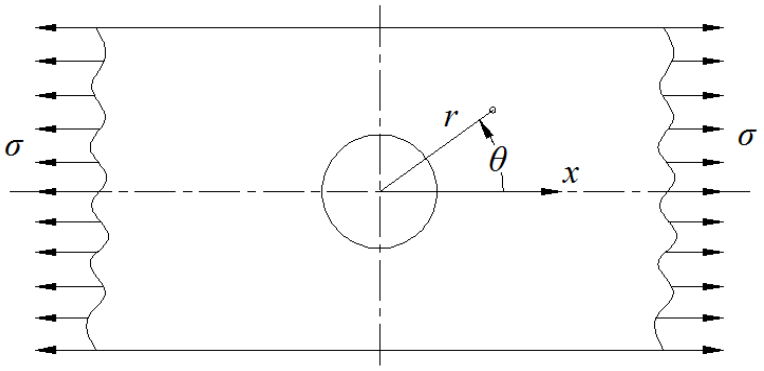

Fig. 1.6 Stress concentration around a small hole in a plate subjected to uniform stress.

The overall stress distributions in the plate are given by $\sigma_{rr}(r,\theta) = \frac{\sigma}{2}\left[\left(1-\frac{a^2}{r^2}\right) + \left(1+3\frac{a^4}{r^4}-4\frac{a^2}{r^2}\right)\cos(2\theta)\right]$, $\sigma_{\theta\theta}(r,\theta) = \frac{\sigma}{2}\left[\left(1+\frac{a^2}{r^2}\right) - \left(1+3\frac{a^4}{r^4}\right)\cos(2\theta)\right]$ and $\sigma_{r\theta}(r,\theta) = -\frac{\sigma}{2}\left[\left(1-3\frac{a^4}{r^4}+2\frac{a^2}{r^2}\right)\sin(2\theta)\right]$, where a is the hole radius (Timoshenko and Goodier (1951)).

1.5 Summary of the thesis

Chapter 1 introduces the subject matter of the proposed work and briefly discusses the contents of the thesis. In this chapter various applications of leaf spring is discussed and construction details along with basic design principles of leaf springs are introduced. This chapter also includes experimental techniques and basic mathematics involved in analysis of the present problem.

In chapter 2, a detailed review of the available literature on stress and deformation analysis of leaf spring and its equivalent model is carried out. The review work is carried out quite extensively with emphasis on analysis methods and experimental techniques for geometric nonlinear analysis of leaf spring, beam, etc. Effects of various system parameters, namely loading condition and boundary condition, on static response of leaf springs and their equivalent models are discussed subsequently.

Chapter 3 reports experimental and theoretical analysis of load-deflection behavior of master leaf spring as curved cantilever beam. This chapter begins with a detailed description of the experimental set-up and then reports experimental determination of deflection profiles

of master leaf spring under loaded conditions. In corresponding theoretical analysis, a semi analytical method is proposed to study large deflection behavior of initially curved cantilever beams under tip concentrated load. Comparisons between the experimental and theoretical results are quite good, and from this comparative study several aspects of leaf spring modeling are identified and reported. The proposed theoretical method is further extended to study large deflection behavior of initially curved beams under distributed and combined loads.

In chapter 4, experimental stress and deflection analysis of master leaf spring under three point bending is reported. This chapter describes design development of a leaf spring testing set-up and experimental procedure to obtain deflection profiles and stress field developed in a master leaf spring under various loading conditions. For the purpose of comparison of experimental stress results with theoretical ones, master leaf spring is modeled as curved beam under three point bending and analysis is carried out using Winkler-Bach curved beam theory. Effects of asymmetric geometry and presence of central drill hole in mater leaf spring are also addressed in this analysis.

Chapter 5 offers the conclusion of the present thesis and highlights the future scope of work, which is then followed by list of references and a bibliography.

Chapter 2

LITERATURE REVIEW

Analysis of leaf spring is ever interesting due to its numerous applications in automotive industry and a huge number of research works are reported in literature. Literature on dynamic analysis of leaf spring is not included in the scope of this review as the present work concentrate on static analysis of leaf spring. Static analysis of a structure entails determination of deflections, stresses, moments, etc. developed in the structure under steady or time independent loading. The parameters of such a problem depend on several factors, for example, boundary condition, loading pattern, initial geometry, etc. To investigate the state of internal stresses produced in the process of bending of a structure, one must examine the corresponding deformation state which takes place within the material. Research works available in literature on stress and deflection analysis of leaf spring under bending type of loading can be broadly categorized in two major categories and they are theoretical and experimental works. In the following sections a concise description of various literature available related to research work on stress and deflection analysis of leaf spring is provided.

2.1 Literature on theoretical work

In theoretical stress and deflection analysis, leaf springs are generally modeled as a bundle of prismatic beams under three point bending, whereas many researchers consider only one half of the spring taking it as a cantilever beam. The following three sub-sections report various literatures related to deflection analysis, stress analysis and combined deflection and stress analysis of leaf spring and their equivalent model respectively. Major research findings reported in individual papers are presented chronologically. Different analysis methods, various system parameters and complicating effects are identified from the reported research papers and they are reviewed subsequently in this chapter.

2.1.1 Deflection analysis

Deflection is the measure to which a structural element is displaced under a load and it may refer to an angle or a distance. Usually deflection is measured with respect to its initial undeformed configuration. The deflection of a member under a load is directly related to the

slope of the deflected shape under that load and can be calculated by integrating the slope function mathematically. Traditionally deflection characteristics of beams are analyzed with small deflection theory which is a simplification of the theory of elasticity in linear domain. The derivation is based on the fundamental Bernoulli-Euler theorem, which states that the curvature is proportional to the bending moment. It is assumed also that bending does not alter the length of the beam.

Later on, many researchers pointed out that for better prediction of large bending behavior of beams, analysis should be carried out through large deflection theory. Modeling of these problems is known to involve geometric nonlinearity as the slope-curvature relation of its deflection curve is nonlinear. Several researchers have also considered effects of combined bending-stretching and transverse shear deformation on deflection behaviors. The following paragraphs briefly describe various literature related to large deflection analysis of structures like leaf springs and beams under various loading conditions.

Bisshopp and Drucker (1945) were the first to point out that the solution for large deflection of a cantilever beam cannot be obtained from elementary beam theory. The basic assumptions of elementary theory are no longer valid as it neglects the square of first derivative in the curvature formula and provides no correction for the shortening of the moment arm as the loaded end of the beam deflects. With this realization they proposed elliptic integral approach for analyzing large deflection problems which was in agreement with experimental observations and still widely used at present. In this theory they have considered the square of the first derivative in the curvature formula and also the correction factors due to shortening of the moment arm.

Wang (1968) proposed a simple numerical method for analyzing non-linear bending of beams based on Bernoulli-Euler theory which states that the bending moment at any point of a beam is proportional to the corresponding curvature. When the slope of the beam is small, its square can be neglected in comparison with unity, thus the expression of the curvature is linearized. Wang pointed out that results based on this approximation cannot be applied in case of large deflection. He proposed a numerical method for analyzing two problems-(1) a cantilever beam bending problem under a concentrated load at the free end and (2) a simply supported beam subjected to a nonsymmetrical load and compared the results successfully with the results of Bisshopp and Drucker (1945).

In the next year, Wang (1969) also studied non-linear bending of both cantilever and simply supported beams subjected to a uniformly distributed load. The expressions for slopes in terms of the horizontal projection of the arc length for beams carrying a uniformly distributed load have been derived. By using numerical methods, the slopes at all points, the maximum deflection, and the horizontal projection of the beam lengths have been obtained.

Wang et al. (1997) presented large deflection problems of beams subjected to a point load with one end fixed and other end allowed to slide freely over a frictionless support. In this work, they have proposed solution of such non-linear problem by using both the elliptic integral method and the shooting-optimization technique, thus providing independent checks on the solutions. Features of this kind of problem are (1) the possibility of two possible equilibrium solutions for a given load magnitude, (2) a maximum (or critical) load and (3) a maximum deformed arc-length for equilibrium.

Beléndez et al. (2002) analyzed the problem of deflection of a cantilever beam, in case of both large and small deflections. Firstly, they obtained the differential equation for the deflection curve in the general case of large deflection and the equations that determine the Cartesian coordinates of each point on the elastic curve. They have also shown that unless small deflections are considered, an analytical solution does not exist, since for large deflections a differential equation with a non-linear term must be solved. This geometrically non-linear equation is solved numerically with the aid of the program Mathematica, without using elliptic functions for the sake of simplicity. Then they obtained the approximation for small deflections from the equations presented for large deflections. Finally, various general numerical results are presented and these are compared with experimental results.

Osipenko et al. (2003) presented a problem where the objective was to find the shapes of the leaves of leaf spring under bending, which was reduced to the problem of finding the densities of the forces of interaction between the leaves. In their analysis, leaf spring is modeled as stack of slim non-uniform curved beams (leaves) with rectangular cross-sections having same widths and different lengths (the lengths decrease upwards). Each leaf is fixed at one end and free at the other end and the loading is applied to the lower leaf in upwards direction. They propounded accurate formulation of the latter problem and proved uniqueness

of the solution. Analytical solution in the special case of two uniform straight leaves are constructed and furnished in this paper.

Kumar et al. (2004) suggested a couple of non-convex search strategies based on the genetic algorithm in the context of large deflection analysis of planar, elastic beams. The first of these strategies is based on the stationarity of the energy functional in the equilibrium state and therefore is considered as weak. The second approach is based on a shooting strategy which directly solved governing differential equation within an optimization frame work and therefore is considered as strong. They have provided several numerical illustrations and verifications with exact solutions. It is observed from numerical results that, while both the methods yield reasonably accurate results, the second approach offers a more efficient and elegant alternative. They concluded with the future scope where these procedures can be applied in the context of finite-rotation (kinematically exact) beam theories and simulations of nonlinear beam dynamics governed by partial differential equations.

Dado and Al-Sadder (2005) developed an approach that approximates the angle of rotation of the beam by a polynomial function to study very large deflection behavior of prismatic and non-prismatic cantilever beams subjected to various types of loadings. The coefficients of the polynomial are obtained by minimizing the integral of the residual error of the governing differential equation and by applying the beam's boundary conditions. In this paper, they have presented several numerical examples ranging from moderately large deflection to very large deflection covering prismatic and non-prismatic cantilever beams subjected to uniform, non-uniform distributed loads and tip concentrated loading in vertical and horizontal directions. However the loads considered in this study are restricted to the non-follower type loads. Cases with different loadings and geometries are compared with MSC/NASTRAN computer package. They also pointed out that the presented scheme handles extreme cases with high accuracy and solution stability while the finite element method as depicted by MSC/NASTRAN failed in predicting these extreme cases.

Sugiyama et al. (2006) reported development of nonlinear elastic leaf spring model for multi body vehicle system. They modeled the distributed inertia and stiffness of the leaves of the spring using the finite element floating frame of reference formulation that accounts for the effect of the nonlinear dynamic coupling between the finite rotations and the leaf deformation. The leaf spring geometry and deformations are modeled using nodal degrees of

freedom defined with respect to the spring body coordinate system. They pointed out that the number of deformation coordinates can be reduced by assuming large leaf deformation but with simple shape. The nonlinear stiffness matrix is first developed for the finite element of each leaf and is used to determine the overall leaf spring stiffness matrix. They discussed the pre-stresses, the contact and friction that characterize the nonlinear behavior of leaf springs. Using the nonlinear leaf spring formulation presented in this study, a detailed multi-body model for a sport utility vehicle is developed. They have also shown that the proposed leaf spring model that accounts for the effect of windup, contact and friction between the spring leaves can be effectively used for assessing the dynamic stability of sports utility vehicles.

Shvartsman (2007) proposed a direct numerical method for large-deflection analysis of a non-uniform spring-hinged cantilever beam under a tip follower force. The mathematical formulation of this problem yields a nonlinear two-point boundary-value problem which reduced to an initial-value problem by change of variables. The resulting problem can be solved without iterations. He has shown that there exist no critical loads in the Euler sense (divergence) for any flexural-stiffness distribution and angle of inclination of the follower force. In this paper he presented the load–displacement characteristics of a uniform cantilever under a follower force normal to the deformed beam axis.

Banerjee et al. (2008) proposed non-linear shooting and Adomian decomposition methods to determine large deflection of a cantilever beam under arbitrary loading conditions. Results obtained only due to end loading are validated using elliptic integral solutions. The non-linear shooting method gives accurate numerical results while the Adomian decomposition method yields polynomial expressions for the beam configuration. With high load parameters, occurrence of multiple solutions is discussed with reference to possible buckling of the beam-column. They applied these two methods to solve a problem of concentrated intermediate loading (cantilever beam subjected to two concentrated self-balanced moments) for which no closed form solution can be obtained. Some of the limitations and recipes to obviate these are included.

Eren (2008) investigated large deflection of cantilever beams of ludwick type material subjected to combined loading consisting of a uniformly distributed load and one vertical concentrated load at the free end. In this study, both material and geometrical non-linearity have been considered. Horizontal and vertical deflections are calculated through Euler-

Bernoulli curvature moment relationship assuming different arc length. Vertical deflections are calculated by using Runge-Kutta method.

Tolou and Herder (2009) analytically investigated large deflection of members of compliant mechanisms. Main objective of this paper is to propose a convenient method of solution for the large deflection problem in compliant mechanisms in order to overcome the difficulty and inaccuracy of conventional methods, as well as for the purpose of mathematical modeling and optimization. In this work, they have considered an element by modeling it as a cantilever beam subjected to vertical end point load which can be used as a building block in more complex compliant mechanisms. First, the governing equation has been obtained for the cantilever beam. Subsequently, the Adomian decomposition method has been utilized to obtain a semi analytical solution. In addition, variations of the parameters that affect the characteristics of the deflection have been examined. The results reveal that the proposed procedure is very accurate, efficient, and convenient for cantilever beams, and can probably be applied to a large class of practical problems for the purpose of analysis and optimization.

Chen (2010) proposed a new integral approach to solve large deflection cantilever beam problems. This method is different from the traditional elliptic integral method while can be converted to the elliptic integral in certain conditions. In this work, he have shown that the proposed method is applicable for any arbitrary loading conditions such as concentrated load, distributed load and combined load. The proposed method is also applicable for variable beam properties such as changing cross-sectional area. He pointed out that application of this approach usually requires only simple numerical techniques and straight-forward solution procedures. Only one first order ODE needs to be solved which is easier than traditional approaches. Standard search or iterative procedures or combination of them are usually adequate for the solution. For concentrated loads on uniform beam, theoretical and numerical analysis showed that this approach is equivalent to the Bisshopp and Drucker (1945) elliptic integral approach. He also presented numerical simulation of the experiment by Beléndez et al. (2003) of cantilever beam bending under a concentrated load and gravity.

Mutyalarao et al. (2010a) proposed a numerical method to obtain deformed configuration of cantilever beam subjected to tip concentrated load, which rotates in relation with the tip-rotation of the beam. Firstly, they derived governing differential equations of the cantilever beam which are nonlinear, amenable to numerical integration. Then, they obtained

a relation for the applied tip-concentrated load in terms of the tip-angle of the beam. When the tip-concentrated load acts always normal to the undeformed axis of the beam (the rotation parameter = 0) there is a possibility of obtaining non-unique solution for the applied load. This phenomenon is also observed for other rotation parameters less than unity. When the tip-concentrated load is acting normal to the deformed axis of the beam (the rotation parameter = 1), many load parameters are obtained for a tip-angle with different deformed configurations of the beam. However, each load parameter corresponds to a tip-angle, which confirms the uniqueness on the solution of non-linear differential equations.

In a later work, Mutyalarao et al. (2010b) also studied large deflection of cantilever beam subjected to a tip-concentrated load whose inclination to the deformed axis of the beam is assumed as constant. The mathematical formulation yields a non-linear two-point boundary value problem amenable to numerical integration. A relation is obtained between the load and the tip-angle of the beam when the tip-concentrated load is normal to the deformed axis of the beam. Many possible loads are found for a specified tip-angle. For the specified load, the tip-angle is found to be unique. However, there is a change in the deformation pattern of the beam having a specified tip-angle with the corresponding multiple loads. This confirms the uniqueness of the solution for the governing non-linear differential equations of a cantilever beam under a tip-concentrated load whose inclination is normal to its deformed axis.

Nallathambi et al. (2010) analyzed large deflections of straight and curved prismatic cantilever beams under follower loads at the tip. They have considered large deflection, the deflection dependent follower load and the initial curved geometry as important features for mathematical formulation which yields non-linear two-point boundary value problem. In this formulation, they used shear force formulation approach which reduced the two point boundary value problem (TPBVP) to an initial value problem (IVP). Fourth order Runge–Kutta method along with one parameter reverse shooting method is applied to the numerical solution to the problem. A novel approach presented in this paper of integrating from the free end to the fixed end of the cantilever beam simply replaced the two parameters shooting with a single parameter shooting yielding several advantages. They finally demonstrated this solution technique for various types of follower tip loads on curved and straight cantilever beams and compared the results with existing results in the literature.

He et al. (2013) proposed a new perturbation method with two small parameters, describing the effect of load and geometry of the problem, to solve nonlinear large deflection problem of initially curved beams under two different boundary conditions. They started with the realization that for beams with gradient, due to the combined influences introduced by loads and gradient, the first derivative item in Euler–Bernoulli equation cannot be neglected thus making the solution of the problem be a nonlinear one. They derived the first and second order approximate analytical solution of the deflection, the rotation and the arc length of the beam, as well as the internal forces of the beam at the end. The results indicate that the choice of two independent parameters may describe comprehensively the nonlinear effects caused by loads and gradient, which enables the approximate solution to be precise enough to be used for the analysis of large-deflection beam with gradient.

Shvartsman (2013) studied large deflection of a curved cantilever beam under a tip-concentrated follower force by direct numerical method. He has shown that after changing the variables, the original non-linear boundary value problem transforms into the initial-value problem for pendulum equation. The resulting initial value problem is solved numerically using a modified Numerov's method. In contrast to the usually used iteration methods (e.g. shooting technique), the problem is solved without iterations by direct numerical method. Some qualitative conclusions were made using Kirchhoff's kinetic analogy. He has also shown that there are no critical loads in the Euler sense (divergence) for any values of the initial curvature and angle of inclination of the follower force. An extension of direct numerical method to curved spring-hinged cantilever subjected to follower force is also proposed. In this paper, some equilibrium configurations of the uniform curved fixed and spring-hinged cantilevers under normal and tangential follower force obtained by direct method are presented.

Tari (2013) studied the problem of determining the parametric large deflection components of Euler–Bernoulli cantilever beams subjected to combined tip point loading. In this paper, they have introduced the beam's deflection characteristic equation governing any combination of loading and deflection parameters. Angular, horizontal and vertical deflection solutions to the Euler–Bernoulli beam's boundary value problem are obtained in terms of the loading parameters by using the recently developed automatic Taylor expansion technique. The parametric solutions are then validated by comparison with the numerical solutions obtained from the numerical differential solver of Mathematica. Exploiting these solutions as

theoretical tools, they have studied beam's angular and axial deflections behavior for several tip point loading conditions. Besides the widely known beam's axial inflection points, they also recognized beam's angular inflection points for the mixed loading condition and showed that the parametric solutions are intelligent in recognizing the right deflection branch for both inflection types.

Sitar et al. (2014) derived governing differential equation for determining large deflections of slender, non-homogeneous beam subjected to a combined loading and composed of a finite number of laminae, which are made of nonlinearly elastic, modified Ludwick's type of material with different stress–strain relations in tension and compression domain. The material properties are varying arbitrarily through the beam's thickness. When the thickness of laminae is sufficiently small and the variation of mechanical properties is close to continuous, the beam can be considered as made of functionally graded material (FGM). The derived equations are solved numerically and tested on several examples. They have shown that the results obtained are in good agreement with those found in the literature.

Mohyeddin and Fereidoon (2014) analyzed large deflections of a straight prismatic shear-deformable simply supported beam subjected to a point load at its mid-span. Governing deferential equations are derived for vertical and horizontal displacements as well as the slope and rotation angle of the beam cross-section based on the Timoshenko beam theory. The system of boundary value problem is solved analytically to yield a closed-form solution. The results are compared with available experimental data and those obtained for Euler–Bernoulli beam in the literature.

Nguyen (2014) studied large displacement behavior of tapered cantilever Euler-Bernoulli beams made of functionally graded material subjected to end forces. The effective Young's modulus of the beams is assumed to be graded in the thickness direction by a power-law distribution. Based on the co-rotational approach, a finite element formulation is derived and employed in the study. An incremental/iterative procedure in combination with the arc-length control method is used in computing the large displacement response of the beams. They presented numerical results which showed that the derived formulation is capable to give accurate results by using just several elements. A parametric study is given to highlight the influence of the material inhomogeneity, taper ratio and taper type on the large

displacement behavior of the beams. They also investigated and highlighted large displacement behavior of beams composed of different constituent materials.

Batista (2015) reported solution for the equilibrium configuration of an elastic beam subject to three-point bending in terms of Jacobi elliptical functions. General equations are derived, and the domain of the solution is established. Several examples that illustrate a use of the solution are discussed. The obtained numerical results are compared with the results of other researchers. In this work, they have also derived an approximation formula by which the beam load is given as a polynomial function of beam deflection. The range of applicability of the approximation is illustrated by numerical examples.

Li and Lee (2015) analyzed bending of a simply supported beam with emphasis on the effect of the horizontal reaction force which is generally neglected for small deflection analysis. Based on Timoshenko's kinematic relation, a governing equation is derived. Three typical cases including uniformly distributed loading, three-point bending and four-point bending are analyzed. Expressions for the deflection and the cross-section rotation are obtained and a non-linear load–deflection relation is derived. They have shown that the results available for Euler– Bernoulli and Timoshenko beams are recovered from the proposed formulation when the horizontal force is neglected. They also discussed the influences of shear deformation and loading position on the transverse deflection and graphically presented the deflection and load–maximum displacement curve. A comparison of the deflections with and without the horizontal reaction force and with experimental data is made. Obtained results are useful in safety design of linear and non-linear beams under complicated loading.

2.1.2 Stress analysis

Stress analysis is a primary task for mechanical engineers involved in the design of structures of all sizes and shapes. In case of structural failures stress analysis is also used to investigate the causes of such failures. Typically, the input data for stress analysis are a geometrical description of the structure, the properties of the materials used for its parts, how the parts are joined, and the maximum or typical forces that are expected to be applied to each point of the structure. In addition, when geometric discontinuity, like central drill hole of master leaf spring, is present in a loaded mechanical part, stress concentration occurs. In

effect, stress increases above the nominal level calculated by conventional mechanics of materials in the vicinity of the discontinuity. This stress concentration effect aggravates failure of such mechanical parts under load.

Fraternali and Bilotti (1997) presented a one-dimensional theory and a finite element model for the stress analysis of laminated curved beams. In this analysis, they have considered moderately large rotations, moderately large shear strains and a different elastic behaviour of the material in tension and in compression. Approximate inter-laminar stress field is obtained by using a penalty technique to enforce the perfect bonding condition between the adjacent laminae of the beam. Finally they have presented some numerical results to show the potential of the proposed finite element model.

Ahmed et al. (2014) investigated development of stresses in a simply supported composite beam with stiffened lateral ends using displacement-potential field. Firstly, they have pointed out that the present problem is a mixed-boundary-value elastic problem and then determined the potential field of the problem by solving a single fourth-order partial differential equation of equilibrium. Stress components are derived in terms of the potential function using Fourier series. In this work, they have considered two different types of stiffeners at the opposing lateral ends of the beam, where the fibres are directed along the beam axis. They have also investigated the effect of beam aspect ratio on the state of stresses at different critical sections of beam. Comparison of the present method with the corresponding solutions of classical beam theory and standard computational method is also presented in this paper.

Amon et al. (1971) considered problem of reducing the stress concentration at a hole in an infinite sheet by reinforcement. They analyzed the problem by describing the sheet according to plane stress elasticity theory and the reinforcement as a beam. Finally they have shown that for a typical reinforcement, the maximum stress can be reduced from 3S to 0.6S, where S is the one-dimensional uniform tension applied to the sheet.

Troyani et al. (2004) studied effect of stress concentration due to presence of U-shaped notches in short flat bars subjected to in-plane bending. In this study, they have considered the effect of length as a significant parameter which is generally neglected in analysis of stress concentration. They have defined a threshold value as transition length and

demonstrated that below this threshold value, magnitude of stress concentration factors are significantly larger than the values calculated through traditional methods. Theoretical stress concentration factors for a wide range of notch radii are calculated using finite element method and presented graphically. The corresponding values of transition lengths are calculated and presented in this paper.

Batista (2011) presented an analytical study on stress concentration around a hole in an infinite plate subjected to uniform load at infinity. Firstly he has presented Muskhelishvili's method in detail and proposed a modified Muskhelishvili's method to calculate stress concentration factors around holes of relatively complex shapes. Finally, he demonstrated applicability of the proposed method through several examples of stress distribution around polygonal holes of a complex geometry utilizing the Schwartz–Chistoffel mapping function.

Mohammadi et al. (2011) presented an analytical calculation for stress concentration factor around a circular hole present in an infinite plate made of inhomogeneous material subjected to uniform biaxial tension and pure shear loading. In this analysis, they have considered radial variations of Young's modulus and Poisson's ratio of the plate material. Governing differential equation of stress concentration factor for biaxial tension is derived and solved. Stress concentration factor for pure shear is calculated by using a Frobenius series solution. Finally, they have analyzed the effect of non-homogeneous stiffness and varying Poisson's ratio on the stress concentration factors.

Nagpal et al. (2011) presented an overview of various techniques developed for analysis and mitigation of stress concentration factor due to presence of discontinuity in flat plate. Determination of stress concentration factor around different discontinuities in a rectangular plate made up of different materials under different loading conditions includes several methods of analysis and they are analytical, numerical and experimental. They have compared several methods and pointed out that a single method can not be suggested for every situation. In this review, they have considered singularities of circular and elliptical holes in rectangular plate.

Castagnetti and Dragoni (2013) investigated Neuber's criterion to study stress concentration in elastic solids due to presence of periodic notches under different loading

conditions. They observed from a critical review that Neuber's method is very accurate for the ideal configuration of a sharp and shallow notch under shear stresses, but the accuracy is very poor for real notches with a large root radius, in particular for normal stresses. In this work, they have proposed two modified expressions for the depth reduction factor and distinguishing between notches under shear or normal stresses. This modification provides very accurate results, and becomes quite useful for real geometries.

2.1.3 Combined deflection and stress analysis

The results of static analysis of a structure are typically a quantitative description of the stress over all those parts and the deformation caused by those stresses. Generally stress and deflection analysis is performed together for designing a structure. The following paragraphs present literatures on combined stress and deflection analysis of leaf springs under different loading conditions.

Rajendran and Vijayarangan (2001) presented optimal design of a composite leaf spring. The design variables (thickness and width of leaf) are optimized using a non-traditional optimization technique called Genetic Algorithm (GA). Main objective of this paper was to reduce the weight of leaf spring which affects vibrational characteristics of vehicle including comfort, directional stability etc. In this work, a reduction of 75.6% weight is achieved when a seven-leaf steel spring is replaced with a mono-leaf composite spring under identical conditions of design parameters and optimization.

Shokrieh and Rezaei (2003) presented design optimization of composite leaf spring using finite element method. Firstly, they analyzed development of stresses and deflections in a steel leaf spring using finite element package ANSYS and verified the results with the existing analytical and experimental solutions. Then, a composite leaf spring made from fiberglass with epoxy resin is designed using these results. In this design, they have considered stresses (Tsai–Wu failure criterion) and displacements as design constraints. The results showed that an optimum spring width decreases hyperbolically and the thickness increases linearly from the spring eyes towards the axle seat. They have concluded with the observation that the optimized composite spring has much lower stresses, higher natural frequency and nearly 80% lower weight without eye units compared to the steel spring.

Rahman et al. (2007) presented design and nonlinear analysis of a parabolic leaf spring. Governing differential equations of the problem are derived and solved numerically to calculate stress and deflection developed in the beam. The numerical analysis demonstrated effects of end shortening geometric nonlinearity on the response of the beam. In this work, they have shown that the actual bending stress calculated by nonlinear theory is 2.30-3.39% less than the values calculated by traditional theories. In addition, the maximum stress occurs at a region far away from the fixed end of the deigned leaf spring. Comparison of the present numerical scheme with results of other researchers is also presented in this paper and they are in good agreement.

Almeida et al. (2011) presented a geometric nonlinear analysis of functionally graded beams using Total Lagrangian approach. In the formulation of the problem, they have incorporated the effect of material gradation considering the beam element effective cross-section rigidities associated to axial, shear and flexural deformation kinematics. Finally, they illustrated the main features of the formulation through two examples and compared stress and deflection behaviors of such functionally graded beams with beams of homogeneous material.

Raghavedra et al. (2012) performed a comparative study between laminated composite leaf spring and steel leaf spring with respect to weight, stiffness and strength. In the present work, they have considered the dimensions of an existing mono steel leaf spring of a Maruti 800 passenger vehicle for modeling. Stress and deflection behaviors of leaf springs made of three different composite materials namely, E-glass/Epoxy, S-glass/Epoxy and Carbon/Epoxy are studied. Stresses and deflections are considered as design constraints in this study. Finally they have furnished results which showed that the laminated composite leaf spring is lighter and more economical than the conventional steel spring with similar design specifications.

Kumar and Teja (2012) analyzed design of a composite leaf spring with the objective of minimizing weight of leaf spring. Firstly, they discussed advantages of composite structures over metallic structures with respect to specific stiffness and strength. The leaf spring is modeled in Pro/E and stress and deflection analysis is done using ANSYS Metaphysics software. Finally, they have presented results which showed that composite leaf spring has superior strength and stiffness and lesser in weight compared to steel.

Cannarozzi and Molari (2013) proposed a stress based formulation for non-linear deflection analysis of curved, extensible, shear flexible, elastic beams. The formulation is based on variational principle which serves as the basis for a finite element analysis. The displacements are derived from the stresses by means of integration. Several numerical examples are presented to illustrate the effectiveness of the approach. This approach also leads to high accuracy of stress and displacement results due to the choice of stresses as primary variables.

Ghodake and Patil (2013) presented stress and deflection analysis of leaf springs made of glass fibre reinforced polymer and steel, using finite element method. The dimensions of an existing conventional steel leaf spring of a light commercial vehicle are taken for evaluation of results. Comparison of stress, deflection and strain energy results between the composite and steel leaf springs are presented in this paper. A reduction in the weight of composite leaf spring is obtained up to 85% compared with steel. In 2013, Pozhilarasu and Pillai also presented a comparative study on the performance of composite (Glass Fibre Reinforced plastic - GFRP) and conventional leaf springs using finite element package ANSYS. In this work, they have fabricated an Eglass/Epoxy composite leaf spring using hand layup method. The composite and steel leaf springs are tested using universal testing machine and the results are compared.

Roy and Saha (2013) applied a geometry updation technique by using variational method to find out deflection profiles of non-uniform beams under various loading conditions. Besides the free end displacement, the variation of stress, strain and the bending moment of the beam having variable material properties with the beam length are obtained by the technique of minimization of total potential energy. The mathematical formulation is based on a variational principle using Galerkin's assumed mode method. The displacement functions are approximated by linear combination of sets of orthogonal coordinate functions, developed through Gram-Schmidt scheme and substituted in the governing equilibrium equation. The final solution of the large displacement geometric nonlinear problem is obtained iteratively with the help of MATLAB computational simulation. They pointed out that the free end displacements and the shortening of projected beam length are greatly affected by the variation in elasticity modulus value. Finally they compared the results with existing results and furnished some new results. They have also shown the influence of

material gradation for various types of exponential and parabolic distribution for three different types of loading.

Parkhe et al. (2014) presented stress and deflection analysis of Carbon fiber epoxy based leaf spring under static load condition by using FEA. In this analysis, the composite mono leaf spring is modeled by considering varying cross-section, with unidirectional fiber orientation angle for each lamina of a laminate. Static analysis of a 3-D model has been performed using ANSYS 12.0. Weight reduction of 22.5% is achieved compared to mono steel leaf spring. In 2014, Rajagopal et al. also reported a comparative study between composite and steel leaf spring with respect to stress and deflection.

2.2 Review on methods of theoretical analysis

Theoretical research works on stress and deflection analysis of beams include different techniques for formulation and solution of such bending problems. These theories exist in individual or in mixed mode and they include analytical, semi analytical, numerical and finite element methods.

2.2.1 Analytical method

Analytical solution to static problems of structures is possible when the analysis is limited to the consideration of linear theory of elasticity. But in case of geometric nonlinear analysis, simple analytical solution is not possible due to the presence of nonlinear terms in governing equations. When non-uniform geometry and geometric discontinuity in a mechanical part are considered, the problems become much more complex. However, analytical solutions to static problems of structures like beams, leaf springs, plates, etc. are proposed by many researchers and they are presented in the following paragraphs.

The first analytical work to deal with the large deflection analysis of beam was that of Bisshopp and Drucker (1945) who proposed elliptic integral approach to solve such geometric nonlinear problem. Osipenko et al. (2003) analyzed leaf spring bending problem by modeling it as a stack of slim curved cantilever beams and constructed analytical solution of the bending problem. Mohyeddin and Fereidoon (2014) considered the effect of shear deformation in large deflection analysis of a straight prismatic beam and proposed closed-form solution based on Timoshenko beam theory. Ahmed et al. (2014) presented elasticity

solution of an initially straight beam and proposed an analytical scheme based on the displacement-potential field. In 2015, Batista proposed solution of large deflection problem of a simply supported beam under three point bending loads in terms of Jacobi elliptic functions. Li and Lee (2015) considered the effect of horizontal reaction force in bending problems of simply supported beams under different types of loading.

In 1971, Amon et al. analyzed the problem of a reinforced hole in a sheet by using plane stress elasticity theory. Later on, many researchers have analyzed effect of stress concentration in the vicinity of geometric discontinuity in a loaded structure. Batista (2011) proposed analytical method based on modified Muskhelishvili's method to calculate stress concentration factors around holes in infinite plates. Whereas, Mohammadi et al. (2011) considered radial variations of Young's modulus and Poisson's ratio of the plate material in this regards. Castagnetti and Dragoni (2013) reviewed Neuber's criterion and proposed two modified expressions in connection with stress concentration in elastic solids due to presence of periodic notches under different loading conditions.

2.2.2 Semi analytical method

Geometric nonlinear analysis of structures like beams, leaf springs, etc. results nonlinear system governing equations. In order to solve such nonlinear problems, several researchers have proposed methods where governing equations of the problems are derived based on classical mechanics and then numerical methods are used for solution purpose. Approaches based on variational principle, stationarity of the energy functional, Lagrangian formulations, etc. have also been reported in literature for solution of such nonlinear structural problems. These approaches are known as semi analytical methods and literatures available related to these methods for static analyses of beams are presented in the following paragraph.

Wang (1969) used finite difference method with Newton-Rhapson iteration technique to investigate load-deflection behavior of uniform beams under distributed load. Wang et al. (1997) presented a comparative study between elliptic integral approach and shooting-optimization technique for large deflection analysis of beams. In their elliptic integral approach, the elliptic integrals are evaluated using iterative technique, without using elliptic functions. Later on, Beléndez et al. (2002) used Mathematica computational platform to solve

elliptic integrals, encountered in large deflection analysis of cantilever beam under concentrated load. Kumar et al. (2004) proposed search strategy based on the stationarity of the energy functional in the equilibrium state for large deflection analysis of initially straight beam. Dado and Al-Sadder (2005) considered very large deflection of a non-prismatic beam under complex load and proposed an approach based on approximation of the angle of rotation of the beam by a polynomial function to solve such beam bending problem. Banerjee et al. (2008) proposed Adomain decomposition method to determine large deflection of beam under arbitrary loading condition. Tolou and Herder (2009) also used Adomain decomposition method to analyze large deflection behavior of members of compliant mechanism. Chen (2010) proposed an integral approach for large deflection study of beam with complex load and varying beam properties. Almeida et al. (2011) presented finite element formulations for large deflection analysis of beams based on total Lagrangian formulation. He et al. (2013) proposed perturbation method based on two small parameters to solve nonlinear large deflection problem of beams with gradient under two different boundary conditions. In this year, approximate analytical solutions employing the recently developed automatic Taylor expansion technique (ATET) to solve large deflection problem was proposed by Tari (2013). Cannarozzi and Molari (2013) presented solution of large deflection problems of beams based on principle of total potential energy. Roy and Saha (2013) proposed a geometry updating technique by using variational method to find out deflection profiles of non-uniform beams under various loading conditions.

2.2.3 Numerical method

As mentioned earlier, closed form solutions to static problems of structures like beams, leaf springs, etc. are few due to the presence of nonlinearity in system governing equations. If non-prismatic and curved beams are considered, the complexity of the problems becomes much greater. In such situation numerical scheme is the only approach available. Widely used numerical approaches in structural analysis include numerical integration techniques based on iterative shooting technique, finite difference method with Newton-Raphson iterative technique, etc. Numerical approaches available in literature for static analysis of beams and leaf springs are presented in the following paragraph.

In 1968, Wang proposed a simple numerical scheme for analyzing nonlinear bending problem of initially straight beams where numerical integrations were carried out by

Simpson's rule. In a paper, Rajendran and Vijayarangan (2001) studied deflection behavior of leaf spring and presented solution technique using genetic algorithms (GA). Later on, Rahman et al. (2007) studied deflections and stresses developed in leaf springs under concentrated loads numerically. Eren (2008) considered both material and geometrical non-linearity in large deflection analysis of beams and proposed an approach based on Runge-Kutta method to obtain its load-deflection characteristics. Large deflection behavior of beams under follower type loading was solved numerically by Shvartsman (2007), Mutyalarao et al. (2010a) and Mutyalarao et al. (2010b). Nallathambi et al. (2010) addressed effect of initial curvature of initially curved beams under follower force and applied fourth order Runge-Kutta method along one parameter reverse shooting method to solve the problem. In a later work, Shvartsman (2013) solved the same problem by using direct numerical method. Sitar et al. (2014) numerically studied large deflection behavior of beams of material with different stress–strain relations in tension and compression domain.

2.2.4 Finite element method

As it is well-known, a system of differential equations can be used to model a physical phenomenon. So, in order to describe relations among the involved quantities of interest, a solution of the differential equation has to be found out. However, governing differential equations of structures for large deflection analyses are nonlinear and for solving such nonlinear equations, a technique has been successfully used where the whole domain of the structure is divided into finite elements of arbitrary shape.

Fraternali and Bilotti (1997) and Pai et al. (2000) presented finite element formulation based on total Lagrangian approach to study large deflection behavior of beams. Sugiyama et al. (2006) developed a nonlinear finite element formulation based on floating frame of reference for nonlinear elasticity analysis of leaf springs. In a paper, Troyani et al. (2004) addressed the effect of length of plates with opposite U-shaped notches subjected to in-plane bending in theoretical stress concentration factors using finite element method. Solutions of geometric nonlinear problems of leaf springs and beams through several commercial finite element packages like ANSYS, ABAQUS, MSC/NASTRAN and NACS etc. have been reported by several researchers in literature. Many papers, for example, papers by Shokrieh and Rezaei (2003), Shankar and Vijayarangan (2006), Hou et al. (2007), Charde and Bhope (2012), Kumar and Teja (2012), Raghavedra et al. (2012), Ghodake and Patil (2013), Parkhe

et al. (2014), Aşık et al. (2014), Ahuett-Garza et al. (2014) presented development of stresses and deflection behavior of leaf springs and beams under different loading conditions by commercial finite element packages.

2.3 Review on types of loading

Development of stresses and deflections in structures like leaf spring, beam, etc. highly depends on the nature of problem parameters. One most important parameter of such a structural problem is type of loading to which the member is subjected. Mechanical loads applied to beams can be divided into two major categories and they are follower type and non-follower type loads. When the angle of inclination of applied load remains fixed with respect to the deformed axis of beam then the applied load is called follower type load. Otherwise the loading condition is referred to as non-follower type loading. Generally non-follower type loading include two types of loads and they are concentrated and distributed loads. On the other hand, follower type loading is mostly concentrated type. The following two sub-sections briefly describe the literatures available related to static analysis of beams and leaf springs under concentrated and distributed loading conditions respectively.

2.3.1 Concentrated load

Large deflection behavior of initially straight beams under concentrated follower type load has been studied numerically by Shvartsman (2007) and Mutyalarao et al. (2010a, 2010b). Whereas, papers by Nallathambi et al. (2010) and Shvartsman (2013) addressed effect of initial curvature of curved beams in deflection behavior under concentrated follower type loading condition.

Large deflection behavior of beams under non-follower type concentrated load was first addressed by Bisshopp and Drucker (1945). Later on, development of stresses and deflections in beams under concentrated loads have been reported by Wang (1968), Wang et al. (1997), Fraternali and Bilotti (1997), Pai et al. (2000), Beléndez et al. (2002), Kumar et al. (2004), Dado and Al-Sadder (2005), Banerjee et al. (2008), Tolou and Herder (2009), Chen (2010), Almeida et al. (2011), Cannarozzi and Molari (2013), Mohyeddin and Fereidoon (2014), Nguyen (2014), Aşık et al. (2014), Ahuett-Garza et al. (2014) and Batista (2015). Static analyses of leaf springs and crane hooks under concentrated loads have also been presented in several research papers (Rajendran and Vijayarangan (2001), Shokrieh and

Rezaei (2003), Shankar and Vijayarangan (2006), Sugiyama et al. (2006), Rahman et al. (2007), Hou et al. (2007), Rashmi (2011), Raghavedra et al. (2012), Charde and Bhope (2012), Kumar and Teja (2012), Roy and Saha (2013) and Parkhe et al. (2014)).

2.3.2 Distributed load

In a paper, Wang (1969) studied large deflection behavior of beams under uniformly distributed loads. Later on, stresses and deflections characteristics of beams under uniformly distributed loads have been addressed by several researchers (Osipenko et al. (2003), He et al. (2013), Cannarozzi and Molari (2013), Ghodake and Patil (2013), Roy and Saha (2013) and Ahmed et al. (2014)). Dado and Al-Sadder (2005) considered non-uniform distribution of loads as well. Chen (2010) pointed out that due to geometric nonlinearity in large deflection analysis, the intensity of the distributed load is not constant along the undeformed axis of the beam. Rather, the load intensity is constant along the axis of the deformed beam. In such cases the loading condition is assumed as non-uniformly distributed over the projected length of the beam.

In 2008, Eren studied deflection behavior of beams under combined action of concentrated and uniformly distributed load. Later on many papers, for examples, papers by Chen (2010), Roy and Saha (2013), Tari (2013), Sitar et al. (2014) and Li and Lee (2015) presented development of stresses and deflections in beams under combined loads.

2.4 Review on types of boundary condition

Boundary conditions are defined as the set of conditions specified for the solution of governing differential equation of a physical system at the boundary of its domain. Deflection characteristics and stress field developed in beam like structures under different loading conditions depend on their boundary conditions. Stress and deformation analysis of leaf spring is generally carried out through two classical beam models and they are fixed-free i.e., cantilever model (Osipenko et al. (2003), Roy and Saha (2013), Shokrieh and Rezaei (2003), Rahman et al. (2007)) and three point bending model (Sugiyama et al. (2006), Kumar and Teja (2012), Raghavedra et al. (2012), Ghodake and Patil (2013), Parkhe et al. (2014)). Many other non-conventional boundary conditions are also considered by several researchers. Literature related to fixed-free, simply supported-simply supported and non-conventional

boundary conditions, in connection with beam bending, are described in the following three sub-sections respectively.

2.4.1 Fixed-free

In 1945, Bisshopp and Drucker analyzed large deflection behavior of beam whose one end is fixed and other end is free i.e., cantilever beam under tip concentrated load. Later on, many research papers, for example papers by Wang (1968), Beléndez et al. (2002), Kumar et al. (2004), Banerjee et al. (2008), Eren (2008), Mutyalarao et al. (2010a), Mutyalarao et al. (2010b), Nallathambi et al. (2010), Tari (2013), Shvartsman (2013), Sitar et al. (2014) reported non-linear static analysis of cantilever beams. Papers by Dado and Al-Sadder (2005), Chen (2010) and Nguyen (2014) considered geometry variation along the length of cantilever beam in large deflection. Tolou and Herder (2009) reported geometric non-linear analysis of members of compliant mechanism. In this study, an element is considered and modeled as a cantilever beam under vertical end point load. They concluded with the future scope that this cantilever model can further be used as a building block in more complex compliant mechanisms. Almeida et al. (2011) analyzed stresses and deflection characteristics of functionally graded beams and furnished two examples of cantilever beams under different type of loading. Cannarozzi and Molari (2013) have shown performance of their proposed approach for non-linear analysis of planar beams through cantilever beam examples.

2.4.2 Simply supported-simply supported

After successful comparison of results for cantilever beam with exact ones, Wang (1968) applied the proposed numerical method to solve bending problem of a simply supported beam under concentrated load. In the next year, Wang extended his work to address large deflection behavior under distributed load. Later on, Fraternali and Bilotti (1997) analyzed development of stresses in laminated curved beams incorporating the effects of large rotation and different behavior of material under tension and compression. In this paper, they have shown the effectiveness of the proposed method through solution of bending problem of an initially straight simply supported beam under concentrated load. Mohyeddin and Fereidoon (2014) considered transverse shear deformation in large deflection analysis of straight simply supported isotropic beam under three point bending. In this analysis, they have pointed out that the reaction forces at supports are not quite vertical, but normal to the beam midline in the absence of frictional forces in large deflection. Batista (2015) analyzed

deflection behavior of beam under three point bending considering both smooth and rough supports. In this study, he has also presented a detail discussion on the effect of the radius of supports. Li and Lee (2015) addressed effect of horizontal reaction force in large deflection analysis of simply supported beam. They pointed out that contact locations between the beam and the supports are somewhat shifted from the original position to attain equilibrium and for smooth simple supports the reaction forces at two ends are normal to the deformed beam.

2.4.3 Non-conventional

Wang et al. (1997) analyzed large deflection characteristics of beam whose one end is hinged and elastically restrained against rotation and the other end is free to move over a frictionless support. Later on, Shvartsman (2007) presented large deflection analysis of beam whose one end is spring hinged and the other end is free and subjected to a concentrated load. In a paper, Cannarozzi and Molari (2013) reported nonlinear analysis of hinged clamped circular arch and shallow hinged arch. In the same year, He et al. presented large deflection analysis of beam with gradient with one end fixed and other end simply supported. Ahmed et al. (2014) presented analysis of stress field in a simply supported composite beam with stiffened lateral ends. In this analysis, two types of stiffeners, namely the axial and lateral stiffeners are considered for the opposing lateral ends of the beam for which the fibers are assumed to be directed along the beam axis.

2.5 Literature on experimental work

Several researchers have used many techniques for stress and deflection analysis of structure like leaf springs and beams under different loading conditions. Experimental works are further classified in two categories on the basis of their goal and they are pure experimental and combined experimental and theoretical. It is observed that combined experimental and theoretical research works on stress and deflection analysis of leaf spring, beam, etc., are available in literature but on the other hand pure experimental works are few.

2.5.1 Pure experimental work

Pure experimental works are performed with the goal of recreating the conditions of actual working environment of a structural component in order to predict its behavior under

such conditions. The following paragraphs briefly describe various literatures related to pure experimental works on stress and deflection analysis of structures.

Ryan and Fischer (1938) carried out experiment using photo-elastic technique to study stress concentration effect due to presence of holes in beams under pure bending. The experimental results are compared with theoretical and experimental results of other researchers. From this study they have proposed rules for design of rectangular beams with centrally located holes under pure bending.

Politch (1985) described three methods for strain measurement and compared with analytical method. These three methods are speckle shearing interferometry (SSI), electrical strain gages and mechanical deflectometers. These methods were applied on a simply supported uniformly loaded plate of composite material. Good agreement was obtained between the measured and the calculated results, at the points of measurement within the range of loading.

Shenhua et al. (1997) carried out experimental work on precision roll-forging of taper-leaf spring of vehicle and results have been used in the design of precision roll-forging process and the dies for the forming of taper-leaf springs. In this work, they determined equations to evaluate the width-extension and slip-forward values that affect the work piece quality and their correcting curves experimentally and proved that such equations are both practical and reliable. Satisfactory results were obtained when the equations were applied to the design of the roll-forging process and dies for forming different taper-leaf springs: there was no flash on the parts, the dimensional accuracy was high and the surface quality was excellent. Industrial applications have shown that the precision roll-forging technique for taper-leaf springs can increase the productivity, decrease production costs and investment in equipment, and meet the requirements for product quality and properties being especially economical and suitable for the production of massive taper-leaf springs.

Al-Qureshi (2001) presented a comparative study on performances of leaf springs made of steel and composite material. Firstly, a leaf spring of glass fiber reinforced plastic was designed and fabricated. Mechanical and geometrical properties of the fabricated leaf spring were similar to those of an existing multi-leaf steel leaf spring. These leaf springs were subjected to a series of laboratory static tests followed by a road test. In the experiment,

springs were mounted on a beam which was attached to the lower platen of a hydraulic testing machine. A specially designed punch was attached to the upper platen of the machine. This study demonstrated that composites can be used for leaf springs which meet the requirements together with substantial weight saving.

Mahdi and Hamouda (2013) presented an experimental investigation on mechanical behavior of hybrid and nonhybrid semi-elliptical springs made of composite material. In this work, compression, tension, torsion and cyclic tests are performed with three types of composites, namely, carbon/epoxy, glass/epoxy and glass/carbon/epoxy. Finally, the results of these tests are presented which showed that the fiber type and ellipticity ratio significantly influenced the spring stiffness. After 1.15 million fatigue cycles, composite semi-elliptical suspension spring's useful stroke is reduced by only 2% of its original height. The relaxation of the composite elliptic spring is very sensitive to the compression rate.

Motra et al. (2014) presented comparison between several strain measurement techniques and analyzed the uncertainty sources incorporated in them. In this work, the geometry of structural steel samples was analyzed by 3D scanner and vernier caliper. Strain values were determined by using three different techniques, namely strain gauge, extensometer and machine crosshead motion. These three techniques of strain measurement are compared in quantitative manner based on the mechanical properties of structural steel. Finally they have concluded with the observation that the extensometer and strain gauge provided reliable data, however the extensometer offers several advantages over the strain gauge and crosshead motion for testing structural steel in tension.

2.5.2 Combined experimental and theoretical work

Combined experimental and theoretical works are carried out with the goal of verifying or establishing the validity of a theoretical simulation study. In the following paragraphs a brief description of literatures available related to combined experimental and theoretical works on stress and deflection analysis of structures like leaf springs, beams, etc. are presented.

Ko (1985) performed a coupon tests to validate their theoretical study on the effect of hole size in stress concentration factor in composite plate. The specimens were tested in a

tensile test machine and load was increased until the specimens failed under uniaxial tension. One specimen without hole was also studied in similar manner to obtain the tensile strength of the material. Comparison is made between experimental and theoretical results of stress distributions around a hole present in a composite plate and presented graphically.

Pai et al. (2000) performed large bending and twisting tests on flexible straight and curved beams to validate their finite element model for large deformation analysis of beams. For the purpose of experimentation of such beams under different loading conditions, two special test fixtures are designed. Finally, they have compared the experimental results with theoretical ones and presented in the paper.

Beléndez et al. (2003) conducted experiment with a steel ruler of rectangular cross-section which was built-in at one end and loaded by a concentrated load at the free end to study load-deflection behavior of a cantilever beam under tip concentrated load. Deflection profile as well as tip deflection and end shortening of the beam are directly measured by using horizontal and vertical rulers.

Shankar and Vijayarangan (2006) conducted a test of steel leaf spring in a leaf spring test rig following standard procedures recommended by SAE to study development of stresses and deflections in it under concentrated load. In this test, the spring is loaded from zero to the prescribed maximum deflection by a concentrated load applied at the centre of the spring. Stresses and deflections of the spring centre are recorded in the load interval of 50 N.

Hou et al. (2007) conducted a static test of glass reinforced plastic (GRP) leaf spring with three different designs of eye-end attachment to obtain stress and deflection developed in the spring. Strain gauges were placed on the top and bottom surfaces of the leaf springs along the fibre direction. Deflection was measured at the centre of the suspension where the load was applied.

Mujika (2007) analyzed three point bending test taking into account shear and local deformation effects in the load application and supports. Indentation tests and three-point bending tests have been carried out on two composite specimens at five different spans. Load–deflection curves have been determined in three fixed strain ranges and a fixed load range. The best results have been obtained for the highest strain range, as local deformation

effects can be considered linear. Local deformation effects can have even more importance than shear effects in the case of small span to depth ratio.

Rashmi (2011) carried out experiment using the concept of photo elasticity to determine stress distribution in a loaded crane hook. A crane hook model made out of a birefringent material was selected for the study which has geometry similar to that of the crane hook. When a ray of light passes through a birefringent material, it experiences two refractive indices. This property of birefringent material is known as birefringence and the present experimental method is developed based on this property.

Charde and Bhope (2012) investigated evaluation of stresses in master leaf over the span using strain gauge technique. Firstly, they pointed out that the maximum stress induced in the master leaf is at support. But due to non-geometric linearity and large deflection behavior the stress may be occurred at any section over the span of leaf spring. They carried out stress analysis of half cantilever master leaf of leaf spring with and without extra full length leave. Four strain gauges were located on the master leaf to determine stresses over the span. Finally, experimental results are verified with the results of finite element method.

Aşık et al. (2014) carried out experiment for determination of stresses and deflections developed in curved glass beam under concentrated load. In this combined experimental and theoretical work, they have performed three point bending tests by applying a constant bending load of 500 N in radial direction only. Strain gauges are mounted on the curved beam and a portable strain indicator is used for strain measurement. In this connection, a computer aided screw-driven testing machine is used to maintain minimum of 2 mm/min loading rate until the load reaches the maximum value, 500 N. Finally, deflection and stress results are compared with theoretical results and presented in graphical forms.

Ahuett-Garza et al. (2014) presented a combined experimental and theoretical study on use of curved beams as large displacement hinges in planar compliant mechanisms. An aluminum model of the mechanism was built and its load-deflection behavior was studied by using a displacement sensor. The analytical and FEA models predicted values within 3% of each other, with a ratio of output to input deflection being about 1. Whereas, the experimental measurements reported the ratio of output to input displacement as 0.9. They have identified several factors which may be the reasons for the deviation. These factors include friction

force produced by the guide on the output pin of the mechanism which is generally neglected in theoretical analysis. In addition, the position of the center of each one of the hinges may not be exactly the same as a normal pinned joint would display.

Ozmen et al. (2015) developed testing and simulation method for the durability of leaf springs based on accelerated fatigue life testing. Load spectra were measured from different vehicles on rough road testing track which contain variable amplitude. Fatigue life of leaf spring is determined using this variable amplitude loading. Afterwards, accelerated spectra were generated for testing and used in newly built fatigue test bench. In this work, they have also performed finite element and multi body simulation calculations and processed load spectra with multichannel fatigue life calculation to generate a virtual test rig.

Chapter 3

ANALYSIS OF LEAF SPRING AS CANTILEVER BEAM

From the literature review, presented in the previous chapter, it is observed that leaf spring is generally analyzed and designed by modeling it as initially curved cantilever beam following large deflection theory. In spite of widespread studies available in this area, there seems to be lack of geometrical nonlinear study for beam which has some initial curvature. Moreover, there is a lack of experimental fidelity in the ensuing models. Most of the available experimental works measure deflection at some points only, whereas experimental measurement of complete displacement field throughout the domain is rare. The present chapter focuses on both experimentally and theoretically large deflection behavior of master leaf spring through cantilever model. Description of the experimental set-up is presented at the beginning of the chapter. Subsequently measurement technique of deflection filed and mathematical modeling of the physical system are reported. Effect of initial curvature of initially curved beam is considered in the present theoretical study. From comparison between experimental and theoretical deflection results, several aspects of cantilever modeling of leaf spring are identified. Further theoretical analysis is carried out to study deflection behavior of initially curved beam under distributed and combined loads.

3.1 Description of experimental set-up

Photograph and schematic diagram of the experimental set-up are shown in Fig. 3.1 (a) and Fig. 3.1 (b) respectively. Major sub-assemblies of the experimental set-up are hydraulic cylinder clamping arrangement (items 1-3), hydraulic cylinder support structure (item 4) and hydraulic power pack (item 9). Detail of the hydraulic cylinder components is shown in Fig. 3.2. A hexagonal cap (item 3) is attached to the head of the ram (item 2) by means of threaded fastening. A hydraulic circuit is formed between the hydraulic cylinder and the hydraulic power pack by using a hose which passes through control valve (item 10). This control valve enables controlling of fluid pressure in the hydraulic cylinder. Main components of hydraulic cylinder support structure are bottom plate and top plate. Details of components of hydraulic cylinder support structures together with its sub-assembled drawing are furnished in Fig. 3.3 (a-c). Main components of hydraulic cylinder support structure are bottom plate and top plate. Bottom plate is mounted on a concrete foundation (item 8) and

top plate is mounted above the bottom plate by using stud, lock nut and washer. The hydraulic cylinder is bolted over the top plate in such a way that the ram can move up and down through the central recess of the top plate. The experimental set-up, housed in Machine Elements laboratory is a general purpose set-up, which is used for clamping various types of structures.

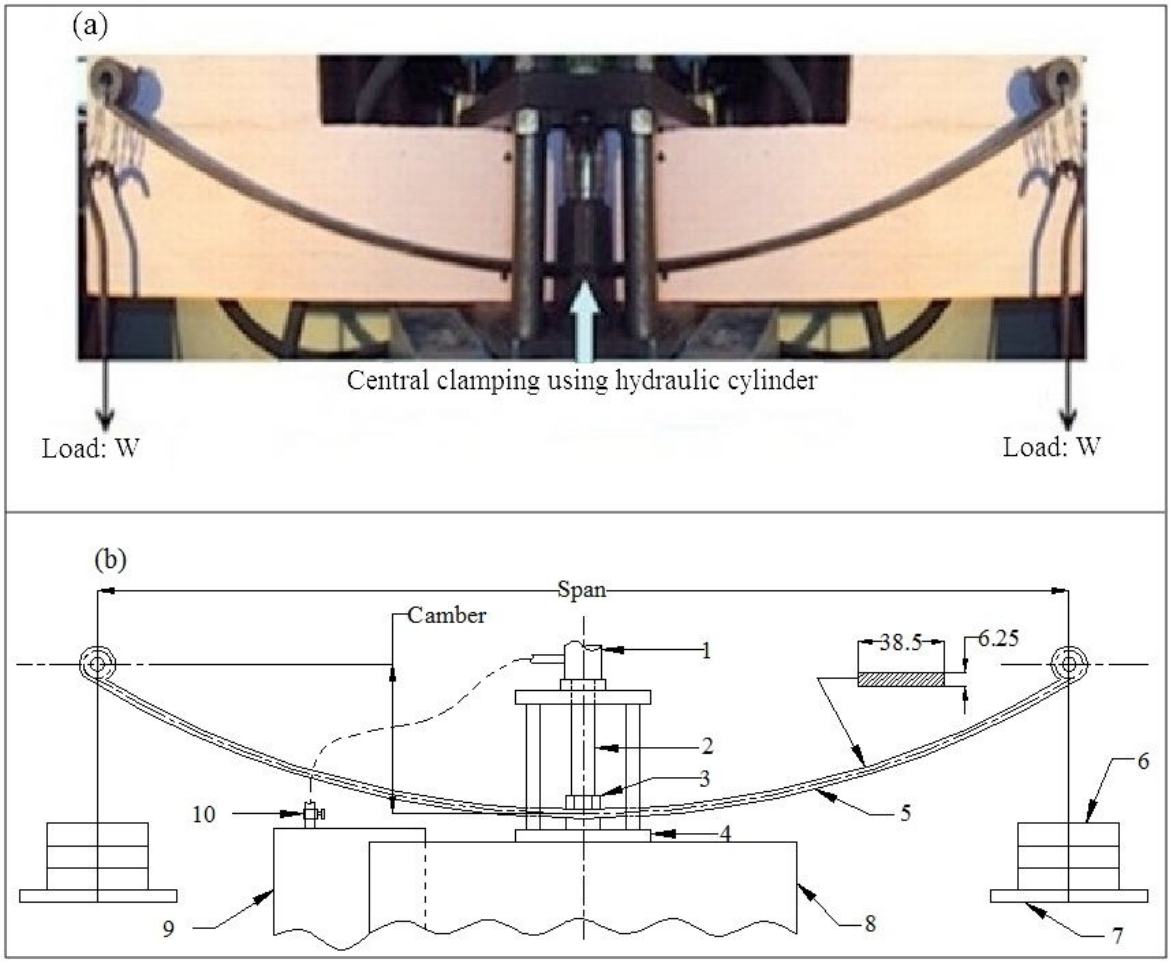

Item	Description
1	Hydraulic cylinder
2	Ram
3	Cap
4	Hydraulic cyl. support structure
5	Master leaf spring

Item	Description
6	Weight
7	Weight pan
8	Foundation
9	Hydraulic power pack
10	Control valve

Fig. 3.1 (a) Photograph and (b) schematic diagram of the experimental set-up.

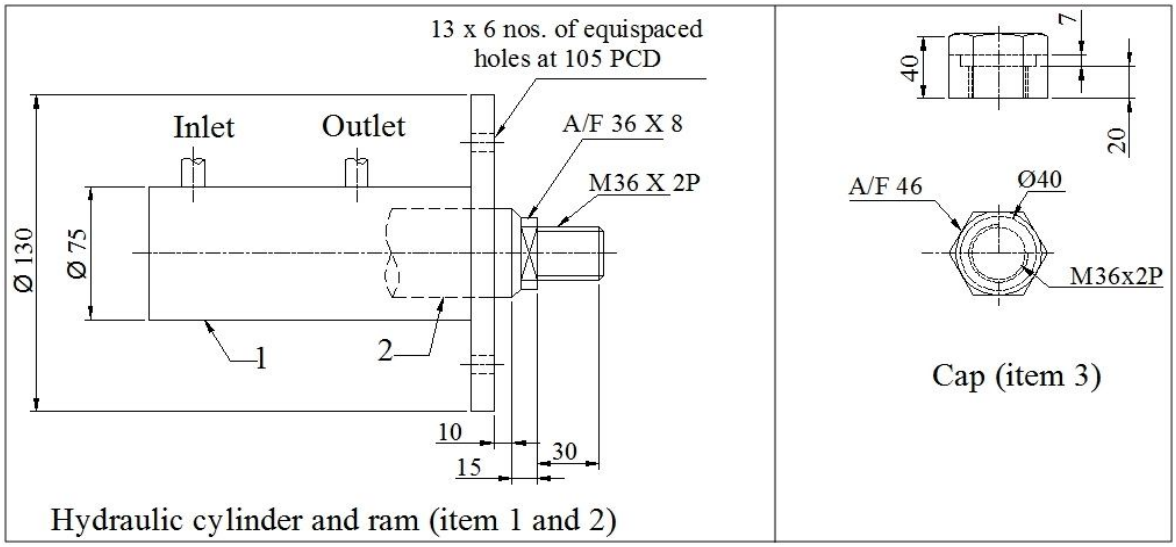

Fig. 3.2 Details of hydraulic cylinder (item 1) and ram (item 2) sub-assembly and the clamping cap (item 3).

To study load-deflection behavior of leaf spring, the master leaf (item 5) of an automobile leaf spring bundle, made from spring steel is procured and placed on the bottom plate of the hydraulic cylinder support structure. Width and thickness of its rectangular cross-section are 38.5 mm and 6.25 mm respectively. The span, camber and arc-length along periphery of the master leaf are measured in its free state and these measurements (in mm) are 866, 129 and 921.8 respectively. The master leaf spring is clamped centrally between the bottom plate and hexagonal head of the ram at a pressure of one ton. Two weight pans (item 7) are connected to the eye ends of the master leaf spring to apply load (item 6) on it. The engagement of ram of the hydraulic cylinder with master leaf spring divides it into two halves. Experimental observation is made in one half of the spring only, which is modeled as cantilever beam with initial curvature in the corresponding theoretical analysis.

3.2 Experimental procedure and observations

It is observed that clamping of the master leaf spring induces a change in its span. In addition, the clamping produces an initial deflection of the spring without application of external load in form of dead weight. Thereafter the spring is loaded symmetrically by placing equal weights on the weight pans at both ends. Central clamping divides the master leaf spring into two symmetric curved cantilever beams and limit load of such a beam is

calculated by using bending stress equation of Winkler-Bach curved beam theory, which is described in the following paragraph.

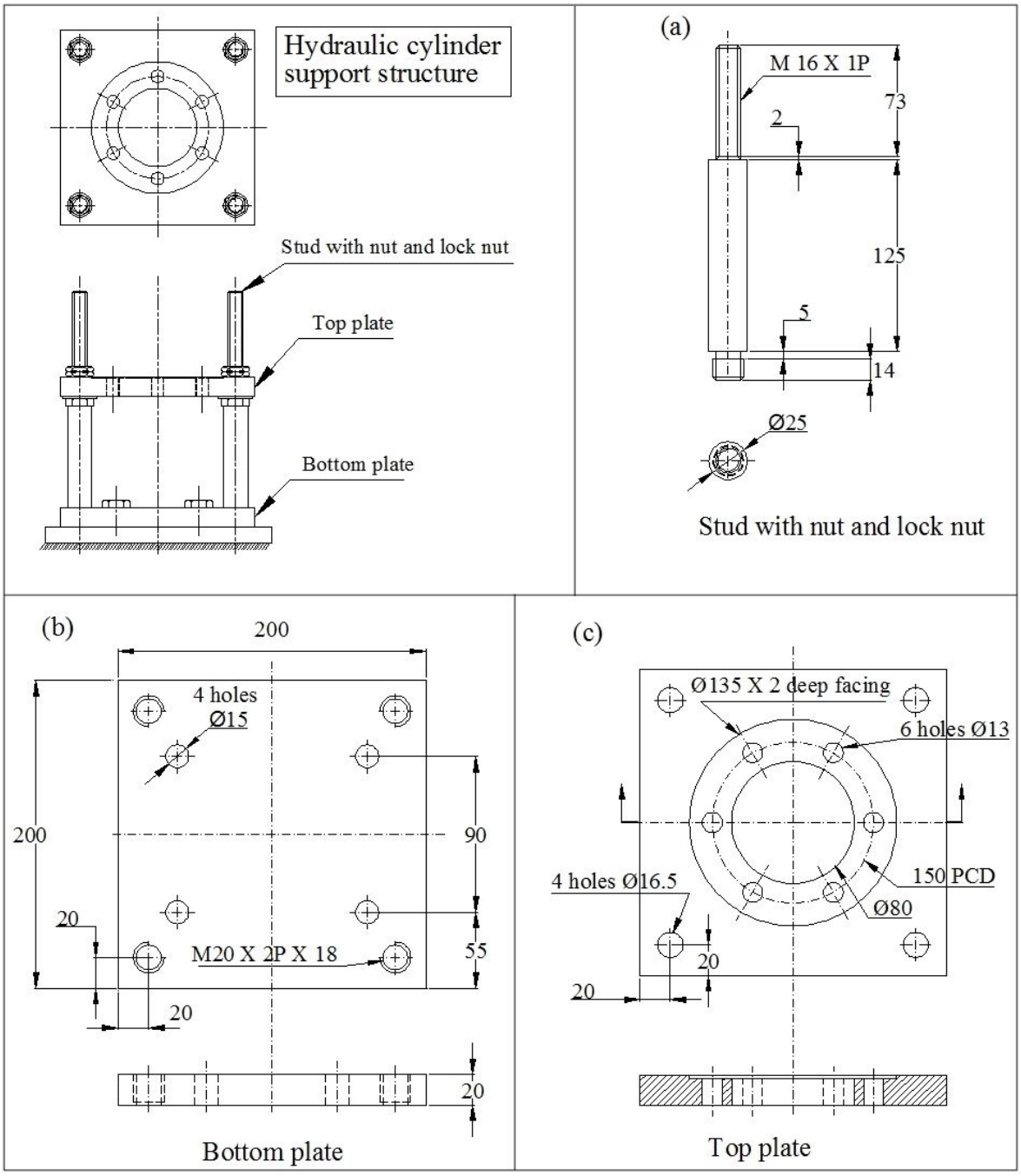

Fig. 3.3 Hydraulic cylinder support structure sub-assembly (item 4) and details of its components-(a) stud, (b) bottom plate and (c) top plate.

Winkler-Bach curved beam theory says that when a curved beam is subjected to pure bending M, the bending stress at any point on the layer with radius of curvature r is given by

$\sigma = \frac{M\,(r_n - r)}{A\,r\,(r_n - r_c)}$, where r_n is radius of curvature of the neutral surface, r_c is radius of curvature of the centroidal surface, A is cross-sectional area of the beam. Induced stress in each half of the master leaf will be maximum at the fixed end and at this location bending moment is given by $M = F\,l$, where F is the applied load and l is half-span of the leaf spring. Now calculation of the limit load only depends on calculations of r_c and r_n. Once profile $y = f(x)$ of left half of the master leaf in its free state is obtained following the procedure discussed in the following sub-sections, radius of curvature of the centroidal surface is calculated at fixed end (i.e., $x = 0$) by using the equation $r_c = \left\{[1 + \left(\frac{dy}{dx}\right)^2]^{3/2} \Big/ \frac{d^2y}{d\,x^2}\right\}\Big|_{x\,=\,0}$. As the cross-section of the master leaf is rectangular of width b and thickness h, radius of curvature of the neutral surface is given by $r_n = \frac{r_2 - r_1}{\ln(r_2/r_1)}$, where $r_1 = r_c - \frac{h}{2}$ and $r_2 = r_c + \frac{h}{2}$. Taking allowable stress as 75% yield stress value of the spring material (1500 MPa) the limit load is calculated and its magnitude is approximately 500 N.

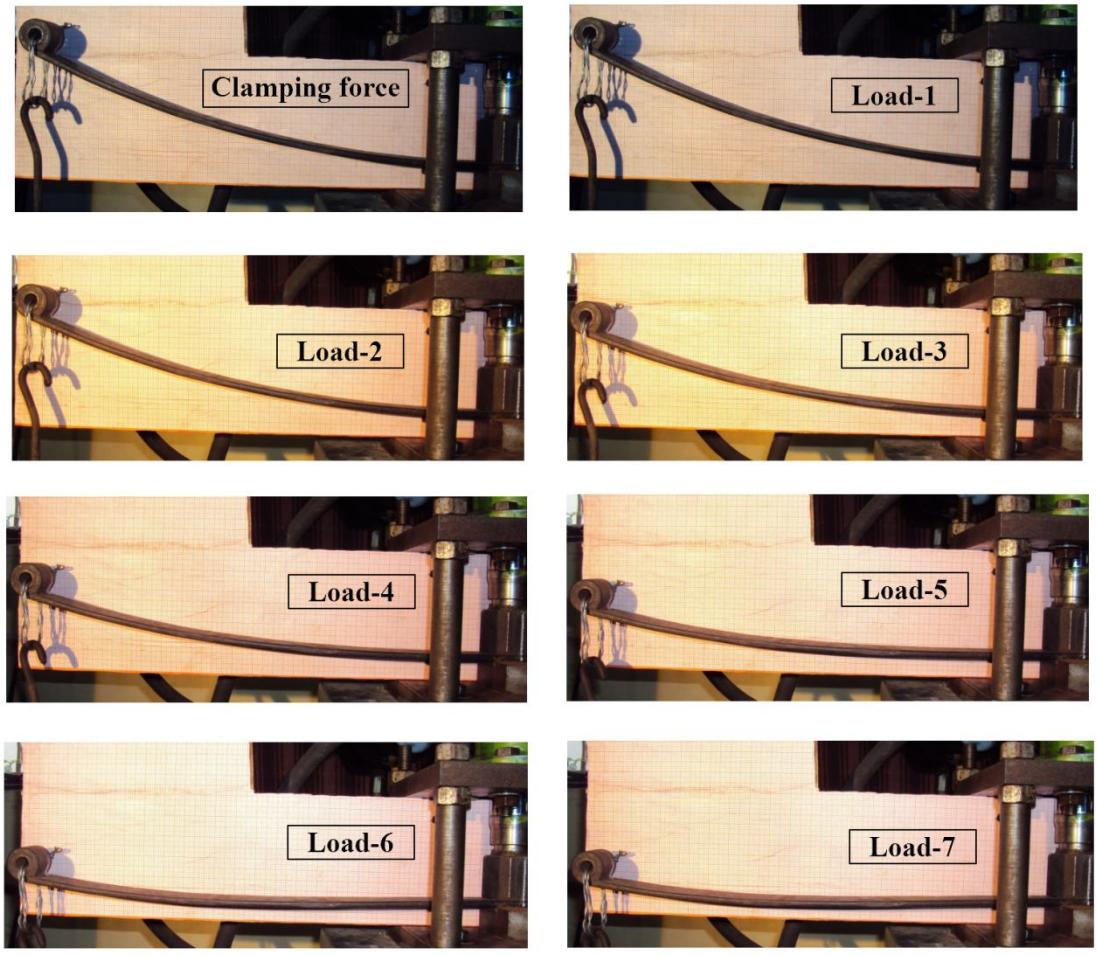

Fig. 3.4 Photographs of deflection profiles of the master leaf under different loading.

Experiment is performed at eight different load steps, where the first load step is designated as clamping force. The other seven load steps are designated as load – 1, 2, 3, 4, 5, 6 and 7 whose magnitudes (in N) are 62.784, 138.321, 211.896, 287.433, 361.989, 438.507 and 460.089 respectively. In each step of loading deflection profile is captured and recorded by using a digital camera (Make: Nikon India Pvt. Ltd., Model: COOLPIX L30, Resolution: 20 MP, Optical zoom: 5x, LCD screen: 7.5 cm). A graph paper is placed immediately behind the spring for the purpose of post processing of the photographs to obtain deflection profiles of the spring under each loading condition. The photographs of deflection profiles under the eight load steps are taken for the left side of the spring only and shown in Fig. 3.4. It is observed that under the maximum load beam has become almost horizontal.

Dynamic behavior of the master leaf spring under load is also observed during the present experimentation and for this purpose a shear mode piezoelectric accelerometer (Make: Kistler Instrument Corporation, Type: 8728A500, Acceleration range: ±500 g (g = 9.80665 m/s^2), Frequency range: 1 Hz–10 kHz (±5%)) is mounted on it using Petro-Wax adhesive. At each load step, the system is excited with the blow of a soft rubber hammer to obtain natural frequency of the master leaf spring under loaded condition. At clamped condition, natural frequency of the master leaf is observed by using a digital storage oscilloscope (Make: Tektronix Inc., Model: TDS 210, Peak detect bandwidth: 50 MHz, Lower frequency limit: 10 Hz). Due to low frequencies of the master leaf spring under the other seven load steps, the oscilloscope is unable to capture signal from the vibrating leaf spring. In these load steps, natural frequencies of the master leaf are obtained through post processing videos, taken during oscillations of the master leaf. Natural frequencies of left half of the master leaf under each load step are tabulated in Table 3.1.

Table 3.1 Natural frequencies of master leaf spring under different load steps

Load	Clamping force	Load-1	Load-2	Load-3	Load-4	Load-5	Load-6	Load-7
Natural frequency (Hz)	20	3.82	2.5	2.33	1.98	1.84	1.67	1.56

3.2.1 Deflection profile through image processing

As mentioned earlier, experimental observation is made only in left half of the master leaf spring. To obtain profile of left half of the master leaf spring in its free state, the master leaf is placed on a graph paper and profiles are drawn along its outer and inner edges. Centres of the left eye end and mounting drill hole are also located on the graph paper and then master leaf is removed. Now centre line of the master leaf is drawn between the outer and inner curvature lines. Thereafter, a perpendicular straight line is drawn on the centre line from the eye centre and this normal point on the centre line is considered as one end of master leaf profile. Other end of the master leaf profile is at the centre of the drill hole which is considered as origin of Cartesian coordinate system (x, y). Projected length of curvature line of left half of the master leaf profile is then divided into ten equal divisions and its profile is obtained as $y = f(x)$ by measuring coordinates of each division point. This profile is then exported in MATLAB® computational platform to calculate arc length of half of the master leaf in its free state, which is found to be 460.9 mm.

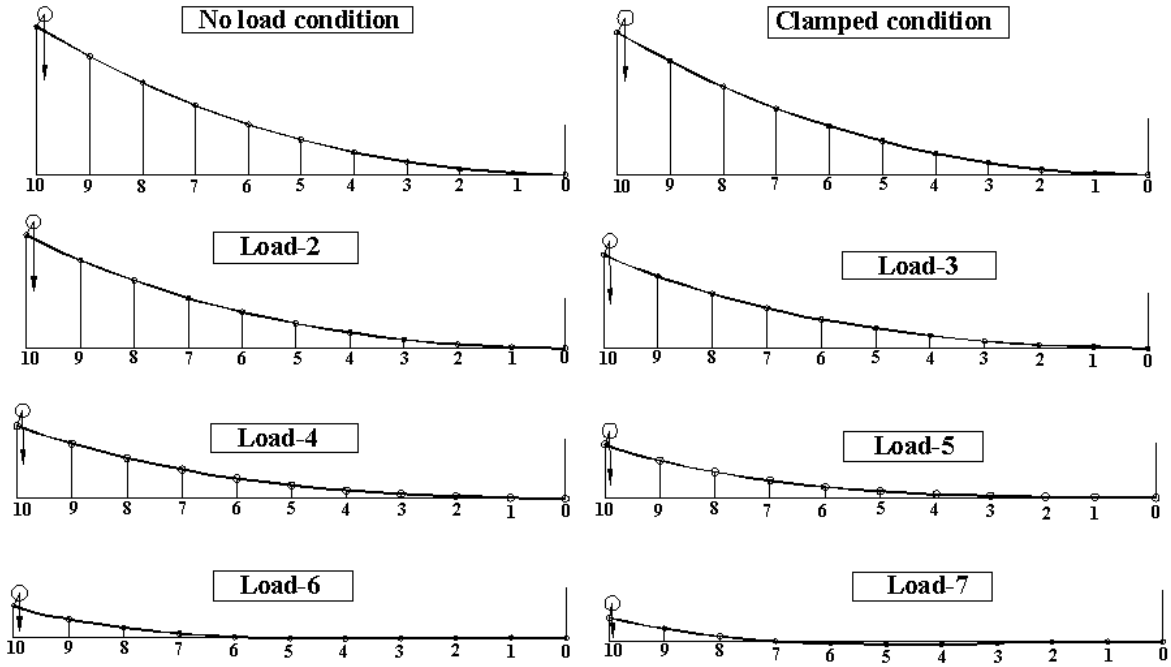

Fig. 3.5 Curvature lines of the master leaf under some applied loads.

On the other hand, deflection profiles of the master leaf in loaded conditions are obtained by post processing photographs. For this purpose, each photograph is taken as

background in the editor of a graph handling software (AutoCAD®) and a curvature line is drawn along the centre line of the loaded beam. The length of the curvature line is measured and the drawing is scaled to equate this length with the initial beam length. Now the projected length of this line is divided into equal ten divisions and (x, y) coordinates are measured at each of the division points. Curvature lines corresponding to each of the load steps excluding load-1 are presented in Fig. 3.5 and in addition, the profile of the spring in its free state is also appended to this figure. Deflection profiles of leaf spring corresponding to the eight loading conditions, as considered in Fig. 3.5, are tabulated in Table 3.2.

Table 3.2 The (x, y) coordinates of curvature line at various locations of the beam under different magnitude of loading

Location number	Load							
	No load	Clamp-ing	Load-2	Load-3	Load-4	Load-5	Load-6	Load-7
0	0.0, 0.0	0.0, 0.0	0.0, 0.0	0.0, 0.0	0.0, 0.0	0.0, 0.0	0.0, 0.0	0.0, 0.0
1	43.85, 1.6	44.01, 1.5	44.7, 1.1	45.13, 1	45.47, 0.8	45.68, 0.49	45.84, 0.16	45.94, 0.1
2	87.7, 4.7	88.02, 4.4	89.4, 4.31	90.26, 2.8	90.94, 2.2	91.36, 0.91	91.68, -0.06	91.88, -0.3
3	131.55, 10.5	132.03, 10.1	134.1, 8.27	135.39, 5.9	136.41, 3.9	137.04, 1.71	137.52, -0.18	137.82, -1.3
4	175.4, 18.8	176.04, 17.7	178.8, 13.84	180.52, 10.6	181.88, 6.6	182.72, 3.08	183.36, -0.47	183.76, -2.1
5	219.25, 29.2	220.05, 28.1	223.5, 21.16	225.65, 16.7	227.35, 11.0	228.40, 5.44	229.20, -0.24	229.7, -2.8
6	263.1, 41.8	264.06, 40.4	268.2, 30.89	270.78, 23.9	272.82, 16.7	274.08, 9.01	275.04, 0.89	275.64, -1.3
7	306.95, 57.5	308.07, 55.1	312.9, 41.12	315.91, 33.5	318.29, 24.2	319.76, 14.10	320.88, 3.86	321.58, 0.4
8	350.8, 76.3	352.08, 73.1	357.6, 55.11	361.04, 45.2	363.76, 33.7	365.44, 21.45	366.72, 8.57	367.52, 4.5
9	394.65, 98.3	396.09, 94.2	402.3, 71.51	406.17, 59.7	409.23, 45.5	411.12, 30.75	412.56, 15.69	413.46, 10.7
10	438.5, 122.6	440.01, 117.9	447, 91.62	451.3, 77.5	454.7, 60.4	456.81, 44.81	458.42, 26.98	459.4, 19.6

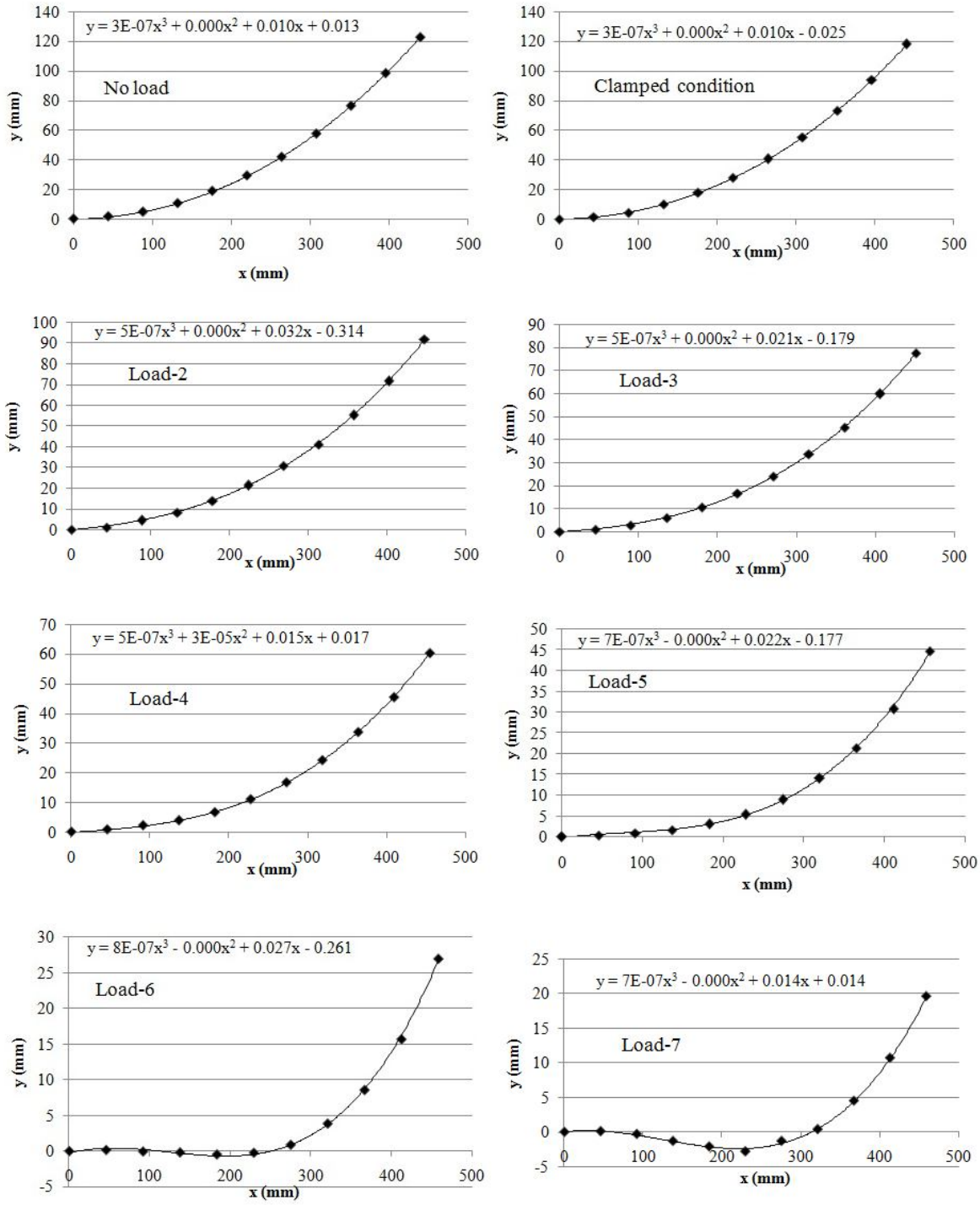

Fig. 3.6 Best fit deflection curves with their equation.

3.2.2 Equations of the deflection curves

The coordinate points of all the deflection profiles are exported in another graph handling software (MS-Excel) to obtain best fit deflection curve and its analytical equation.

The best fitted deflection profiles of the master leaf together with their analytical equations under the eight load steps, as considered in Fig. 3.5, are shown in Fig. 3.6.

3.2.3 Post processing of experimental results

Deflections of the master leaf spring due to applied loads are observed at the tip and they are tabulated in Table 3.3. It is obvious from Table 3.2 that the spring has deflected at clamped position, although no external load in the form of dead weights has been applied. Deflection of the tip at clamped position with respect to the initial no load configuration is 4.7 mm. This deflection is due to bending effect of clamping force acting at the contact surface of head of the ram of hydraulic cylinder and the leaf spring. The clamping effect is modeled through an equivalent force at the tip, which is unknown at this stage, but need to be calculated for obtaining the actual experimental load-deflection behavior.

Table 3.3 Observed load-deflection behavior of the tip

Applied load (dead weight) (N)	Tip-deflection (mm)
62.784	8.8
138.321	26.28
211.896	40.4
287.433	57.5
361.989	74.6
438.507	93
460.089	98.3

Table 3.4 Actual load-deflection behavior of the tip

Load (N)	Tip-deflection (mm)
0	0
20.9634	4.7
83.7474	13.5
159.2844	30.98
232.8594	45.1
308.3964	62.2
382.9542	79.3
459.4704	97.7
481.0524	103

The best fit linear load-deflection curve is obtained from data points of Table 3.3, as shown in Fig. 3.7, and it does not pass through origin. Using MATLAB® software, the load-deflection curve is shifted so as to pass through origin and the equation of the best fit line is $y = 0.2242x$, which is also shown in Fig. 3.7 by solid line with dots on it. Now corresponding to tip-deflection 4.7 mm, clamping force is calculated as 20.9634 N. Hence, this additional tip load is considered to capture the effect of initial clamping, although in

actual case the spring has a locked up moment. It should also be noted that the magnitude and direction of this locked up moment gets changed with the application of external load at different load levels. However following the present proposition, the corrected load-deflection behavior of the tip is given in Table 3.4. Actual experimental loads (in N) are calculated by adding the clamping force with every applied load and their new values are given in Table 3.4. Similarly the tip deflection due to clamping is also added with the observed tip deflections during experiment.

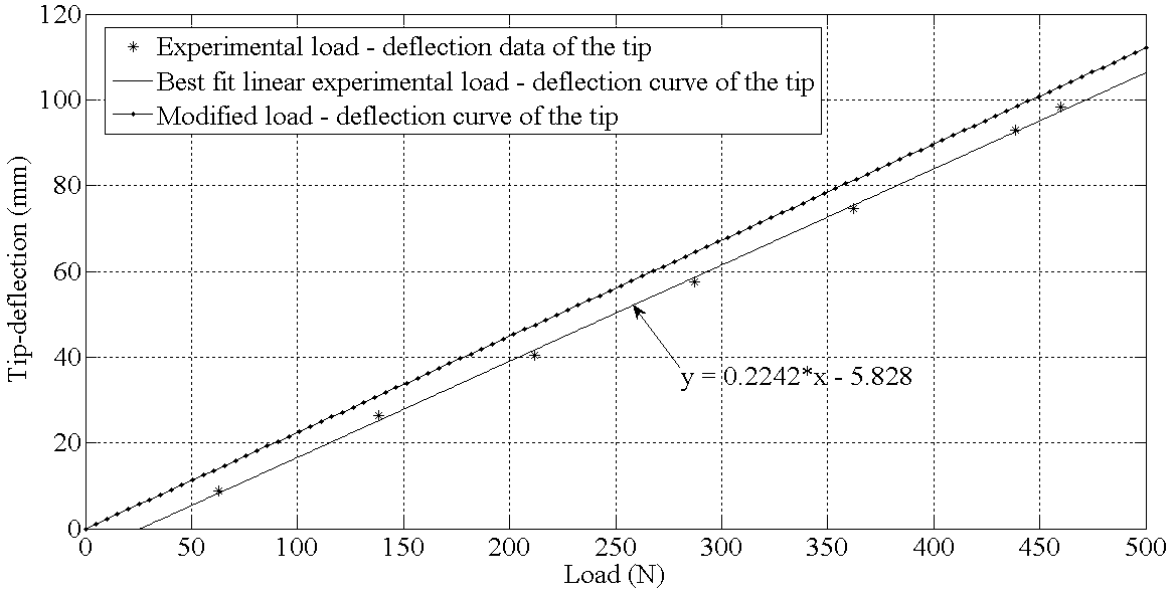

Fig. 3.7 Experimental and modified best fit linear load-deflection behavior of tip.

3.3 Mathematical formulation

In theoretical analysis, the physical system is modeled as cantilever beam with initial curvature subjected to tip concentrated load. To study large deflection behavior of such initially curved cantilever beam, large deflection behavior of initially straight cantilever beam under tip concentrated load is first studied. Large deflection problem of cantilever beams is generally analyzed in curvilinear coordinate system. Euler Bernoulli beam theory in curvilinear coordinate system (s, n) is $1/\rho = M/EI$, where curvature $1/\rho = d\varphi/ds$. So Euler Bernoulli bending moment-curvature relationship is given as follows,

$$EI\frac{d\varphi}{ds} = M, \tag{3.1}$$

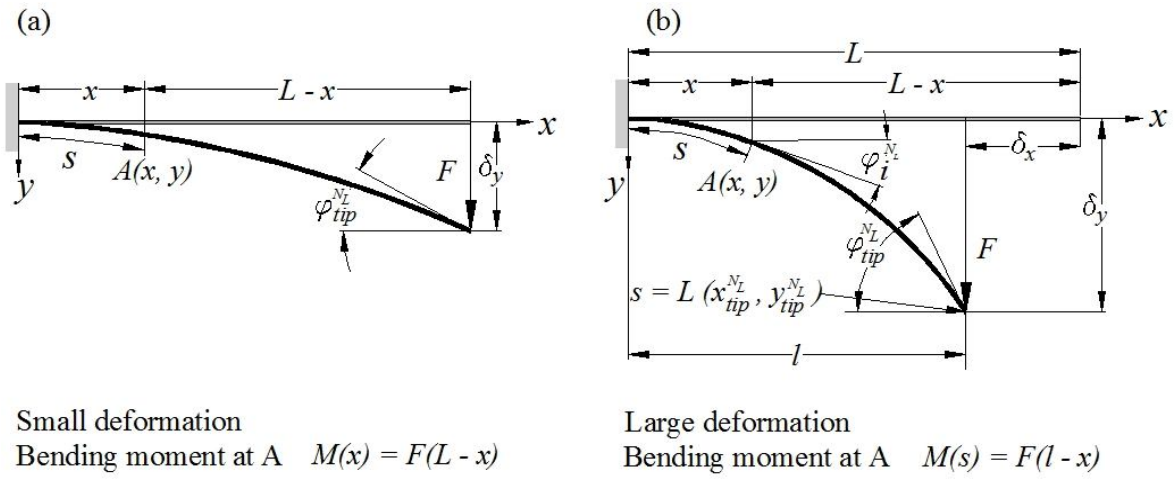

Fig. 3.8 (a) Small deflection and (b) large deflection of a cantilever beam.

where φ is the slope dy/dx at location s, and it is also the measure of normal direction n. Equation (3.1) is valid for both small and large deflection analysis but bending moment is computed differently as shown in Fig. 3.8. For the purpose of computation, φ is designated as φ_j^i, where $i\ (= 1, \ldots, N_L)$ is the measure of load and $j\ (= 1, \ldots, N_g\ /\ N_f)$ correspond to the location. Slope φ is usually measured in (x, y) coordinate system but it is also expressed as $\varphi(s)$ along s coordinate. When large deflection analysis is carried out in Cartesian coordinate system (x, y), the curvature is given by $\frac{1}{\rho} = \frac{d^2y}{dx^2} / [1 + (\frac{dy}{dx})^2]^{(\frac{3}{2})}$. However in the analysis of small deflection problems, the curvature is approximated as $\frac{1}{\rho} = \frac{d^2y}{dx^2}$, and as a consequence the domain of x becomes $0 \leq x \leq L$, i.e., the beam stretches with increase in loading as shown in Fig. 3.8 (a). On the other hand, in large deflection bending analysis of cantilever beams, it is assumed that the length of the beam does not change with loading. Hence the domain of s remains unchanged and spans from 0 to L $(0 \leq s \leq L)$. To maintain constancy in beam length, the domain of x changes with loading, spanning from 0 to the projected length l of the beam, as shown in Fig. 3.8 (b). The first derivative of Eq. (3.1) with respect to s yields,

$$EI \frac{d^2\varphi}{ds^2} = \frac{dM}{ds}. \tag{3.2}$$

The bending moment M at location s is,

$$M(s) = F\,(l - x). \tag{3.3}$$

Differentiating Eq. (3.3) with respect to s and comparing with Eq. (3.2) the following non-linear differential equation is obtained.

$$EI\frac{d^2\varphi}{ds^2} + F\cos\varphi = 0. \tag{3.4}$$

Equation (3.4) is derived by taking into account the geometrical relations $\cos\varphi = \frac{dx}{ds}$ and $\sin\varphi = \frac{dy}{ds}$. The equation is multiplied by $\frac{d\varphi}{ds}$ to yield $EI\frac{d\varphi}{ds}\frac{d^2\varphi}{ds^2} + F\cos\varphi\frac{d\varphi}{ds} = 0$ and after carrying out some mathematical manipulations, it is expressed as,

$$\frac{d}{ds}\left[\frac{EI}{2}\left(\frac{d\varphi}{ds}\right)^2 + F\sin\varphi\right] = 0. \tag{3.5}$$

Equation (3.5) is integrated and the associated constant of integration is evaluated by using boundary conditions i) $\varphi = \varphi_{tip}^{N_L}$ and ii) $\frac{d\varphi}{ds} = 0$ at $s = L$. $\varphi_{tip}^{N_L}$ represents the slope $\frac{dy}{dx}$ corresponding to load F at load step number N_L. Hence Eq. (3.5) becomes,

$$\left(\frac{d\varphi}{ds}\right)^2 = \frac{2F}{EI}\left(\sin\varphi_{tip}^{N_L} - \sin\varphi\right). \tag{3.6}$$

Using a normalized load parameter α $\left(= \frac{FL^2}{2EI}\right)$ [Beléndez et al. (2002)], the above equation is expressed as,

$$L\left(\frac{d\varphi}{ds}\right) = 2\sqrt{\alpha}\sqrt{\left(\sin\varphi_{tip}^{N_L} - \sin\varphi\right)}. \tag{3.7}$$

Upon integration, the equation provides arc length s as a function of φ through the relation,

$$\frac{s}{L} = \frac{1}{2\sqrt{\alpha}}\int_0^{\varphi}\frac{d\varphi}{\sqrt{\left(\sin\varphi_{tip}^{N_L} - \sin\varphi\right)}}. \tag{3.8}$$

Noting that $s/L = 1$ at the free end of the beam, Eq. (3.8) solves for the unknown slope $\varphi_{tip}^{N_L}$ corresponding to load parameter α, from iterative solution of the following relation.

$$2\sqrt{\alpha} = \int_0^{\varphi_{tip}^{N_L}}\frac{d\varphi}{\sqrt{\left(\sin\varphi_{tip}^{N_L} - \sin\varphi\right)}}. \tag{3.9}$$

An appropriate transformation of Eqs. (3.7) and (3.8), obtained by using the relations $\frac{d\varphi}{ds} = \cos\varphi\,\frac{d\varphi}{dx}$ and $\frac{d\varphi}{ds} = \sin\varphi\,\frac{d\varphi}{dy}$, yields the (x, y) coordinate at any location s, as given below.

$$\frac{x}{L} = \frac{1}{\sqrt{\alpha}}\left[\sqrt{\sin\varphi_{tip}^{N_L}} - \sqrt{\left(\sin\varphi_{tip}^{N_L} - \sin\varphi\right)}\right], \tag{3.10}$$

$$\frac{y}{L} = \frac{1}{2\sqrt{\alpha}}\int_0^{\varphi}\frac{\sin\varphi\,d\varphi}{\sqrt{\left(\sin\varphi_{tip}^{N_L} - \sin\varphi\right)}}. \tag{3.11}$$

The coordinate $(x_{tip}^{N_L},\ y_{tip}^{N_L})$ at the free end of the beam provides beam shortening $(\delta_x = x_{tip}^0 - x_{tip}^{N_L})$ or stretching $(\delta_x = x_{tip}^{N_L} - x_{tip}^0)$ corresponding to load F at load step N_L. In

addition the tip coordinate also provides the tip deflection $\delta_y = y_{tip}^0 - y_{tip}^{N_L}$, which may be in vertically upward or downward direction.

3.3.1 Deflection profiles of initially straight cantilever beam

In order to obtain $\varphi_{tip}^{N_L}$ as a function of α, Eq. (3.9) is integrated between 0 and $\varphi_{tip}^{N_L\,max}$ for different value of $\varphi_{tip}^{N_L}$. The results provide the relationship $\varphi_{tip}^{N_L}$ vs. α, as shown in Fig. 3.9. The deflection profiles are now obtained from Eqs. (3.10) and (3.11) and their plots are shown in Fig. 3.10 for different values of load parameter. It is reported earlier that for a given value of α, axial stretching (or shortening) of the tip δ_x is determined from tip co-ordinate $x_{tip}^{N_L}$, but for other coordinate values of x, axial stretching has some other value $\delta_x(s)$. Similarly δ_y is the particular value at $s = L$ and in general it is also a field variable in s. Coordinate $x(s)$ is readily obtained from Eq. (3.10), but evaluation of $y(s)$ from Eq. (3.11) requires evaluation of another elliptic integral, called as incomplete integral of second kind.

The deflection profile, as reported in this section, pertains to an initially straight beam (i.e., $\varphi_{tip}^0 = 0$). However a leaf spring has an initial curvature and hence the boundary condition $\varphi_{tip}^0 = 0$ at the free boundary is not valid here. The deflection behavior of such an initially curved cantilever beam is analyzed by a numerical method as presented in the next section.

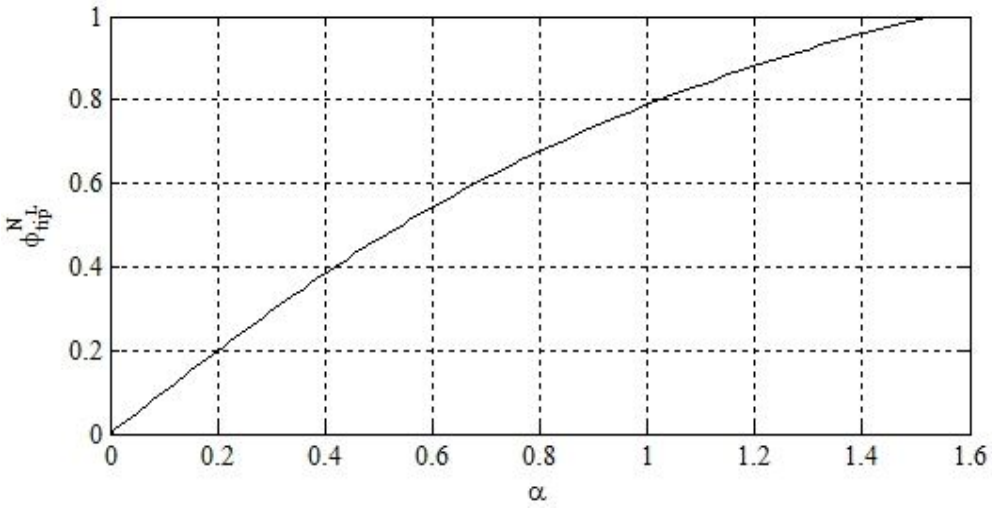

Fig. 3.9 Inter relationship for $\varphi_{tip}^{N_L}$ vs. α.

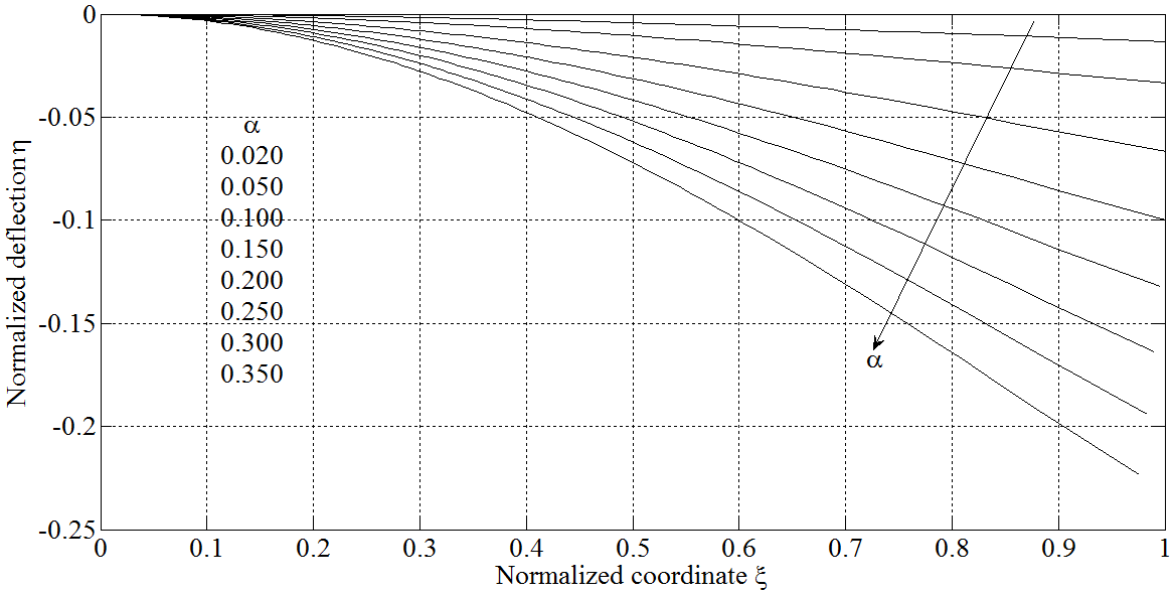

Fig. 3.10 Deflection profiles of straight cantilever beam for different values of load parameter α.

3.3.2 Deflection profiles of initially curved cantilever beam

The deflection profile of a curved beam may be represented in x, y as well as in s, n coordinate system, as highlighted for point A in Fig. 3.8 (b). The correlation between these two systems is established by the relation $s = \int_0^s ds = \int_0^x \sqrt{[1 + (\frac{dy}{dx})^2]}\, dx$. The Cartesian coordinates of the leaf spring under study is noted in its unloaded condition and a best fit polynomial equation of the curved profile $y = f(x)$ is established. This equation provides slope $\frac{dy}{dx}$ and hence arc length s is obtained as a function of x. By using the reverse relation $x(s)$, the x coordinates are determined for a number of equidistant points N_f along the arc length. Obviously for these points, $s_i = i(L/N_f)$, where $i = 1, \ldots, N_f$.

The load deflection behavior of an initially straight beam is known analytically as described in the previous section. Now N_f number of points are taken on the cantilever beam with initial straight profile having coordinates $(x_i^{N_L}, 0)$, i=1,…, N_f. The distance of these points from origin are known and they are a measure of its arc length as well. At each of these points axial shortening $\delta_x(s)$ and vertical deflection $\delta_y(s)$ are calculated for a load step

N_L. The same N_f number of points is also located on the initially curved leaf spring and x, y coordinates of these points are calculated. To get the elastic curve of the leaf spring at the current load step N_L, $\delta_x(s)$ is added to the x coordinate and $\delta_y(s)$ is subtracted from the y coordinate of the elastic curve in its previous configuration. Considering a cantilever beam with known initial curvature, deflection profiles are computed for different α values and the results are shown graphically in Fig. 3.11.

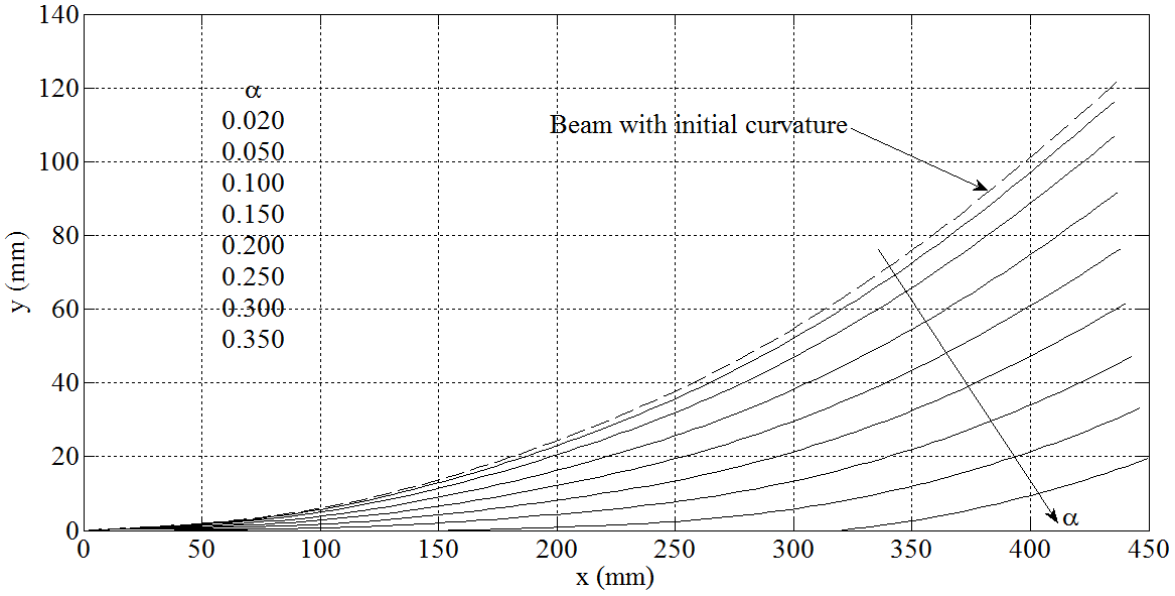

Fig. 3.11 Deflection profiles of cantilever beam with initial curvature for different values of load parameter α.

3.4 Comparison between experimental and theoretical results

Load parameters α are calculated from the actual experimental load and the slope at the free end of the beam $\varphi_{tip}^{N_L}$ is calculated for each of these load parameters from α vs. $\varphi_{tip}^{N_L}$ correlation. When α and $\varphi_{tip}^{N_L}$ are known, it is easy to obtain deflection profiles of the loaded spring as shown in Fig. 3.12. The figure also shows comparison between the theoretical and experimental deflection profiles for loads (in N) 159.2844, 232.8594 and 308.3964. Deflections at the tip of the beam are obtained from deflection profiles and this theoretical load-deflection behavior is shown in Fig. 3.13. The figure also shows comparison between the experimental and theoretical load-deflection behavior of the tip.

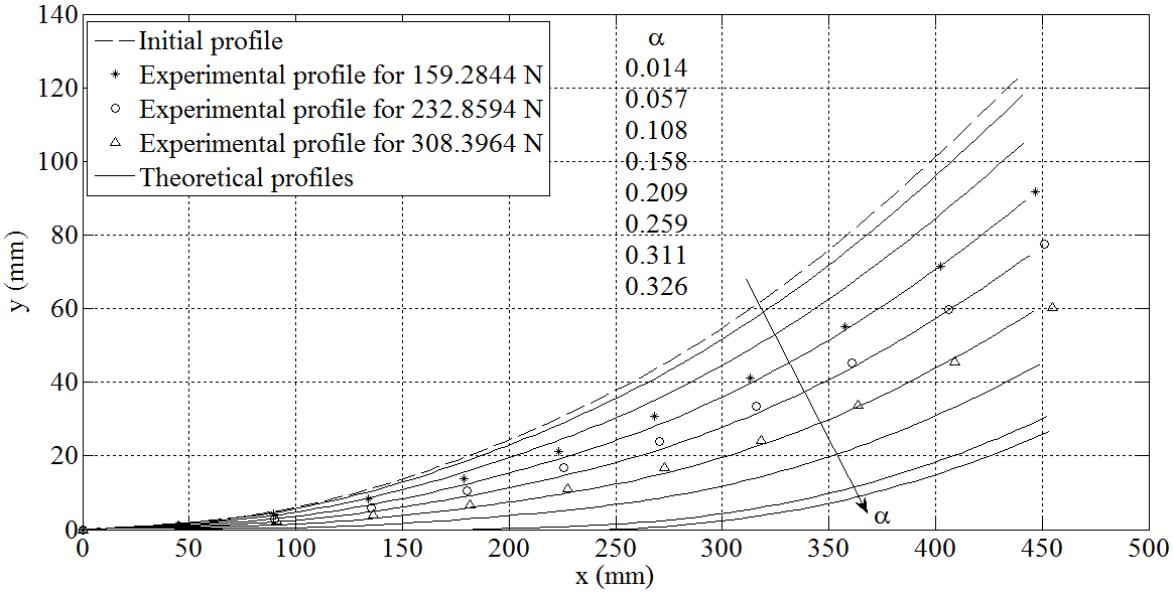

Fig. 3.12 Experimental and theoretical deflection profiles of master leaf spring.

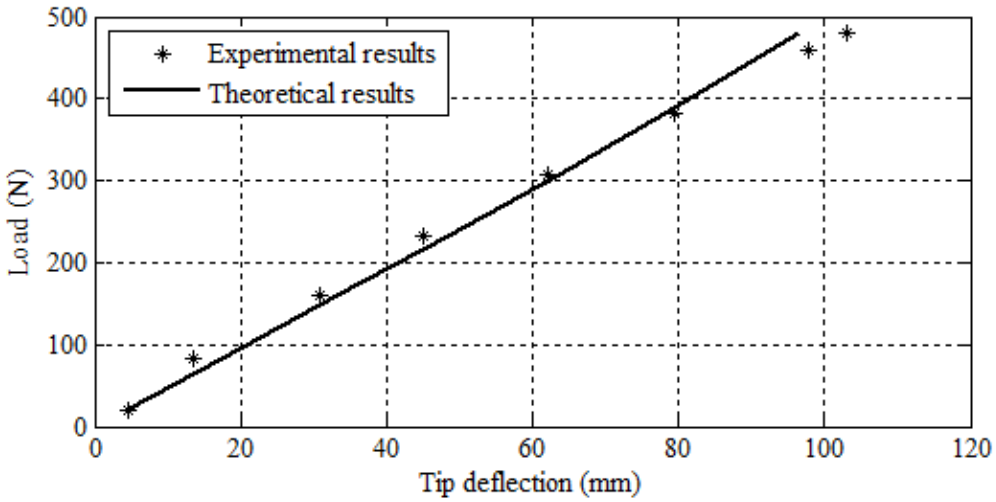

Fig. 3.13 Experimental and theoretical load-deflection behavior of the tip of the master leaf spring.

The theoretical and experimental results match quite well and the slight difference in the progressive and the digressive nature between them may be caused due to the following insufficiencies in modeling.

I. The physical system is modeled as a cantilever beam of uniform cross-section throughout the length, but leaf spring has a geometry variation at the tip portion.

II. Theoretical analysis is carried out for tip concentrated loading, but actual load application point has an eccentricity with respect to the centre line of the beam, as

may be seen in Fig. 3.5. Similarly, the length of the spring is assumed to be constant, but due to the eccentricity, effective length of the spring is changing at each loading condition.

III. The ideal clamping requires a line load, but in actual experimental set up the contact at hydraulic cylinder head is of finite size. Due to this clamping deficiency, the profile of the deflected spring shows a point of inflection at higher values of applied load. Present analysis is not done with due consideration for actual locked up moment, the magnitude of which is changing in the course of experiment.

3.5 Large deflection analysis under distributed and combined load

After successful validation of the proposed numerical method for large deflection analysis of curved cantilever beam under tip concentrated load with experimental results, further analysis is carried out on large deflection analysis of cantilever beam under distributed and combined loading. These problems are not readily solvable by using elliptic integrals and hence the iterative method of solution in Cartesian coordinate system, as proposed by Chen (2010) has been used. The large deflection behavior of an initially straight beam is solved first and after appropriate validation, new results are obtained for initially curved beams. The schematic diagram of the present problem is shown in Figs. 3.14 (a, b) for uniform and combined loading.

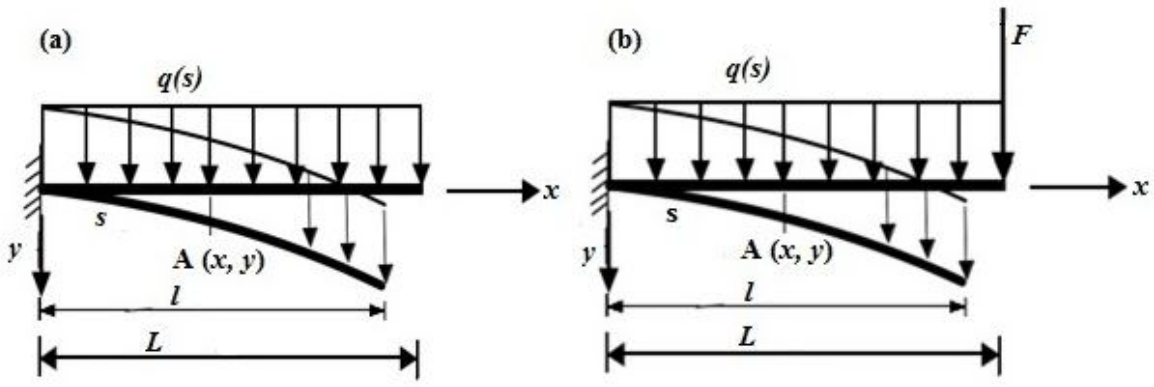

Fig. 3.14 Cantilever beam subjected to (a) uniform and (b) combined loading.

A brief description of the direct integration method is furnished here for ready reference. To carry out large deflection analysis in Cartesian coordinate system (x, y), the

slope curvature relation $\frac{1}{\rho} = \frac{d\varphi}{dx} / [1 + \varphi^2]^{(\frac{3}{2})}$ is used, where φ is the slope $\frac{dy}{dx}$ at location s. From the moment curvature relation $\frac{1}{\rho} = M/EI$, following relation is established,

$$\frac{d\varphi}{[1+\varphi^2]^{(\frac{3}{2})}} = \frac{M(x)}{EI}\, dx. \tag{3.12}$$

Integration of the above differential relation over the domain '0 to s', i.e., from clamped end to the point A of Fig. 3.8 (b), yields

$$\int_0^{\varphi} \frac{d\varphi}{[1+\varphi^2]^{(\frac{3}{2})}} = \int_0^{x} \frac{M(x)}{EI} dx. \tag{3.13}$$

It is easy to evaluate the left hand side integral as $\frac{\varphi}{\sqrt{1+\varphi^2}}$ and substituting $\frac{dy}{dx}$ for φ, the left hand side is finally evaluated as $\frac{dy}{ds}$. The right hand side of the equation is designated as $G(x, l)$ following the notation of Chen (2010). Finally some mathematical manipulations lead to the following two differential equations as given in Eqs. (3.14) and (3.15).

$$ds = \left(1/\sqrt{1 - G^2}\right) dx, \tag{3.14}$$

$$dy = \left(G/\sqrt{1 - G^2}\right) dx. \tag{3.15}$$

Equation (3.14) is evaluated iteratively with assumed values of l until the condition $\int ds = L$ is satisfied, and subsequently Eq. (3.15) is solved with known value of l.

3.5.1 Deflection profiles for uniformly distributed and combined load

When the cantilever beam is under uniformly distributed load, the bending moment at location s is $M(s) = \frac{P}{l}(l - x)^2/2$. It should be noted that the magnitude of uniformly distributed load is a function of the current beam configuration, because the total transverse load $P = q(s)\, l$ is conserved at all times and for all configurations. Thus $G(x, l)$ is found to be [Chen (2010)],

$$G(x, l) = \frac{q}{2EI}(l^2 x - x^2 l + x^3/3) = \frac{P}{2EI}\left(lx - x^2 + \frac{x^3}{3l}\right). \tag{3.16}$$

Using Eq. (3.16), Eqs. (3.14) and (3.15) are converted into

$$ds = \left(1/\sqrt{1 - (\frac{P}{2EI})^2 \left(lx - x^2 + \frac{x^3}{3l}\right)^2}\right) dx, \tag{3.17}$$

$$dy = \left((\frac{P}{2EI}) \left(lx - x^2 + \frac{x^3}{3l}\right) / \sqrt{1 - (\frac{P}{2EI})^2 \left(lx - x^2 + \frac{x^3}{3l}\right)^2}\right) dx. \tag{3.18}$$

Equation (3.17) is solved iteratively to get projected length l and once the appropriate value of l is obtained, deflection profile of the beam is obtained by solving Eq. (3.18), as mentioned in the previous section.

When the cantilever beam is under combined uniform and tip concentrated loading, the bending moment at location s is $M(s) = F\,(l-x) + \frac{P}{l}(l-x)^2/2$. Thus $G(x,l)$ is found to be

$$G(x,l) = \frac{P}{2EI}\left(lx - x^2 + \frac{x^3}{3l}\right) + \frac{F}{EI}\left(lx - \frac{x^2}{2}\right). \tag{3.19}$$

Equations (3.14) and (3.15) are now converted into

$$ds = \left(1/\sqrt{1 - \left[\frac{P}{2EI}\left(lx - x^2 + \frac{x^3}{3l}\right) + \frac{F}{EI}\left(lx - \frac{x^2}{2}\right)\right]^2}\right) dx, \tag{3.20}$$

$$dy = \left(\left[\frac{P}{2EI}\left(lx - x^2 + \frac{x^3}{3l}\right) + \frac{F}{EI}\left(lx - \frac{x^2}{2}\right)\right]/ \sqrt{1 - \left[\frac{P}{2EI}\left(lx - x^2 + \frac{x^3}{3l}\right) + \frac{F}{EI}\left(lx - \frac{x^2}{2}\right)\right]^2}\right) dx. \tag{3.21}$$

The solution can easily be done in this case also, following the above mentioned numerical method.

3.5.2 Validation of results

To carry out validation with the available results, intensity of the uniformly distributed load is defined in a non-dimensional form as

$$\bar{q} = \frac{qL^3}{EI}. \tag{3.22}$$

However, in case of combined loading, no such non-dimensional load parameter can be prescribed and hence results are presented in dimensional plane. The problem of a cantilever beam bending under simultaneous action of a concentrated load and gravity is validated with Chen (2010). In this comparative study, the values of the system parameters are L= 0.4 m, E = 194.3 GPa and I = 1.333×10^{-13} m^4. The weight of the beam P (= 0.3032 N) produces uniformly distributed load and in addition, the beam is acted upon by concentrated load F at tip. Three different cases for F = 0, 0.098 and 0.196 N are taken up

and Fig. 3.15 (a) shows the deflection profiles for these loading conditions in dimensional plane. It is observed that comparison with the results of Chen (2010) is matching quite well.

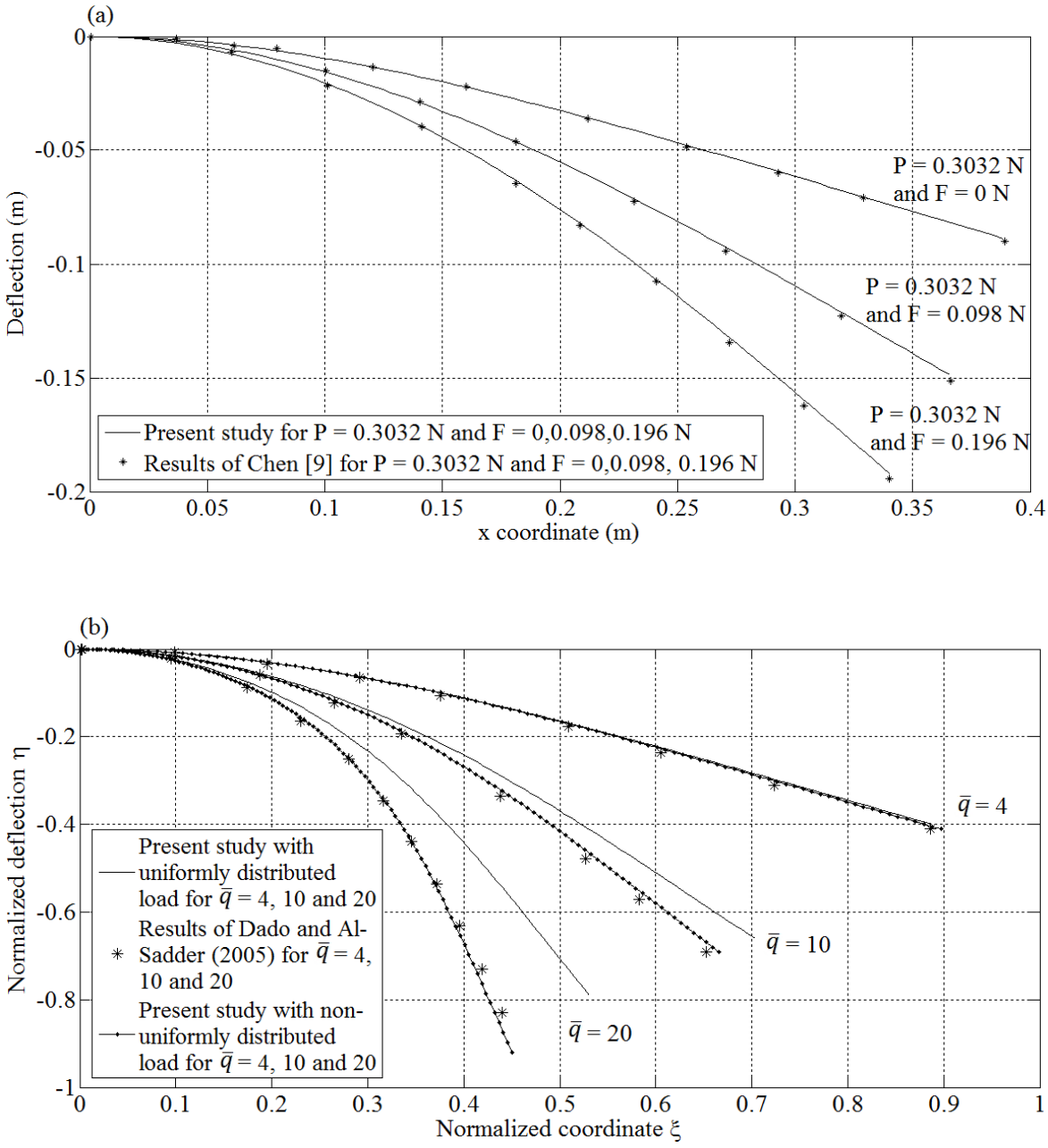

Fig. 3.15 Numerical simulation of the results of (a) Chen (2010) and (b) Dado and Al-Sadder (2005).

To validate the proposed method when the beam is under uniformly distributed load only, numerical results presented by Dado and Al-Sadder (2005) for a prismatic slender cantilever beam bending problem is simulated. For any prescribed value of $\bar{q}$ we can find

out the dimensional value $q_0\ (= P/L)$ by using the relation, $q_0 = \bar{q}l\,\frac{EI}{L^4}$, where q_0 is the initial value of uniformly distributed load at straight configuration of the beam. Numerical computation is carried out for the aforesaid beam geometry and the computational results are shown by solid lines in Fig. 3.15 (b) for load intensities $\bar{q}$ = 4, 10 and 20. It is obvious from the figures that results are not matching with the results of Dado and Al-Sadder (2005, [Fig.-5]) appropriately.

The discrepancy is coming from the assumption that load intensity $q(s) = P/l$ remains constant along x axis for the beam configuration under consideration. However the intensity of the distributed load is constant along the arc length and one must consider the net vertical component of such a loading condition. The expressions of bending moment $M(x)$ and the function $G(x,l)$ are evaluated following the proposed change in loading condition and they are reported in the next section. Hence Fig. 3.15 (b) contains another set of results which are indicated by solid lines with dots on them and observation on those lines is also reported in the next section.

3.5.3 Non-uniformly distributed load

As mentioned earlier, the intensity of the distributed load $q = \frac{P}{l}$ is constant along the arc length but it is not constant along the projected length. At location x ($0 \le x \le l$) the vertical component of q is

$$q_n(x) = \frac{q}{cos\varphi}. \tag{3.23}$$

For a known distribution of loading q_n, shear force $V(x)$ and bending moment $M(x)$ are given by the following relations, for the point A of Fig. 3.14.

$$V(x) = \int_x^l q_n(x)\,dx, \tag{3.24}$$

$$M(x) = \int_x^l V(x)dx. \tag{3.25}$$

Thus $G(x,l)$ is found to be

$$G(x,l) = \int_0^x \frac{M(x)}{EI}dx. \tag{3.26}$$

It is observed from Eqs. (3.23) – (3.26) that, determination of $G(x,l)$ is a stepwise procedure starting from a known distribution of loading q_n. To determine q_n one must know two field variables φ and q apriori, where φ is a function of q. The coupled

problem is solved numerically by using an iterative method, in which the final load value is reached with increment $\Delta\bar{q}$. At load step i, a load increment $\Delta\bar{q}$ is given on the current load value of $i\Delta\bar{q}$, i= 1, 2,…, N_L. The corresponding dimensional load intensity q_0 is obtained from the relation ${q_0}^i = \bar{q}l^i\frac{EI}{L^4}$, where l^i is the current projected length. At this load step the incremented value of total transverse load P is calculated as $P^i = {q_0}^i L$, which is uniformly distributed over the current projected length l^i. So intensity of the distributed load is given by $q^i = \frac{P^i}{l^i} = \bar{q}\frac{EI}{L^3}$, i=1, 2,…, N_L. Net vertical component field of the load intensities are calculated as $(q_n)_j^i = \frac{(q)^i}{cos\ (\varphi_j^{i-1})}$, i=1, 2,…, N_L and j=1,…, N_f. As mentioned earlier the search procedure begins with an assumed projected length l^i for load step i. N_f number of points are taken between '0 to l^i' and at each of these points shear force, bending moment and the function $(G(x, l^i))_j^i$, i = 1,…, N_L and j = 1,…, N_f, are calculated from Eqs. (3.24), (2.25) and (3.26) respectively. Once the function is determined, $(\frac{ds}{dx})_j^i$ is calculated from Eq. (3.14) and this is numerically integrated between '0 to l^i' to find arc length s^i, i = 1,…, N_L. l^i value is adjusted until the condition $\{(L - s^i)/L\} < \varepsilon_{err}$ is satisfied. Once l^i is calculated from the search procedure, deflections at N_f points are obtained from Eqs. (3.26) and (3.15).

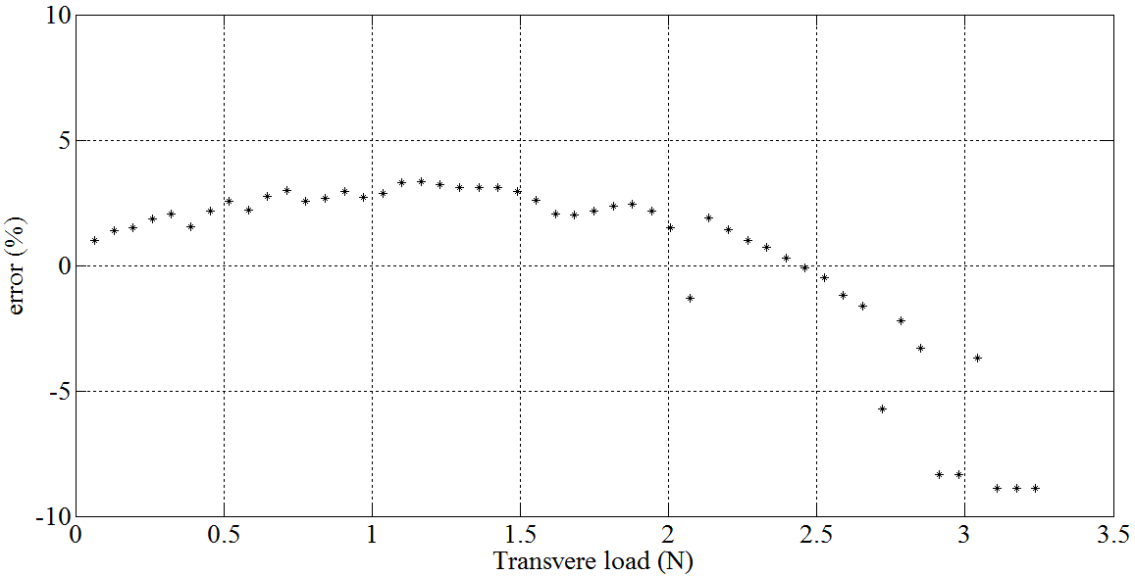

Fig. 3.16 Transverse load vs. error plot.

At load step i, with known value of l^i one can check the total transverse load P_{cal}^i by numerically integrating $(q_n)_j^i$ over the domain 0 to l^i, i = 1,…, N_L and j=1,…, N_f, which

ideally should be equal to P^i. In the computation scheme this is a source of error and this is accounted for in each load step through post-processing. This error is calculated as $\{(P^i - P^i_{cal})/P^i\}$ and plotted against transverse load P^i which is shown in Fig. 3.16. This is clearly seen from the figure that error is bounded between -8.89 % and 3.34 % and in general error increases with load. This indicates that selection of a proper error limit value ε_{err} is a function of the loading. However in the present work computation is carried out within 0.01% error. Fig. 3.15 (b) shows the deflection profiles for non-dimensional load intensities $\bar{q}$ = 4, 10, 20 and these results are successfully validated with the results of Dado and Al-Sadder (2005, [Fig.-5]).

3.5.4 New results for cantilever beam with initial curvature

New results are furnished for an initially curved beam considering the geometry of the master leaf spring mentioned in experimental work. The load deflection behavior is observed under two different loading conditions: uniform and combined. Under uniform loading four different distributed loads, totaling 232, 308, 383 and 460 N are considered. In case of combined loading a base distributed load 232 N is considered and on top of that three different tip concentrated loads 76, 151 and 228 N are imposed. Load deflection behavior under above said loading conditions is determined by using the method of superposition mentioned in section 3.3.2 and the results are shown in Fig. 3.17.

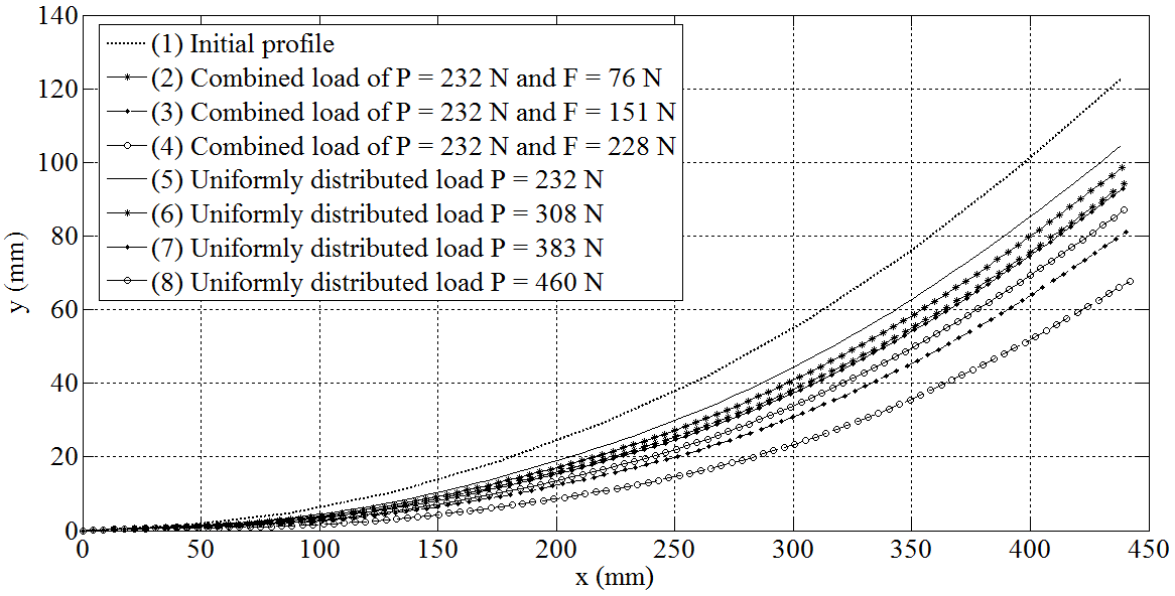

Fig. 3.17 Load-deflection behavior of the master leaf spring under uniformly distributed and combined loads.

It is clearly seen from Fig. 3.17 that deflections under uniformly distributed loads are less compared to those under combined loads when the magnitude of total vertical load is same. As a particular case, it may be noted that for the cases of uniform and combined loading as shown by curves 8 and 4, the magnitudes of total transverse loads are same.

Chapter 4

ANALYSIS OF LEAF SPRING UNDER THREE POINT BENDING

In the previous chapter, load-deflection behavior of a master leaf spring is studied by considering only one half of the spring. In that analysis, geometry of the spring is assumed symmetric and effect of clamping is modeled through an equivalent constant force acting at the tip. This equivalent force of clamping moment is predicted by an indirect approach through post processing. But in actual case this clamping effect changes with loading and highly dependent on spring geometry. In order to overcome such insufficiencies in modeling, a new leaf spring testing rig is designed and presented in this chapter. In the present analysis, whole geometry of the leaf spring is considered and thus the chapter begins with a detailed study of geometry of the specimen i.e., the master leaf spring. Subsequently details of the experimental set-up and measurement procedures are described and results of the experimentally observed deflection and strain fields are reported. Mathematical formulation of the corresponding theoretical model is furnished and a comparative study is carried out. The chapter concludes with some reporting on stress concentration effect, observed at the location of central drill hole of the master leaf.

4.1 The specimen geometry

Cross-section of the master leaf spring is rectangular and its width and thickness are measured by using vernier caliper and they are 38.5 mm and 6.25 mm respectively as already reported in the earlier chapter. In addition, inner and outer diameters of each eye end of the master leaf spring are measured by using outside caliper and inside caliper. From these measurements, pitch circle diameters of the eye ends are determined. The master leaf spring is then placed on a graph paper and its profile is drawn along the outer and inner edges. Centres of the eye ends and mounting drill hole are also located on the graph paper and then the spring is removed from the graph paper. A straight line is drawn between these centres, which is the span of the leaf spring. Now pitch circles are drawn at eye centres and centre line of the master leaf spring is drawn between the outer and inner curvature lines of its profile making its ends tangential to the roller pitch circles. These points of tangencies are denoted by A_1 and B_1 for left roller and right roller respectively. Profile of the master leaf spring in its

free state is shown in Fig. 4.1 through schematic diagram. In Fig. 4.1, major dimensions (span, camber and arc length) of the master leaf spring are shown and enlarged details of eye ends and mounting drill hole are shown separately. Midpoint of the span is considered as origin of Cartesian coordinate system and another perpendicular straight line is drawn at this point. x, y coordinates of twenty one equally spaced points (indicated as 2, 3, 4, …, 22 in Fig. 4.1) on the centre line together with two points of tangencies A_1 and B_1 (indicated as 1 and 23 in Fig. 4.1) are measured with respect to origin and tabulated in Table 4.1. The tabulated values indicate that leaf spring geometry is not symmetric about its mid-point. It is apparent that the centre of the drill hole is not passing through the midpoint of span and the eccentricity between them is 1.6 mm.

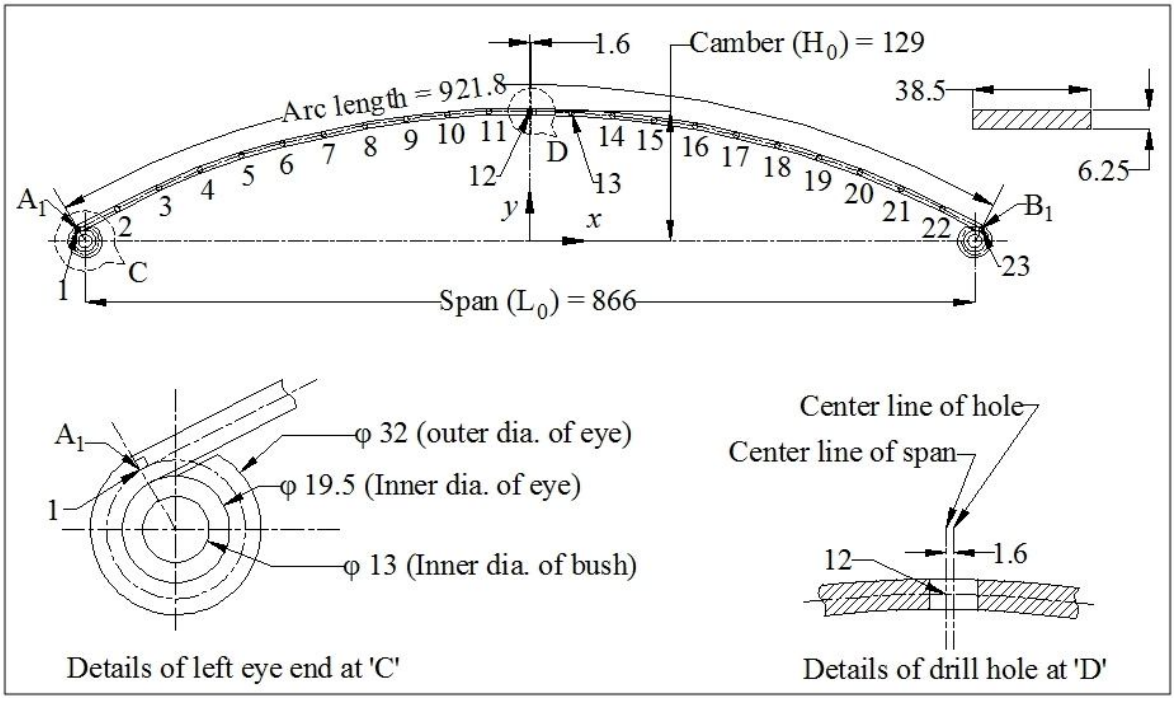

Fig. 4.1 Profile of the master leaf spring in its free state.

Photograph of the master leaf spring in its free state is shown in Fig. 4.2. As shown in Fig. 4.2 (b), twenty one equally spaced points (indicated as 1, 2, 3, …, 21) are marked on the master leaf spring along its centre line, using prick punch to determine profile of the leaf spring under load. These marked points are used as reference in subsequent geometry measurement of the master leaf spring under loaded condition.

Table 4.1 x, y coordinates at various measurement locations of the master leaf spring in its free state

Loc.	1	2	3	4	5	6	7	8	9	10	11
x	-439.3	-400	-360	-320	-280	-240	-200	-160	-120	-80	-40
y	11.4	33	52	68.5	84	96	107	114	120.5	125	128

Loc.	12	13	14	15	16	17	18	19	20	21	22	23
x	0	40	80	120	160	200	240	280	320	360	400	439.1
y	129	128	125	121	115	106.5	97	84	68.5	52	32.5	11.5

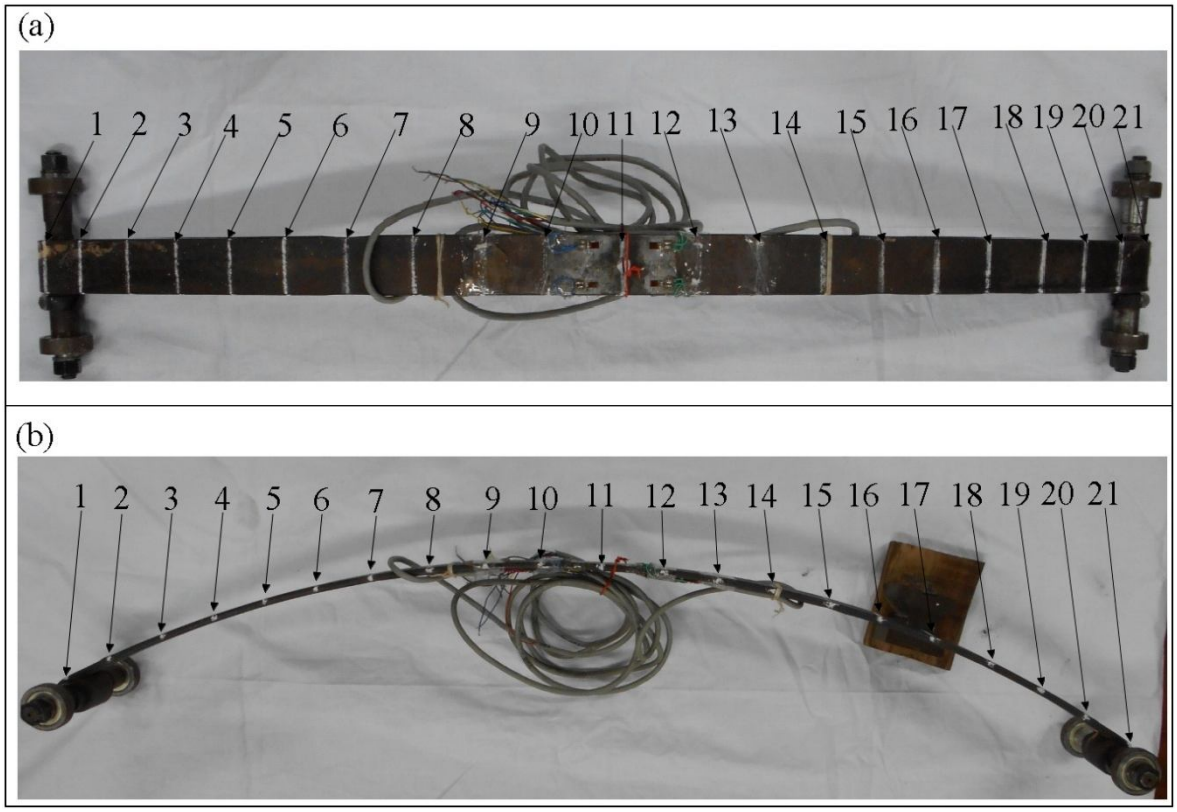

Fig. 4.2 Photographs of the master leaf spring - (a) top view and (b) front view.

4.2 Description of experimental set-up

To study development of stresses and deflections in leaf spring under bending type of loading, a special leaf spring testing rig is designed and set-up in Machine Elements laboratory. This experimental set-up simulates three point bending test. Detail descriptions of

the measurement instruments and the components of the experimental set-up together with their manufacturing details are presented in the following sub-sections.

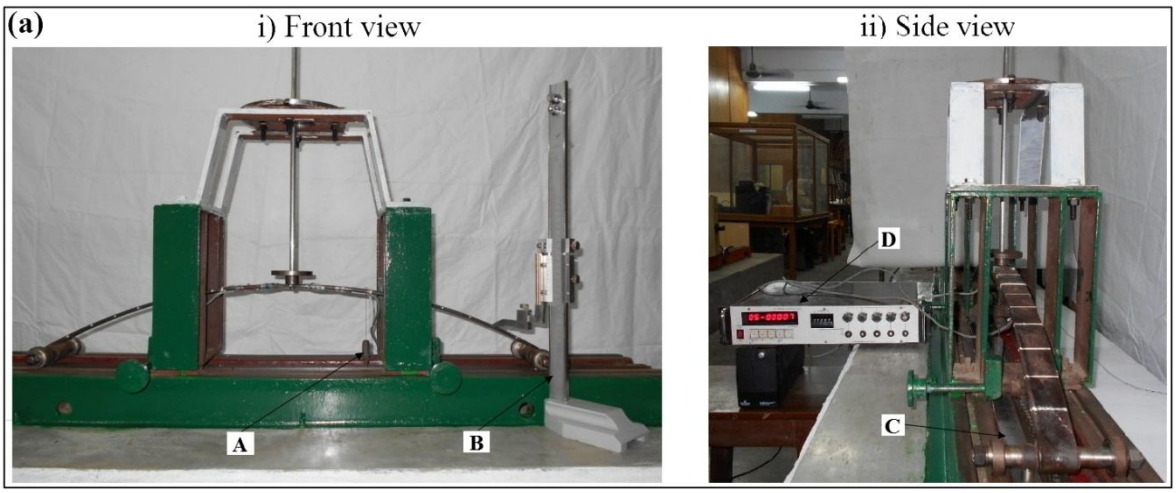

Item	Description
A	Plumb
B	Height gauge

Item	Description
C	Scale
D	Strain indicator

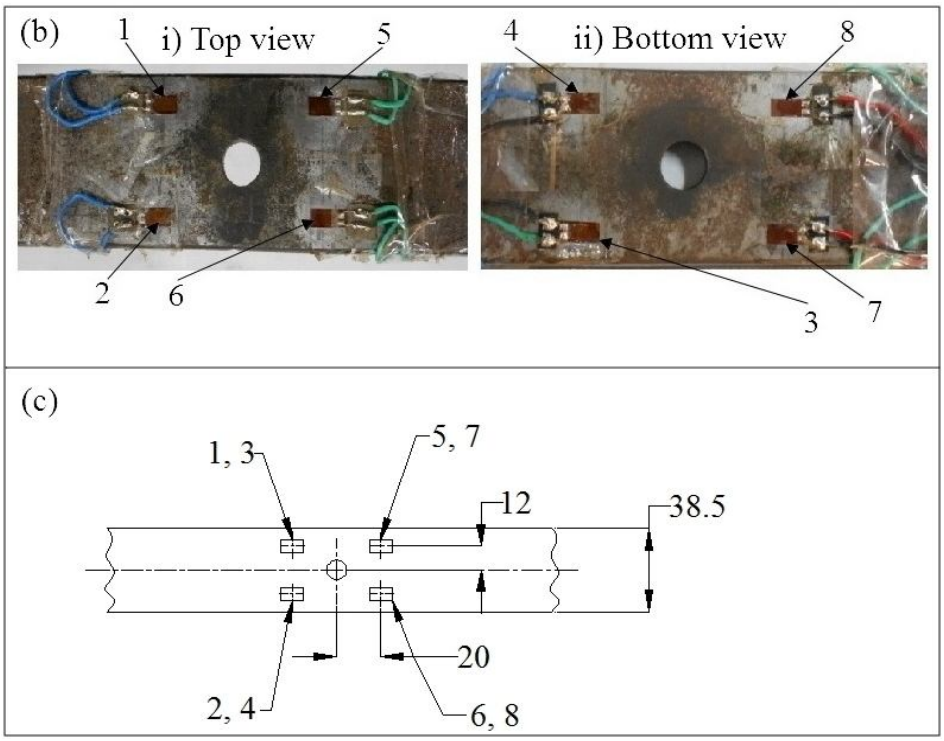

Fig. 4.3 (a) Photographs of the experimental set-up taken from i) front and ii) right sides, (b) photographs at the locations of strain gauges on the master leaf spring taken from i) top and ii) bottom and (c) schematic diagram of strain gauges.

4.2.1 The measurement instruments

It is said that a photograph is worth over thousand words and hence photograph of the experimental set-up is shown in Fig. 4.3 (a), taken from front and right sides of the set-up. Some measurement contrivances are also shown in Fig. 4.3 (a) and marked as items A-D, and in addition, the digital camera used in previous experiments, is also used to capture snapshots of deflection profiles. Details on strain gauge mounting and circuit connection can be found in strain gauge manual (TML, Tokyo Sokki Kenkyojo Co., Ltd.) and operation manual of strain indicator (Syscon Instruments) respectively. As it is shown in Fig. 4.3 (b), strain gauges 1 and 2 are located on the top surface of the master leaf spring at distance 20 mm from the centre of the drill hole in left side, whereas strain gauges 3 and 4 are placed on the bottom surface at the same location. Similarly strain gauges 5 and 6 are placed on the top surface and strain gauges 7 and 8 are placed on the bottom surface at same distance in the right side of the drill hole. Figure 4.3 (c) shows location of the eight strain gauges which are mounted on the master leaf spring along longitudinal direction, through schematic diagram. Detail specifications of the measurement instruments are given in page 76 and their photographs are shown in Fig. 4.4.

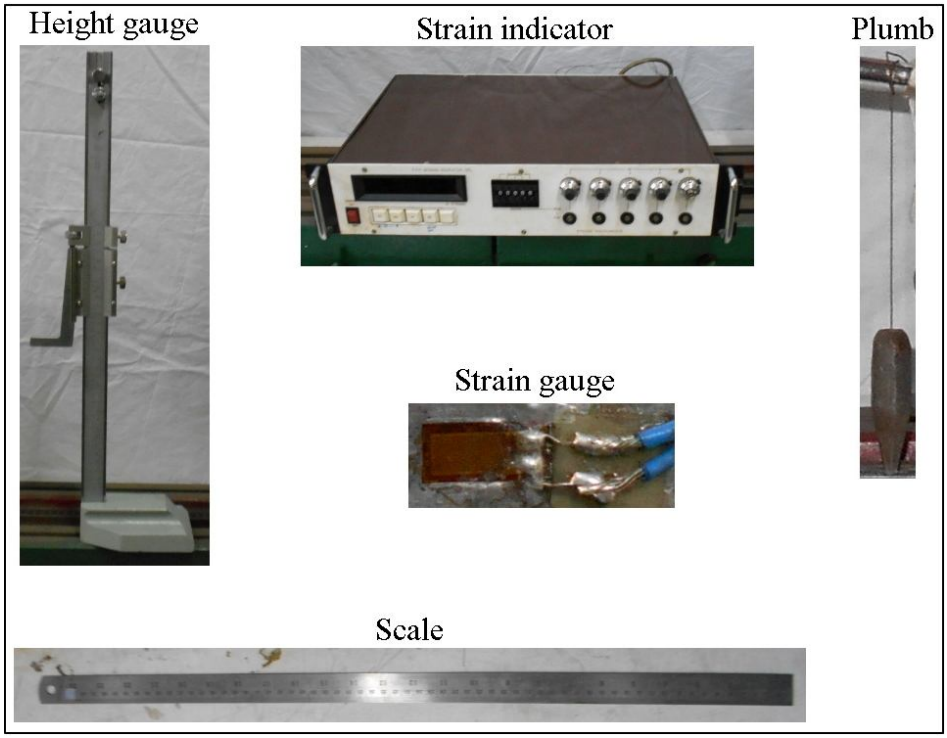

Fig. 4.4 Photographs of measurement instruments.

Specifications of the measurement instruments

I. Strain gauge

Make - Tokyo Sokki Kerkyujo Company Limited

Type - Foil type

Batch No. – 93 28090

Gauge factor – 2.10±1%

Gauge length – 5 mm

Gauge resistance - 350±1.0 Ω

Temperature compensation – $11x10^{-6}$ /º C

Transverse sensitivity – 0.3%

II. Strain indicator

Make – Syscon Instruments

Serial No. - 8117

Display – On a 3 ½ digit, 12.5 mm character height, seven segment, red LED

Measuring range - ±2000 micro strains

Accuracy - Within ±0.2% of the range

No of inputs - 05

Acceptable bridge configuration - (a) Full Bridge and (b) Half Bridge

Acceptable gauge resistance – 100 Ω to 1000 Ω

Operating temperature - + 10º C to + 45º C

Power supply requirement - 230V ± 10 %, 50 Hz, AC mains

Cabinet - 420mm (W) × 088mm (H) × 295mm (D)

III. Height gauge

Make – Aerospace

Range – 0 – 300mm

Least count – 0.02 mm

IV. Scale

Make – Kristeel – Shinwa

Range – 0 - 600mm

V. Plumb

Specially designed plumb to suit the purpose of experiment

Material – En 24

4.2.2 The component details of support structure

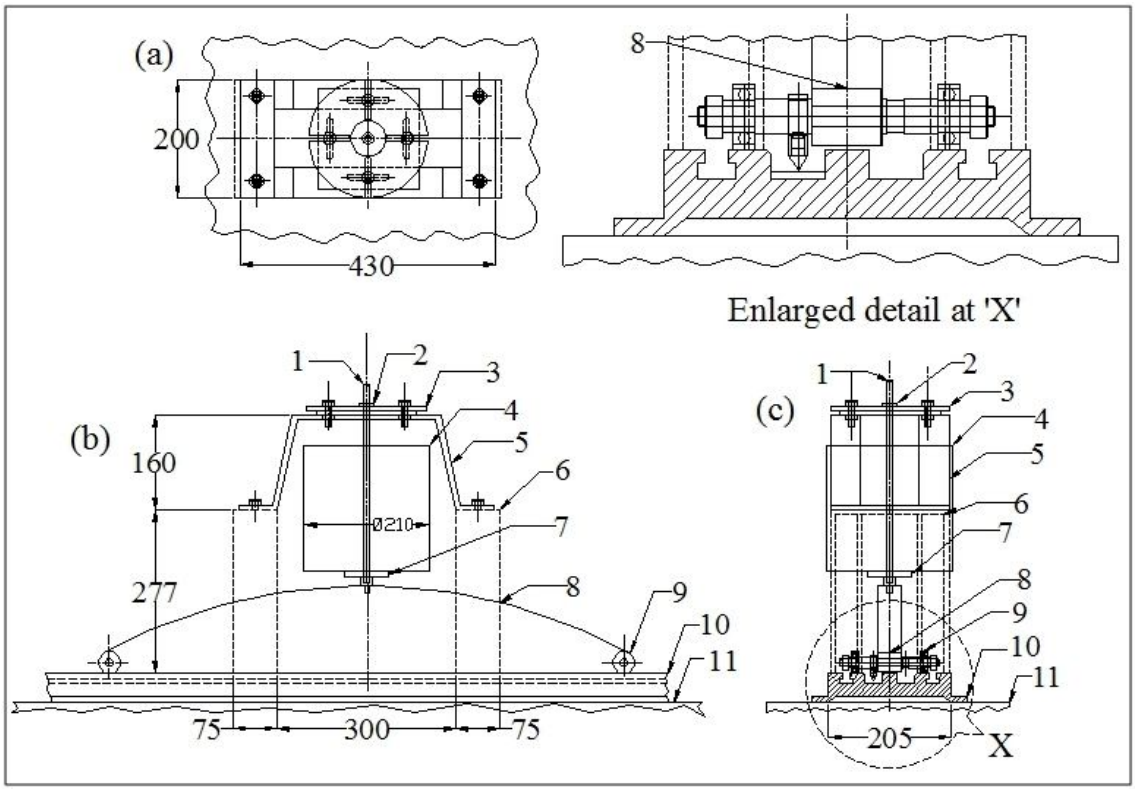

Item	Description
1	Vertical guide rod
2	Bush for guide rod support
3	Guiding disc
4	Slotted discs for loading
5	Bridge
6	Box structure

Item	Description
7	Load connector
8	Master leaf spring
9	Roller support sub-assembly
10	C.I. bed
11	RCC foundation

Fig. 4.5 Schematic diagrams of the experimental set-up (a) top view, (b) front view and (c) side view.

The schematic diagrams of the set-up corresponding to Fig. 4.3 (a) are shown in Fig. 4.5 (a-c), which indicate some major dimensions. The kernel of the set-up is the master leaf of an automobile spring assembly (item 8), which is mounted on a machined cast iron bed (item 10) by using roller supports at the ends (item 9). Some of the features of the roller supports are shown in the enlarged detail 'X' of Fig. 4.5, whereas the major roller support sub-assembly details are shown separately in Fig. 4.6 (a). Individual component details of roller support arrangement are shown in Fig. 4.6 (b) and discussed afterwards. Manufacturing

drawings of other components of the experimental set-up are furnished in Fig. 4.7 (a, b), classified under a) load supporting and b) load imparting components. The following paragraph provides a general description of the set-up and descriptions in greater details are furnished subsequently.

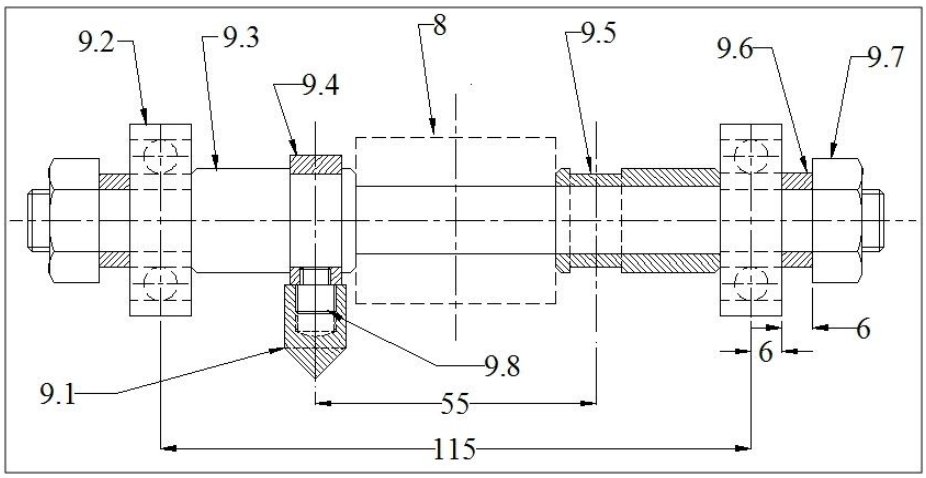

Item	Description
9.1	Fixed plumb pointer
9.2	Ball bearing
9.3	Pin
9.4	Ring

Item	Description
9.5	Spacer
9.6	Washer
9.7	Nut (M 12 X 1.25 mm)
9.8	Plumb pin

Fig. 4.6 (a) Roller support sub-assembly (item 9).

The set-up, as shown in Fig. 4.5, is mounted over the cast iron (C.I.) bed, which rests on a RCC foundation (item 11). Two box structures (item 6) are mounted on the C.I. bed through chain-gear mechanism. This mechanism enables the box structures to move in horizontal direction over the C.I. bed, so that distance between them can be adjusted to carry out experiment with leaf springs of different sizes. However, for the present experimentation, the box structures are made fixed with 300 mm distance between them. The C.I. bed, RCC foundation and box structures are available in the laboratory as part of general purpose of experimentations. The two box structures are indicated by dotted lines in schematic diagram of the experimental set-up to maintain clarity. A bridge structure (item 5) is bolted over the box structures and the guiding disc (item 3) is again bolted over the bridge structure after proper centre line alignment of load line. These two components constitute the overall load support structure to house the loading components.

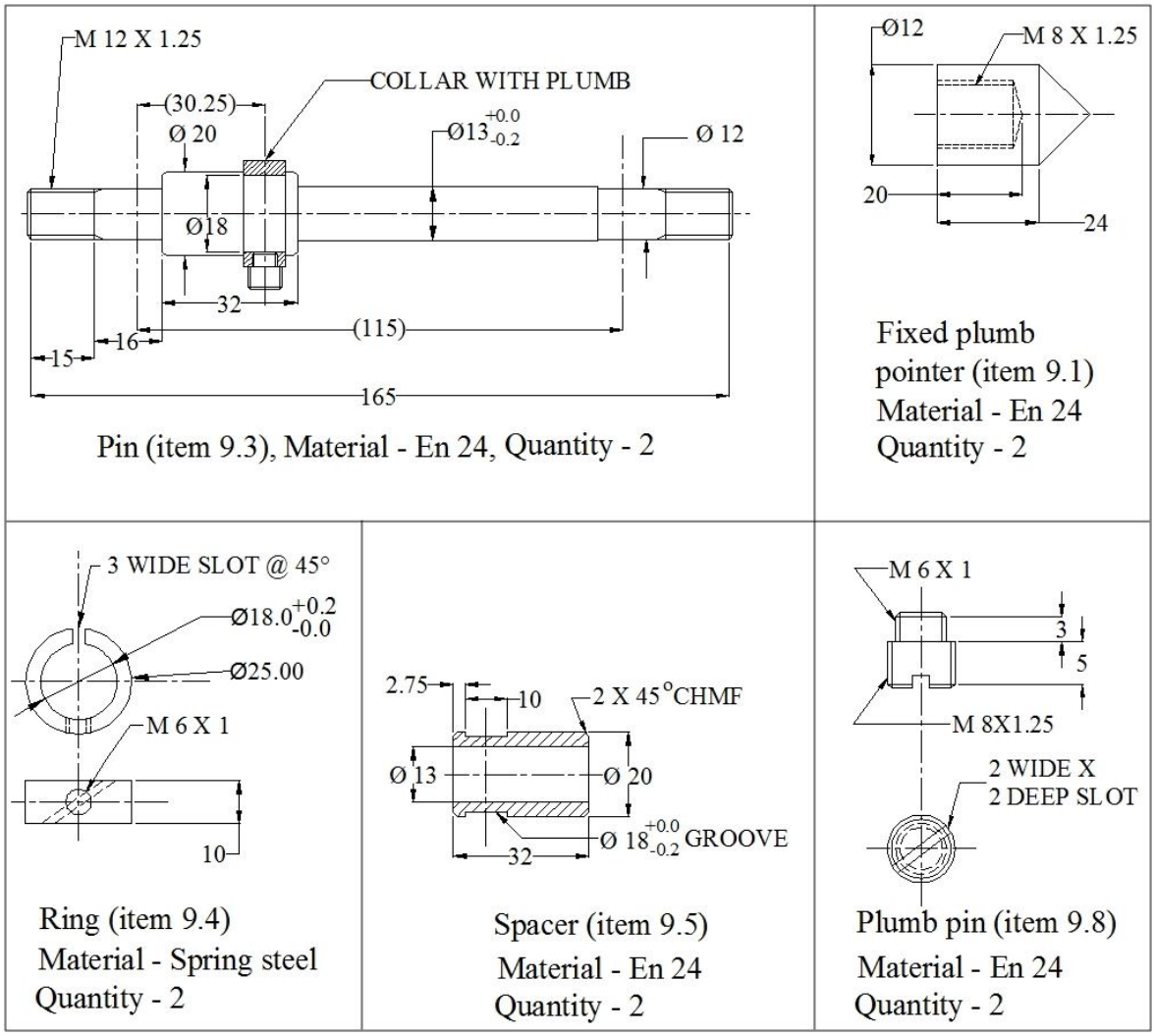

Fig. 4.6 (b) Detail of roller support sub-assembly components.

As shown in Fig. 4.6 (a), each roller support mainly consists of one pin (item 9.3), one spacer (item 9.5) and two ball bearings (item 9.2). Presence of ball bearings in roller support offer frictionless movement of the two halves of the spring about vertical load line. Components of each roller support are assembled together with each eye end of master leaf spring by using nut and washer. A threaded pin (item 9.8) is screwed into the ring (item 9.4) of each roller support sub-assembly and a fixed plumb pointer (item 9.1) is attached to that pin by means of threaded fastening. When leaf spring is loaded by placing slotted discs (item 4) over load connector (item 7), fixed plumb pointers move in horizontal direction along with the roller supports. To measure horizontal movements of these fixed plumb pointers, two steel rules are placed in grooves of the cast iron bed. The zero values of the scales are set with reference to the vertical load line and they are used to record roller movement towards left and right directions respectively.

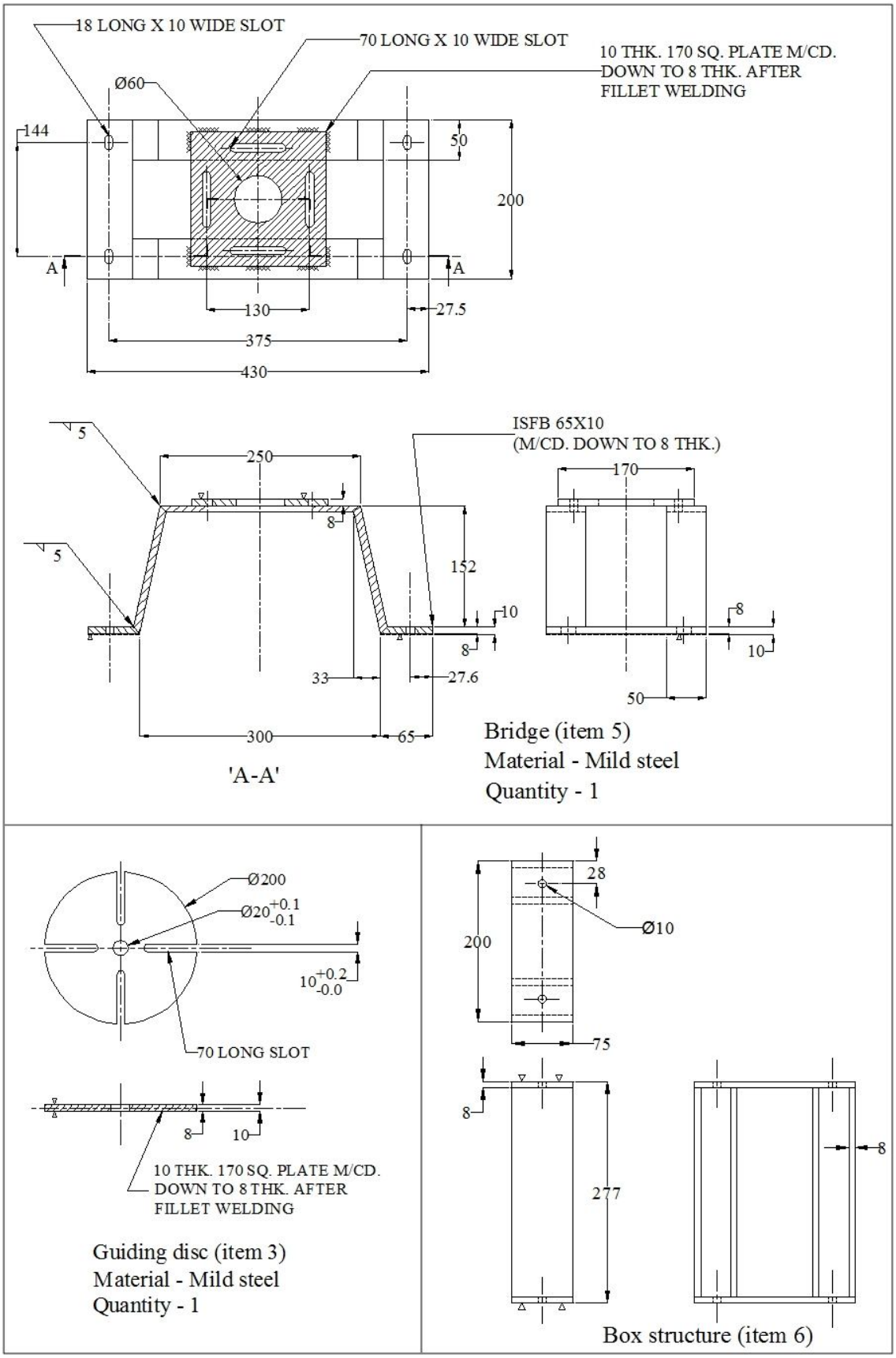

Fig. 4.7 (a) Details of bridge, guiding disc and box structure (components of overall load support structure).

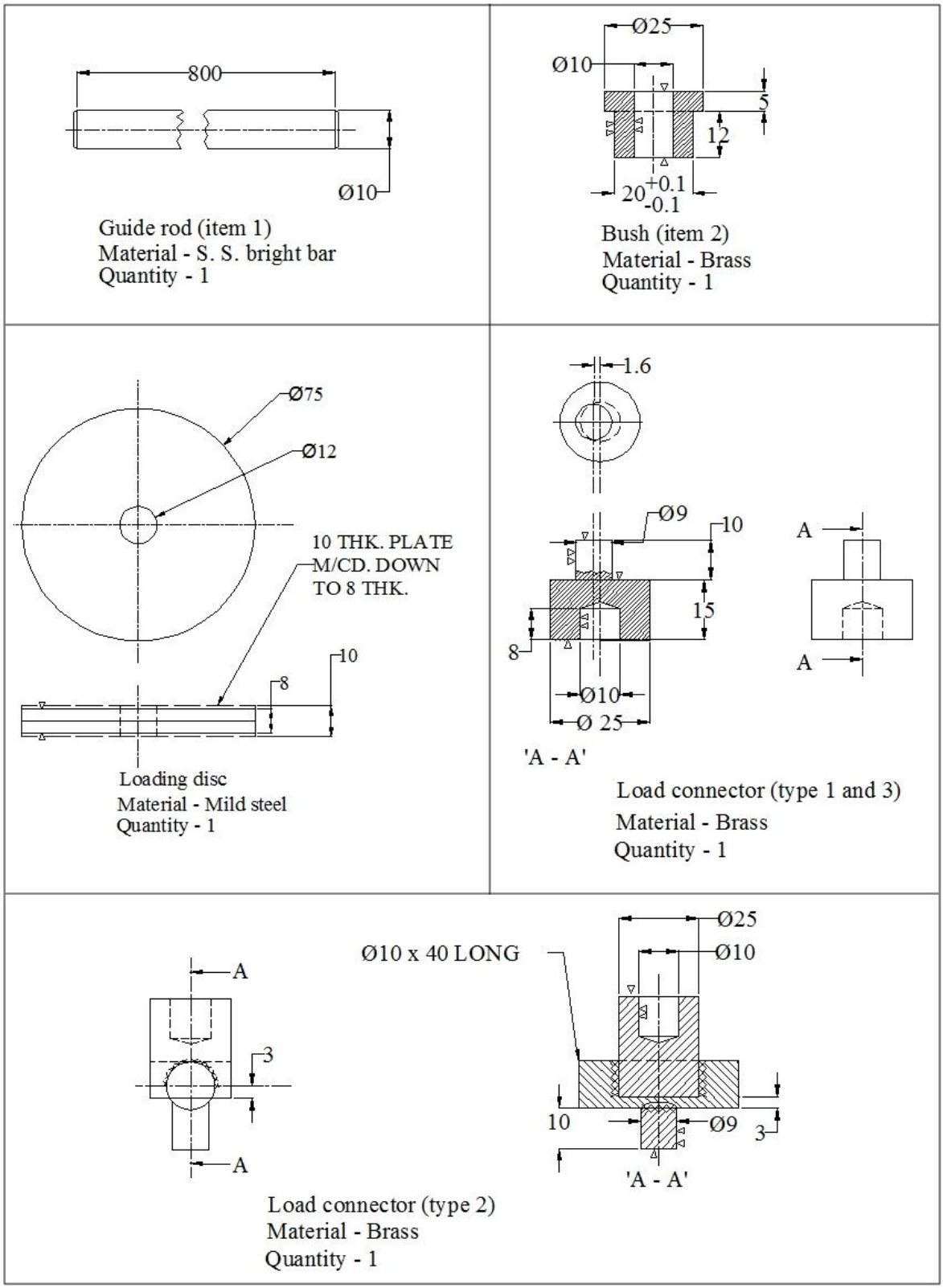

Fig. 4.7 (b) Details of guide rod, bush and load connector (items used to impart load).

The items used to impart load on the spring include guide rod (item 1), bush (item 2) and load connector (item 7) and their detailed drawings are furnished in Fig. 4.7 (b). Different

types of load connectors are used to produce line contact or area contact with leaf spring, at the location of arc length centre. Each load connector consists of a loading pin and a loading disc. Projected part of the loading pin is inserted in the drill hole of the master leaf spring and loading disc is placed over the pin. The vertical guide rod is then fitted to the loading pin through the central hole of the loading disc. The upper end of the guide rod passes through the bush, which is fitted on the guiding disc to restrict horizontal movement of the load.

4.3 Experimental procedure and observations

During experimentation, the master leaf spring is placed in the test rig in such a way that the central drill hole is in right side of geometrical centre line, when seen from the front of experimental set-up. As mentioned earlier, there are two types of load connector – area contact type and line contact type. Line contact type load connector produces eccentric loading with eccentricity 1.6 mm. Whereas, area contact type load connector produce concentric loading in one setting and eccentric loading with eccentricity 3.2 mm in reverse setting (due to the fact that area contact type load connector has eccentricity of 1.6 mm in itself). These three types of load connector settings are further referred as type 2, 1 and 3 respectively. For each of the loading conditions, loading is increased gradually by placing slotted discs over the particular type of load connector. The limit load is calculated by using bending stress equation of Winkler-Bach curved beam theory and taking 75% of yield stress value of spring steel material. Experimentation is carried out at seven different load steps (i = 1, …, 7) under each type of load connectors and i = 0 indicates the free state of the leaf spring. The first load step (i = 1) is designated as pre load, as no disc weight is mounted on load connector, but the guiding rod and load connector attachment produces an initial load on the leaf spring. For area and line contact type load connectors the pre load values are 8.142 N and 8.535 N respectively.

4.3.1. Deflection profiles

Experimental measurements for determination of deflection profile of the loaded leaf spring are not straight forward, as in the case of its measurement in free state. Deflection profiles of the master leaf spring under different loading conditions are determined by using two different techniques – direct measurement technique and indirect measurement technique. Results coming from these two measurement techniques and comparison between them are presented in the following three sub-sections.

4.3.1.1. Direct measurement technique

Table 4.2.1 x, y coordinates of marked points (refer Fig. 4.2) for load connector type 1

Location number	Load (N)						
	Pre load	83.679	159.216	234.753	310.290	384.846	470.193
2	-400, 31.55	-404, 30.55	-405, 30.55	-406, 26.95	-406, 27.55	-409, 26.55	-409, 25.55
3	-355, 52.55	-359, 51.55	-361, 47.55	-362, 44.95	-362, 43.05	-363, 42.05	-363, 37.55
4	-313, 70.55	-316, 67.05	-319, 62.55	-319, 57.95	-319, 54.55	-319.5, 52.55	-321, 47.55
5	-269, 87.55	-270, 81.55	-270, 76.55	-272, 72.95	-274, 69.15	-274, 62.55	-274, 56.55
9	-92, 123.55	-93, 116.55	-94, 104.55	-94, 97.75	-95, 90.25	-95, 83.05	-95, 71.05
10	-48, 126.55	-49, 118.05	-51, 108.05	-51, 100.35	-51.5, 92.75	-52, 84.55	-52, 73.05
11	0, 127.55	0, 120.05	0, 109.55	0, 101.35	0, 92.85	0, 85.55	0, 74.05
12	50, 126.55	51, 119.55	52, 108.55	53, 101.05	54, 90.75	55, 84.55	56, 73.05
13	96, 123.55	97, 114.55	99, 104.55	95, 96.35	96, 88.85	96, 81.05	96, 71.05
14	140, 116.55	140, 109.55	142, 98.55	143, 92.15	144, 85.85	145, 78.55	146, 69.55
17	274, 85.55	275, 81.55	276, 75.05	277, 69.65	277, 66.22	278, 61.55	279, 57.55
18	322, 69.55	323, 65.55	325, 60.55	326, 57.35	326, 55.45	327, 50.65	327, 48.05
19	366, 51.55	366, 48.95	370, 45.55	372, 43.05	373, 41.05	373, 38.55	373, 37.75
20	404, 33.55	405, 31.96	410, 28.05	411, 27.95	412, 27.55	413, 27.55	413, 25.05

As mentioned earlier, there are twenty one equally spaced points marked on the leaf spring along its centre line. At a particular load step under a particular load connector, span of the leaf spring is obtained directly from the readings of fixed plumb pointers along horizontal scale (item C). Horizontal coordinates (x) of the marked points are determined by taking

projections of these points over the horizontal scale by using a separate plumb (item A). Camber of the leaf spring is measured by using a height gauge (item B) and y coordinates of other marked points are also obtained by using the height gauge. However, out of the twenty one marked point, experimental reading is available in fourteen points only as the tip of the height gauge could not reach at seven locations. The observations are tabulated in Tables 4.2.1, 4.2.2 and 4.2.3 for the three different types of load connectors.

Table 4.2.2 x, y coordinates of marked points (refer Fig. 4.2) for load connector type 2

Location number	Load (N)						
	Pre load	84.072	159.609	235.146	310.683	385.239	470.586
2	-404, 33.85	-407, 33.15	-407.5, 32.65	-411, 29.95	-412, 29.65	-417, 28.65	-419, 25.95
3	-361, 52.15	-365, 51.35	-365.5, 49.65	-366, 47.95	-368, 43.15	-371, 41.65	-373, 38.95
4	-316, 72.15	-322, 67.65	-323, 63.15	-323, 60.95	-324, 56.65	-326, 53.15	-328, 46.75
5	-273, 89.35	-277, 82.15	-278, 78.15	-279, 72.95	-280, 67.25	-281, 62.35	-283, 53.75
9	-97, 122.15	-97, 114.85	-97, 107.55	-97, 99.75	-98, 92.35	-98, 81.95	-99, 68.95
10	-55, 126.15	-55, 118.25	-56, 111.55	-56, 103.35	-57, 94.85	-58, 85.25	-59, 72.35
11	0, 127.65	0, 120.05	0, 112.15	0, 104.35	0, 94.95	0, 85.65	0, 71.35
12	45, 127.15	45, 119.05	45, 111.15	45, 103.05	45, 92.85	45, 85.55	45, 70.95
13	90, 122.15	90.5, 115.55	90, 107.25	90.5, 99.35	91, 90.95	92, 84.95	93, 68.95
14	133, 116.15	134, 110.35	135, 102.95	136, 95.15	136, 87.95	136, 81.95	138, 66.65
17	267, 84.65	267, 82.15	272, 77.05	272, 75.05	272, 70.65	272, 63.05	280, 55.15
18	314, 68.85	316, 66.15	321, 63.65	322, 60.35	322, 57.55	323, 54.25	324, 46.75
19	359, 51.15	360, 49.15	365, 47.55	367, 46.05	367.5, 43.15	368, 42.65	370, 37.15
20	398, 33.65	400, 33.15	405, 32.15	407.5, 30.15	408, 29.65	406, 28.65	411, 27.45

Table 4.2.3 x, y coordinates of marked points (refer Fig. 4.2) for load connector type 3

Location number	Load (N)						
	Pre load	83.679	159.216	234.753	310.290	384.846	470.193
2	-402, 34.68	-404, 34.18	-408, 31.18	-409, 30.68	-411, 30.18	-412, 27.48	-415, 23.99
3	-359, 53.38	-362, 50.08	-365.5, 47.28	-367, 46.38	-369, 45.18	-370, 41.98	-372, 37.99
4	-315, 72.58	-318, 67.38	-320, 63.28	-322.5, 61.88	-323.5, 59.38	-323.5, 52.48	-324, 47.99
5	-272, 84.98	-272.5, 82.38	-273, 78.18	-275, 74.68	-276, 69.18	-277, 61.98	-280, 54.49
9	-95, 124.18	-96, 116.38	-97, 107.38	-98, 101.18	-98, 92.18	-99, 81.48	-99.5, 72.59
10	-53.5, 127.38	-54, 119.18	-56, 109.18	-56.5, 103.88	-56.5, 96.38	-56.4, 83.48	-56.5, 73.79
11	0, 127.48	0, 119.18	0, 110.28	0, 105.18	0, 96.88	0, 85.48	0, 73.99
12	49, 127.48	49, 119.05	49, 110.38	49.5, 103.68	49.5, 94.88	49.5, 83.28	49.5, 72.99
13	93.5, 123.38	94, 116.08	94.5, 106.38	95, 100.18	99, 91.38	99.5, 81.48	99.6, 71.99
14	134, 117.18	135, 109.68	136, 102.18	136.5, 97.78	137, 89.38	137.5, 78.48	138, 68.49
17	367, 86.78	268, 83.48	269, 78.58	269.5, 75.48	270, 68.68	272.5, 61.48	273, 54.79
18	318, 70.38	319, 66.78	321, 63.38	322, 61.48	323, 57.08	324, 50.68	325, 46.19
19	362, 52.38	363, 48.98	365, 47.38	367, 45.88	368, 41.18	370, 37.98	372, 35.19
20	400, 33.18	401, 32.68	403, 32.28	405, 31.68	407, 31.18	410, 26.48	413, 25.99

4.3.1.2. Indirect measurement technique

At each step of loading, deflection profile of the master leaf spring is captured from front by using a digital camera and recorded in computer for post processing. Photographs of deflection profiles at each load step under the three types of load connectors are presented in Figs. 4.8.1, 4.8.2 and 4.8.3.

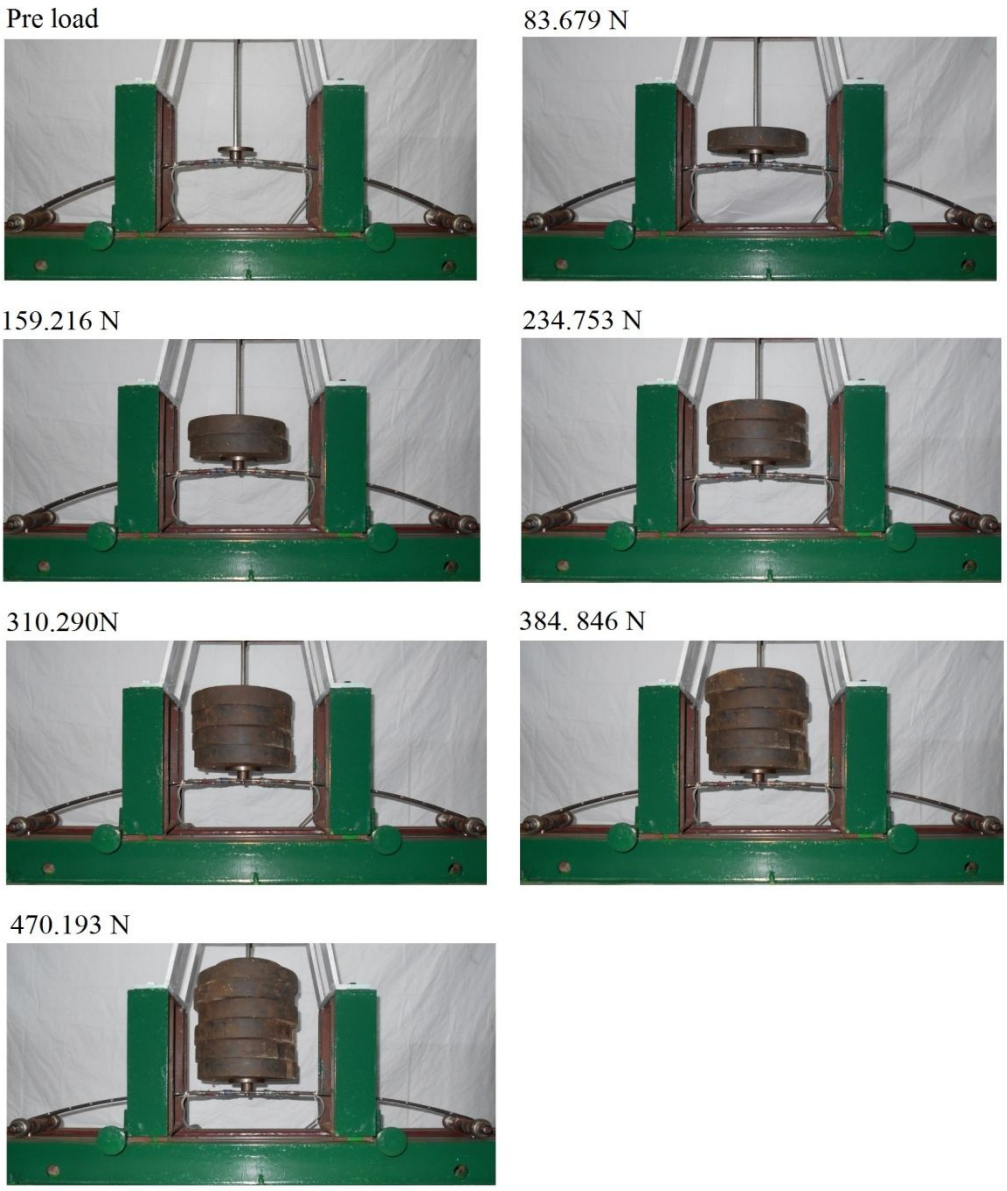

Fig. 4.8.1 Photographs of the master leaf spring at different load steps under load connector type 1.

Taking each photograph of Fig. 4.8 as background in the editor of AutoCAD® software, centres of the rollers are located. Then the horizontal line between the two roller centres and the vertical load line are drawn. Intersection point of these two straight lines is considered as origin of present coordinate system. Thereafter, roller pitch circles are drawn and the centre line of the master leaf is drawn making its ends tangential to the roller pitch circles. These points of tangencies are denoted by A_1 and B_1 for left roller and right roller respectively. Two straight lines are drawn between left eye centre and A_1 and between right eye centre and B_1 respectively. Reaction forces coming from roller supports acts along these

straight lines at left and right ends of master leaf spring respectively. Angles of these straight lines with negative and positive x axis are denoted by α_L and α_R (refer Fig. 4.9) and called reaction force angles at left and right rollers respectively. Then the drawing is scaled with respect to the origin by using appropriate scale factors along x and y direction. Scaling along x direction is done with respect to the span of the master leaf at that particular load step. Whereas, scaling along y direction is done with camber of the spring at that particular load step. AutoCAD® drawings of curvature lines of the master leaf spring, constructed from the photographs of leaf spring, shown in Fig. 4.8, are presented in Figs. 4.9.1, 4.9.2 and 4.9.3.

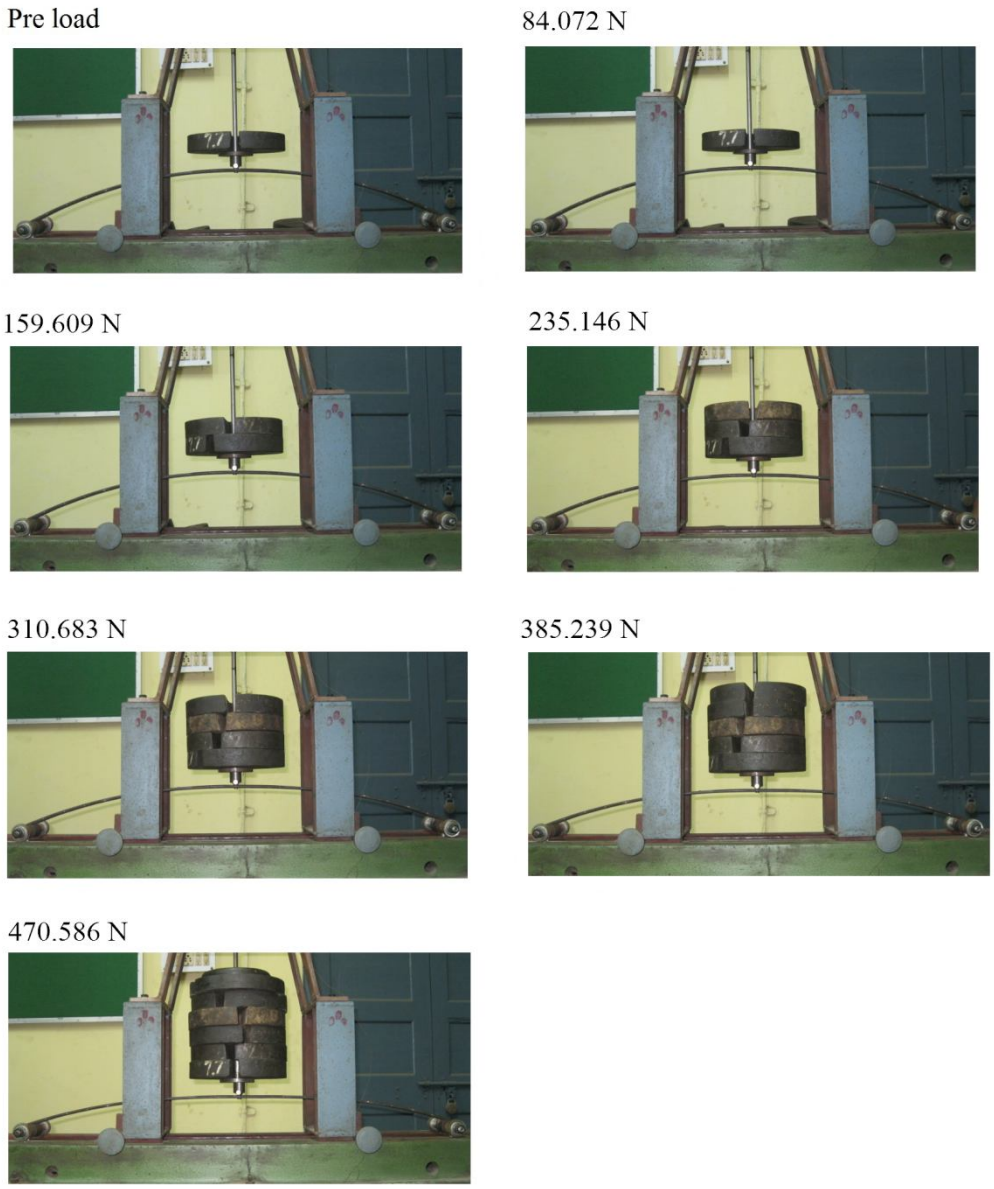

Fig. 4.8.2 Photographs of the master leaf spring at different load steps under load connector type 2.

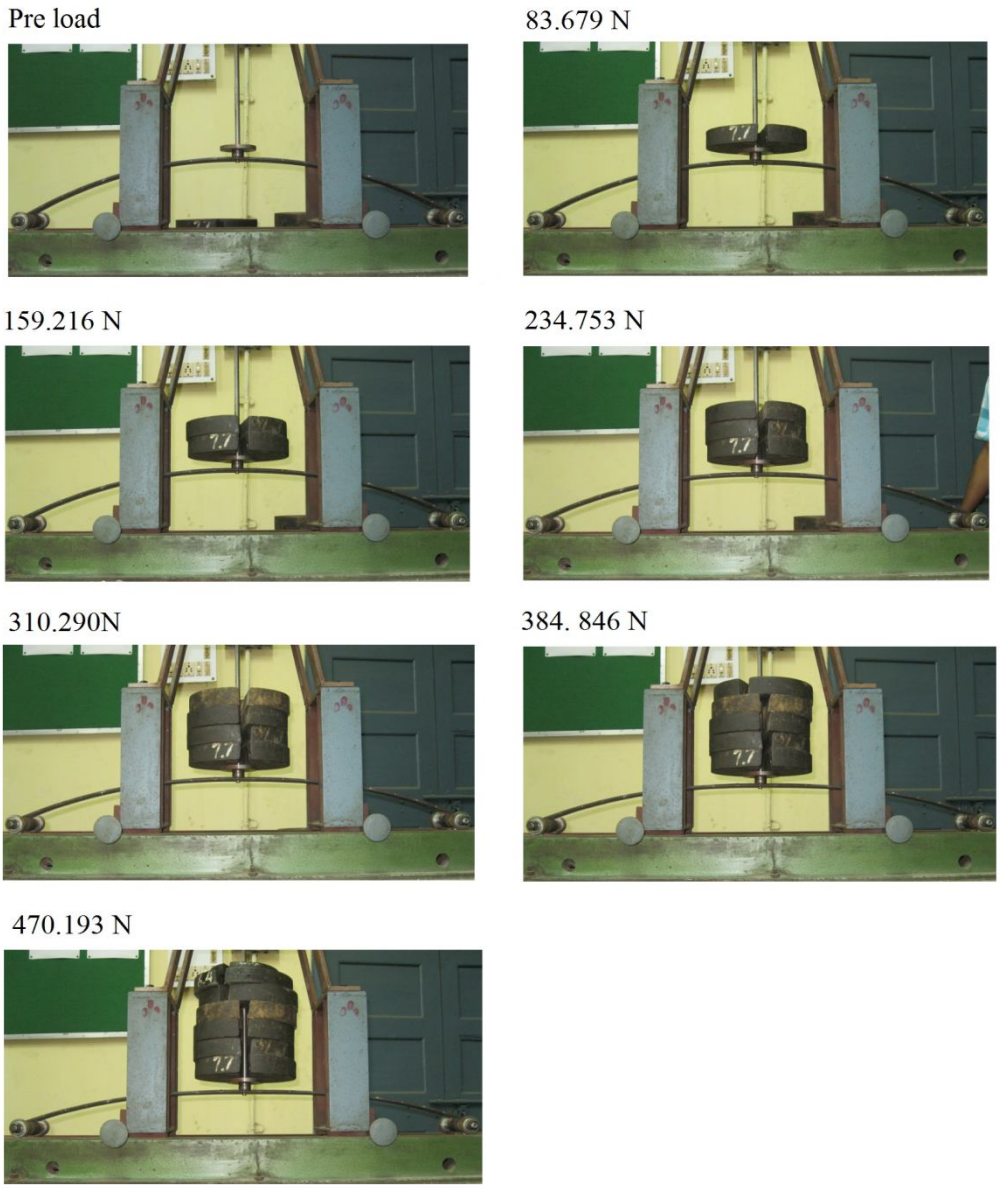

Fig. 4.8.3 Photographs of the master leaf spring at different load steps under load connector type 3.

Now the projected length of curve $\overset{\frown}{A_1B_1}$ is divided into twenty equal divisions. x, y coordinates of each division points are measured from the drawing and exported in a data file by using an auto-lisp code. For each type of load connector, seven such data files are generated with appropriate file names. At each step of loading under each type of load connector, reaction force angles α_L and α_R and arc length of master leaf spring $\overset{\frown}{A_1B_1}$ are measured and tabulated in Tables 4.3.1, 4.3.2 and 4.3.3 for load connectors 1, 2 and 3 respectively.

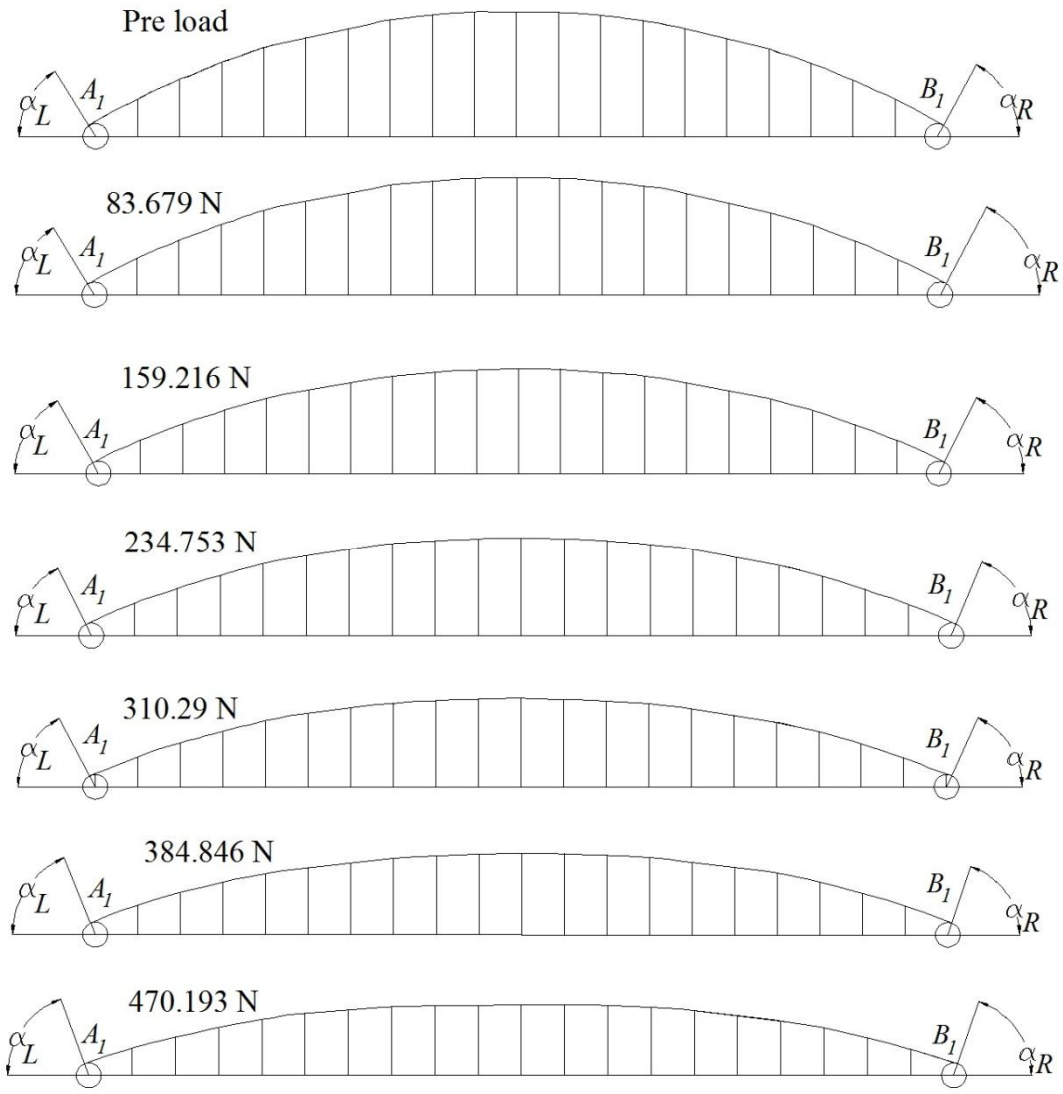

Fig. 4.9.1 Curvature lines of the master leaf spring at different load steps under load connector type 1.

Table 4.3.1 Variations of reaction force angles and arc length with load under load connector 1

Load (N)	α_L (º)	α_R (º)	Arc ($\overset{\frown}{A_1B_1}$) length (mm)
Pre load	58	62	918.51
83.679	59	62	919.39
159.216	61	64	924.67
234.753	63	67	923.80
310.290	65	68	923.38
384.846	68	72	922.53
470.193	70	73	925.72

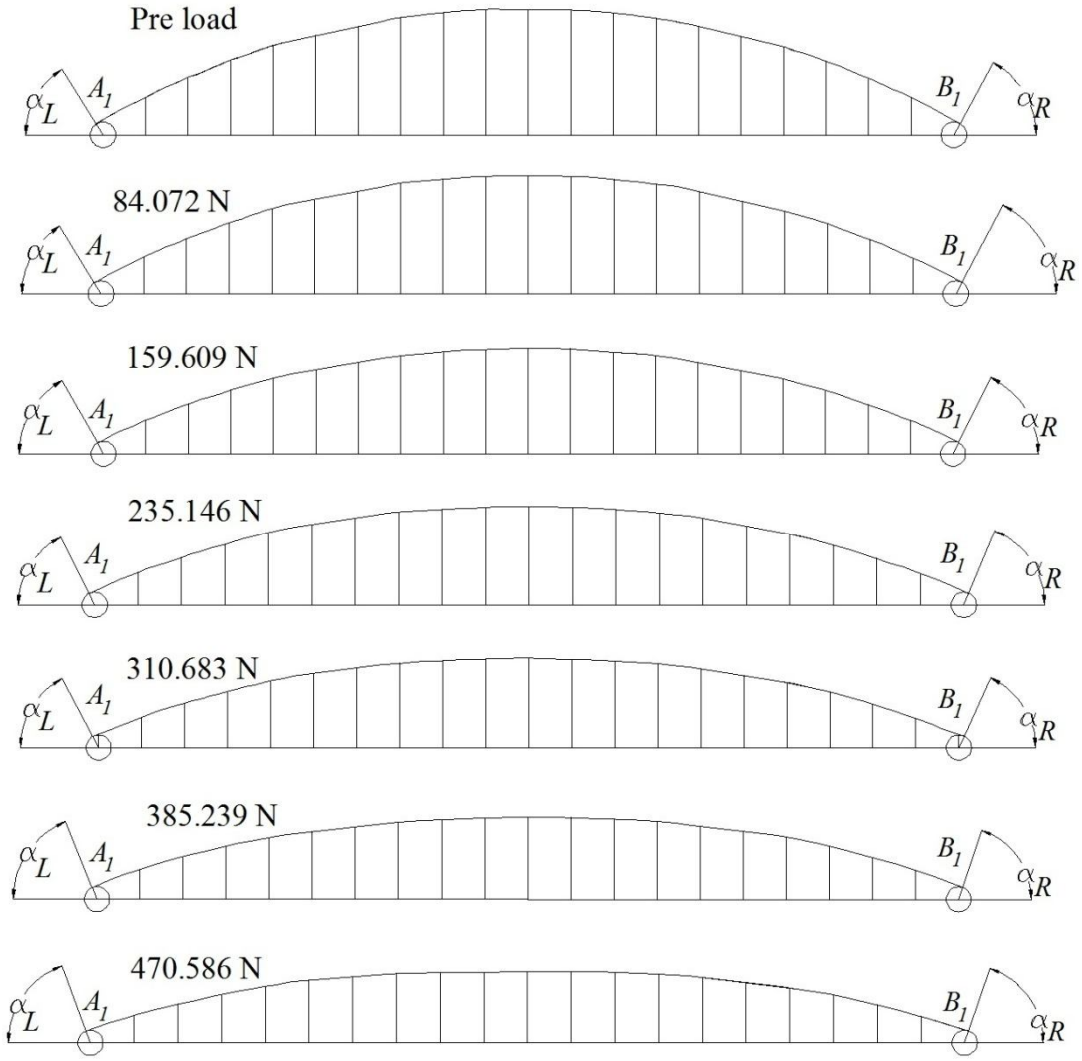

Fig. 4.9.2 Curvature lines of the master leaf spring at different load steps under load connector type 2.

Table 4.3.2 Variations of reaction force angles and arc length with load under load connector 2

Load (N)	α_L (º)	α_R (º)	Arc ($\overset{\frown}{A_1B_1}$) length (mm)
Pre load	58	62	925.18
84.072	60	64	924.07
159.609	62	64	924.99
235.146	64	67	925.76
310.683	65	68	926.48
385.239	66	72	925.28
470.586	68	75	925.61

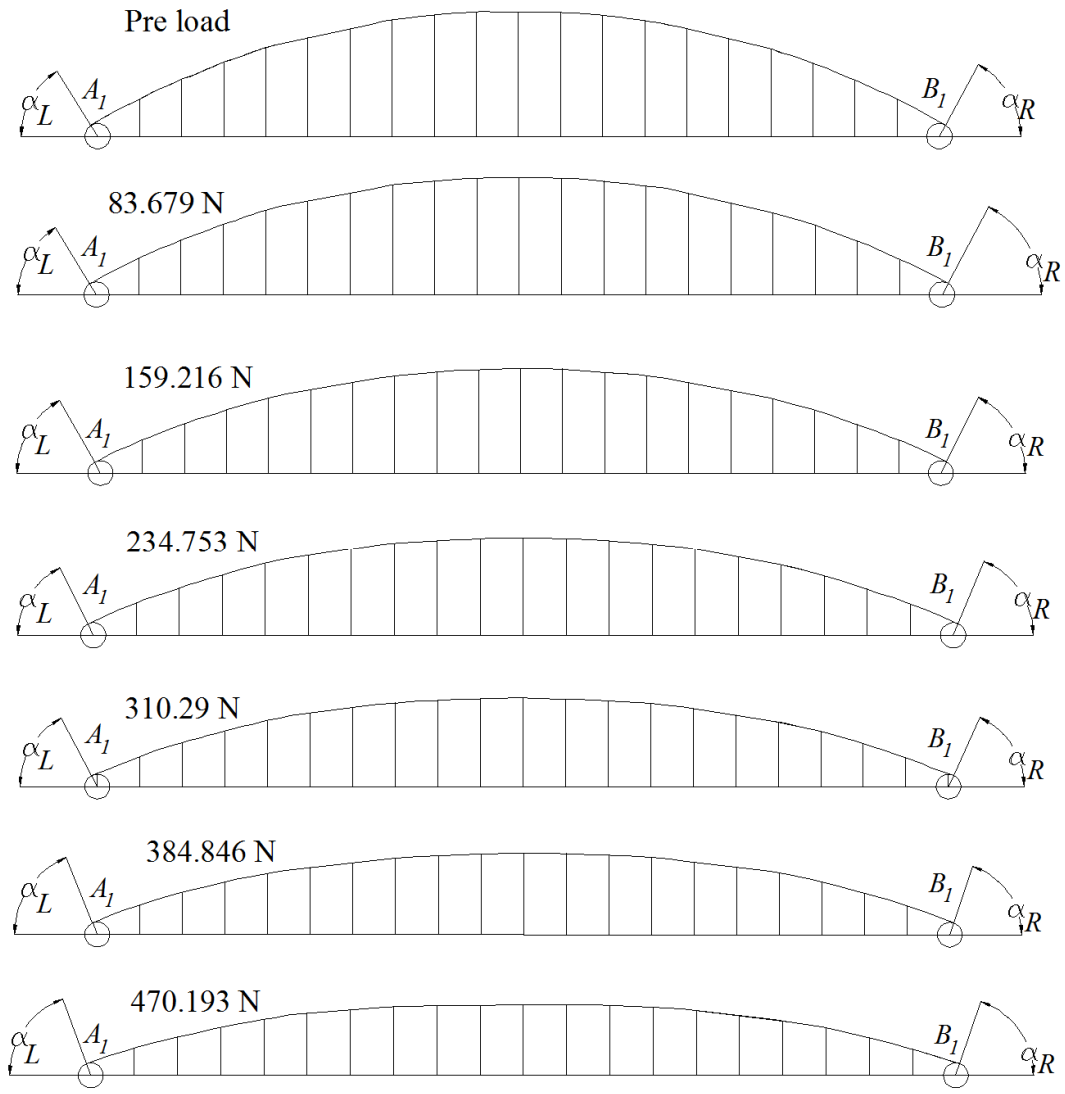

Fig. 4.9.3 Curvature lines of the master leaf spring at different load steps under load connector type 3.

Table 4.3.3 Variations of reaction force angles and arc length with load under load connector 3

Load (N)	α_L (°)	α_R (°)	Arc ($\overset{\frown}{A_1B_1}$) length (mm)
Pre load	60	61	921.69
83.679	62	62	917.93
159.216	63	64	919.8
234.753	63	64	925.16
310.290	64	65	923.25
384.846	66	67	926.48
470.193	67	68	927.26

4.3.1.3. Comparison between the measurement techniques

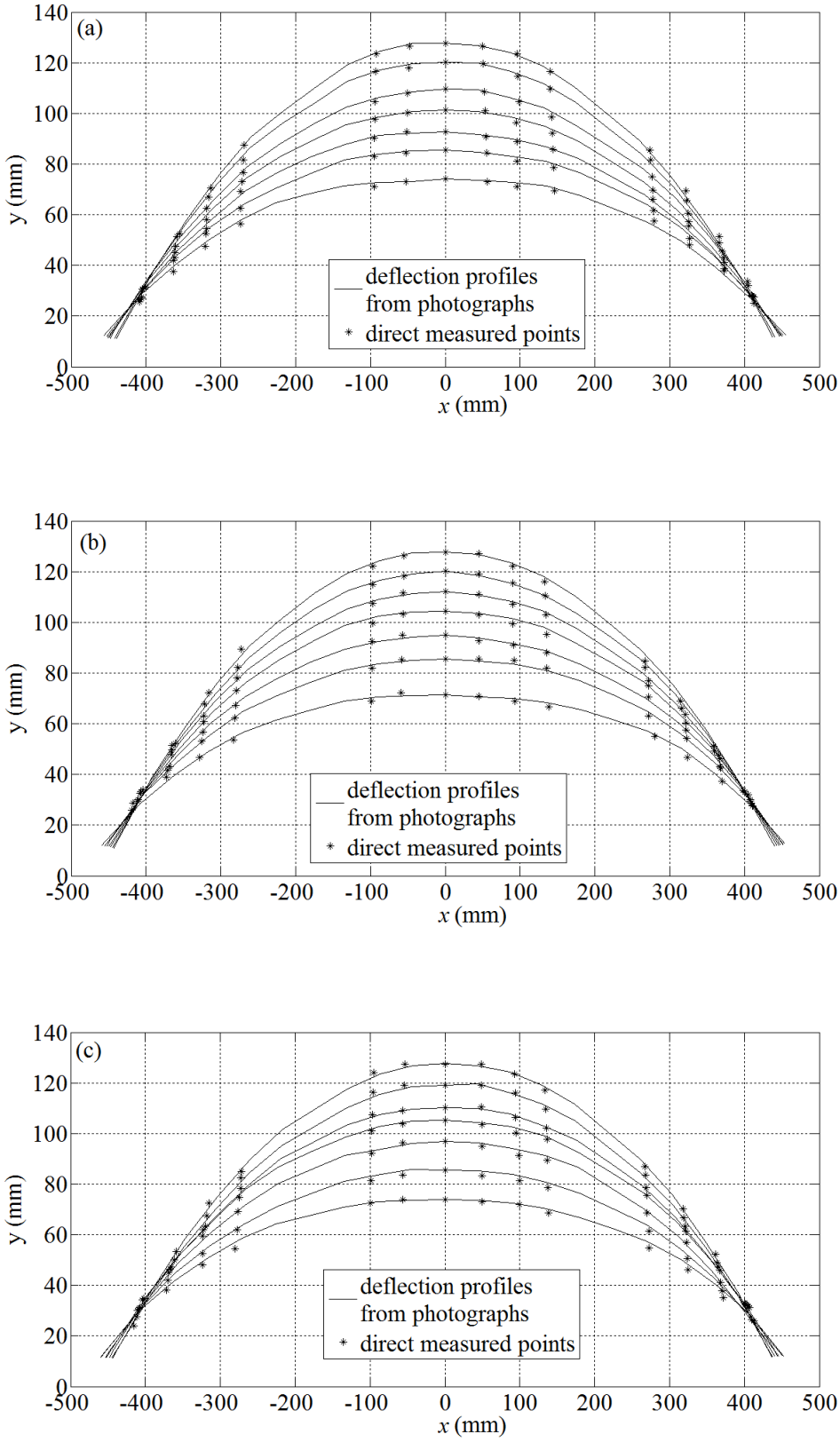

Fig. 4.10 Deflection profiles of the master leaf spring at different load steps under (a) load connector 1, (b) load connector 2 and (c) load connector 3.

The data files obtained from AutoCAD® by post processing photographs, are exported in MATLAB® computational platform. Deflection profiles of the master leaf spring under each of the loading conditions are drawn once again as MATLAB® plots. These deflection profiles, coming from each type of load connectors, are clubbed together and presented in Fig. 4.10 (a-c). The figure also shows results from direct measurement and hence a comparison between the two measurement methods are results obtained. Effect of loading type on the patterns of deflection profiles, produced by the three load connectors are carried out corresponding to the maximum load and shown in Fig. 4.11. It is observed that line contact type load connector has some effect on deflection profile.

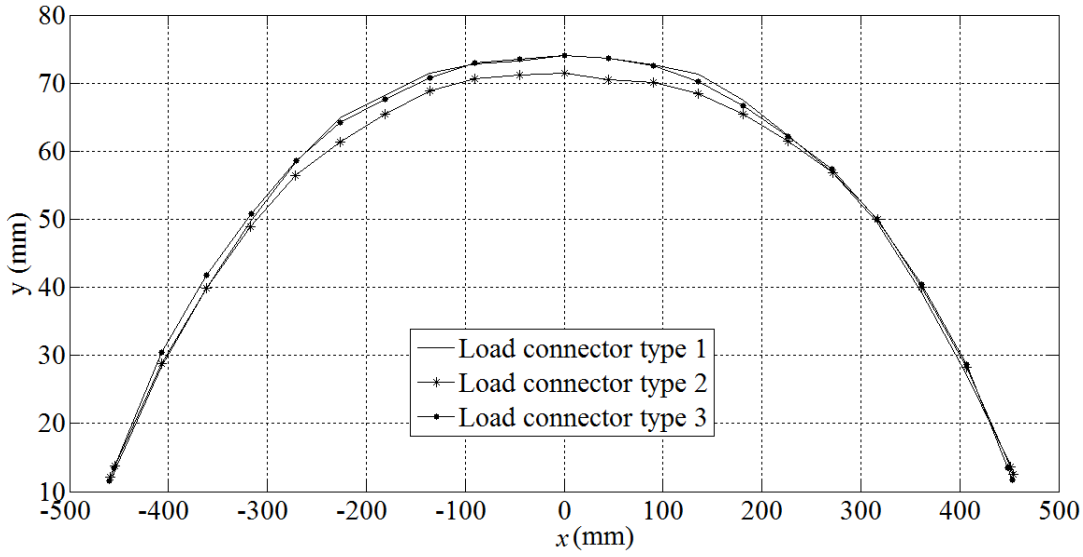

Fig. 4.11 Effect of load connector type on deflection profile.

4.3.2. Strain readings

Strains developed at the location of strain gauges in left side of the drill hole are measured by using a full-bridge circuit with strain gauges 1, 3, 2 and 4, whereas, strain gauges 5, 7, 6 and 8 are used to measure strains in right side of the drill hole (refer Fig. 4.3 (b)). At pre-load condition, each circuit is balanced by setting zero in the strain indicator. Strain readings, indicated in strain indicator at different loading conditions, are presented in Tables 4.4.1 and 4.4.2 for left and right sides respectively.

Table 4.4.1 Strain readings (micro) at left side

Load (N)	Load connector		
	Type 1	Type 2	Type 3
75.537	388	401.75	361.375
151.074	779.625	783.875	674.875
226.611	1179.375	1113.25	1103.875
302.148	1598.5	1560.125	1556.875
376.704	2025	1876.25	1877.875
462.051	2362.5	2300.75	2315.25

Table 4.4.2 Strain readings (micro) at right side

Load (N)	Load connector		
	Type 1	Type 2	Type 3
75.537	381.125	403.5	363.5
151.074	768.125	788.375	677.875
226.611	1173.125	1120.25	1119.25
302.148	1589.5	1570.625	1542.375
376.704	1994.5	1888.875	1905.625
462.051	2341	2316.5	2348.25

Individual strain gauge readings are also observed at each loading condition by using quarter-bridge circuits. A dummy gauge is used to complete each quarter-bridge circuit, which is mounted on a piece of the same material as the leaf spring. These individual strain gauge readings are presented in Tables 4.5.1, 4.5.2 and 4.5.3 for load connectors 1, 2 and 3 respectively.

Table 4.5.1 Individual strain gauge readings (micro) under load connector 1

Load (N)	Individual strain gauge readings							
	1	2	3	4	5	6	7	8
75.537	-160	-158	160	161	-168	-166	156	156
151.074	-332	-350	330	325	-352	-346	363	346
226.611	-553	-544	525	522	-544	-580	473	565
302.148	-721	-705	711	715	-741	-746	710	713
376.704	-926	-914	878	902	-962	-878	895	924
462.051	-1033	-1110	1072	1099	-1118	-1175	1075	1125

Table 4.5.2 Individual strain gauge readings (micro) under load connector 2

Load (N)	Individual strain gauge readings							
	1	2	3	4	5	6	7	8
75.537	-333	-396	340	250	-309	-320	355	365
151.074	-678	-788	745	530	-702	-680	715	755
226.611	-1058	-1207	1190	825	-1087	-1150	1100	1135
302.148	-1400	-1565	1532	1117	-1325	-1505	1475	1515
376.704	-1770	-1868	1860	1360	-1837	-1900	1845	1810
462.051	-2208	-2477	2410	1620	-2205	-2355	2225	2365

Table 4.5.3 Individual strain gauge readings (micro) under load connector 3

Load (N)	Individual strain gauge readings							
	1	2	3	4	5	6	7	8
75.537	-313	-168	158	163	-393	-378	365	378
151.074	-785	-341	325	327	-793	-792	755	748
226.611	-1238	-517	504	502	-1180	-1185	1162	1162
302.148	-1650	-707	687	693	-1593	-1618	1519	1599
376.704	-2137	-869	826	887	-2001	-2028	1914	1956
462.051	-2506	-1068	1047	1069	-2430	-2497	2492	2475

4.4 Theoretical stress analysis

For the purpose of comparison of experimental stress results with theoretical ones, master leaf spring is modeled as curved beam subjected to three point bending. Stress field developed in such curved beam under different loading conditions is calculated by using Winkler-Bach curved beam theory. Mathematical formulation of the problem and comparison between theoretical and experimental stress results are presented in the following two sub-sections.

4.4.1 Mathematical formulation

Free body diagram (FBD) of the master leaf is shown in Fig. 4.12 (a) by modeling it as an initially curved beam under three point bending. The FBD is drawn in equilibrium position attained after application of load and point A_1 is considered as origin of the present coordinate system O_{xyz}. At a particular load step, distance of load line from O_{xyz} is L_W, where horizontal restraining force P develops with load W due to the geometric asymmetry

of the master leaf. Reaction forces at left and right ends of the curved beam are R_L and R_R respectively coming from the roller supports. The lines of action of these forces make angle α_L and α_R with negative and positive x axis. Reaction force coming from left roller R_L has components (P_{xL}, P_{yL}) and in case of the right end roller, components of R_R are (P_{xR}, P_{yR}).

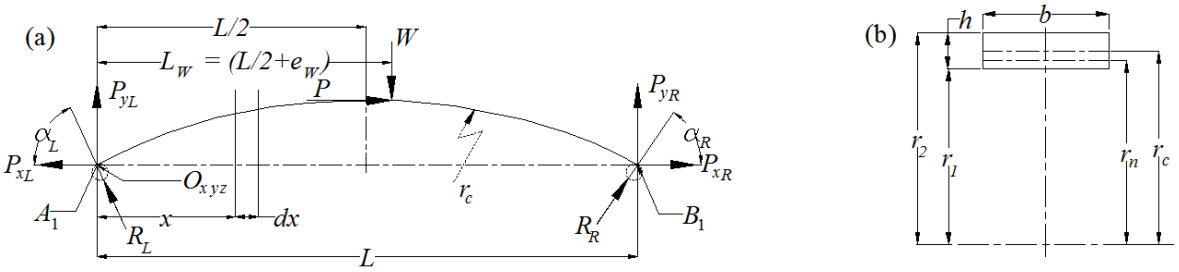

Fig. 4.12 (a) Free body diagram and (b) cross-section of curved beam in normal plane.

From force equilibrium condition in vertical and horizontal directions: $W = P_{yL} + P_{yR}$ and $P = P_{xL} - P_{xR}$. Taking moment of all forces about point A_1, $P_{yR} = (WL_W + PH_W)/L$ and $P_{yL} = W - P_{yR}$, where H_W is y coordinate of master leaf profile at $x = L_W$. Horizontal components of reaction forces at left and right ends are $P_{xL} = P_{yL}/\tan\alpha_L$ and $P_{xR} = P_{yR}/\tan\alpha_R$ respectively, which yields restraining force P at load application point. At location x ($0 \leq x \leq L$) shear force and bending moment are given by,

$$V_x = \begin{cases} P_{yL}, & 0 \leq x \leq L_W \\ P_{yL} - W, & L_W \leq x \leq L \end{cases} \tag{4.1}$$

$$M_x = \begin{cases} P_{yL}\,x + P_{xL}\,y, & 0 \leq x \leq L_W \\ P_{yL}\,x + P_{xL}\,y - W(x - L_W) + P(H_W - y), & L_W \leq x \leq L \end{cases} \tag{4.2}$$

According to Winkler-Bach formula, bending stress developed in the beam at location x ($0 \leq x \leq L$) is given by,

$$\sigma_{bx} = -M_x\,y/A\,e(r_n - y). \tag{4.3}$$

For rectangular cross-section, as shown in Fig. 4.12 (b), radius of curvature of neutral axis is given by $r_n = h/[\ln(r_2/r_1)]$.

4.4.2 Comparison with experimental results

Profiles of the master leaf spring under each of the load connectors are exported in MATLAB® computational platform. Now N_f (number of computational points within the

domain of the physical system) number of points is taken on the leaf spring profile and at each of these points bending moment is calculated from Eq. (4.2). As the leaf spring profile has non-uniform curvature, radii of curvature of its centroidal axis and neutral axis are calculated numerically at each of the N_f points. Thereafter, bending stress is calculated at each point from Eq. (4.3). Stress fields developed in the master leaf at different load steps under load connector type 1 are presented in Fig. 4.13. The stress fields produced by other two load connectors are also shown in the figure corresponding to the maximum load, and it is observed that effect of loading type variation is insignificant.

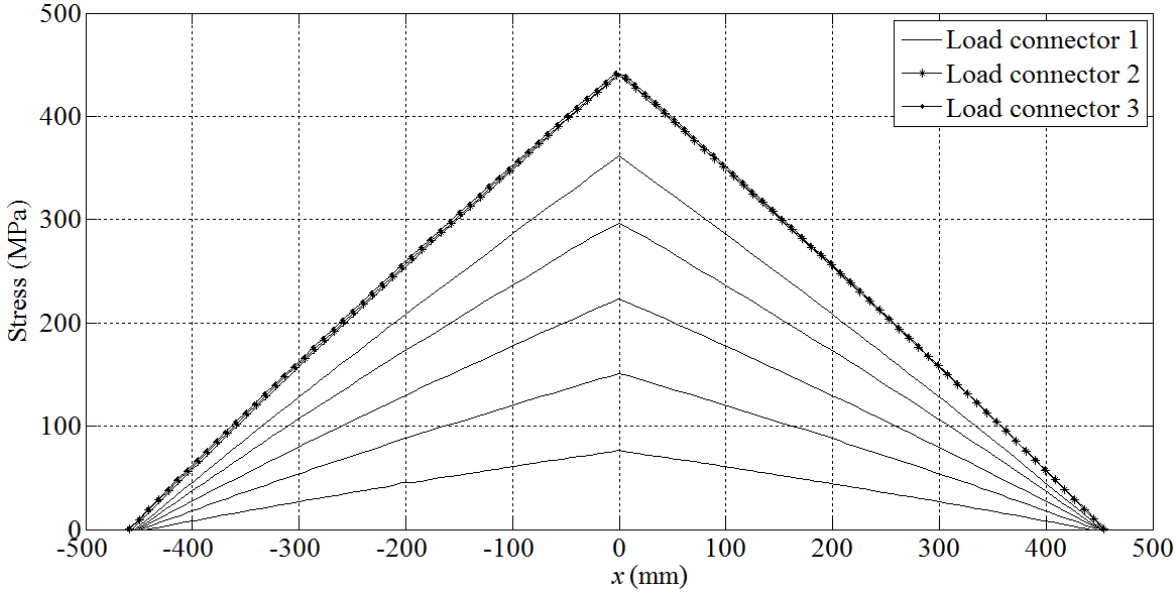

Fig. 4.13 Stress field developed in the master leaf under load connector 1 and effect of connector type on stress field.

Experimental strain values, presented in Tables 4.4.1 and 4.4.2, are multiplied by modulus of elasticity of the spring material (considered as 207 GPa) to get stresses developed at the locations of strain gauges in left and right sides of the hole under each load step. These experimental stresses developed in the master leaf under load connector type1 are presented in Fig. 4.14. Figure 4.14 also show theoretical stress values at the locations of strain gauges under load connector type 1 calculated from stress field presented in Fig. 4.13. Individual plots of experimental and theoretical stress are regular indicating definite trends in results but they are not matching and the error increases with the load. The presence of hole in master leaf spring might be a possible source of error.

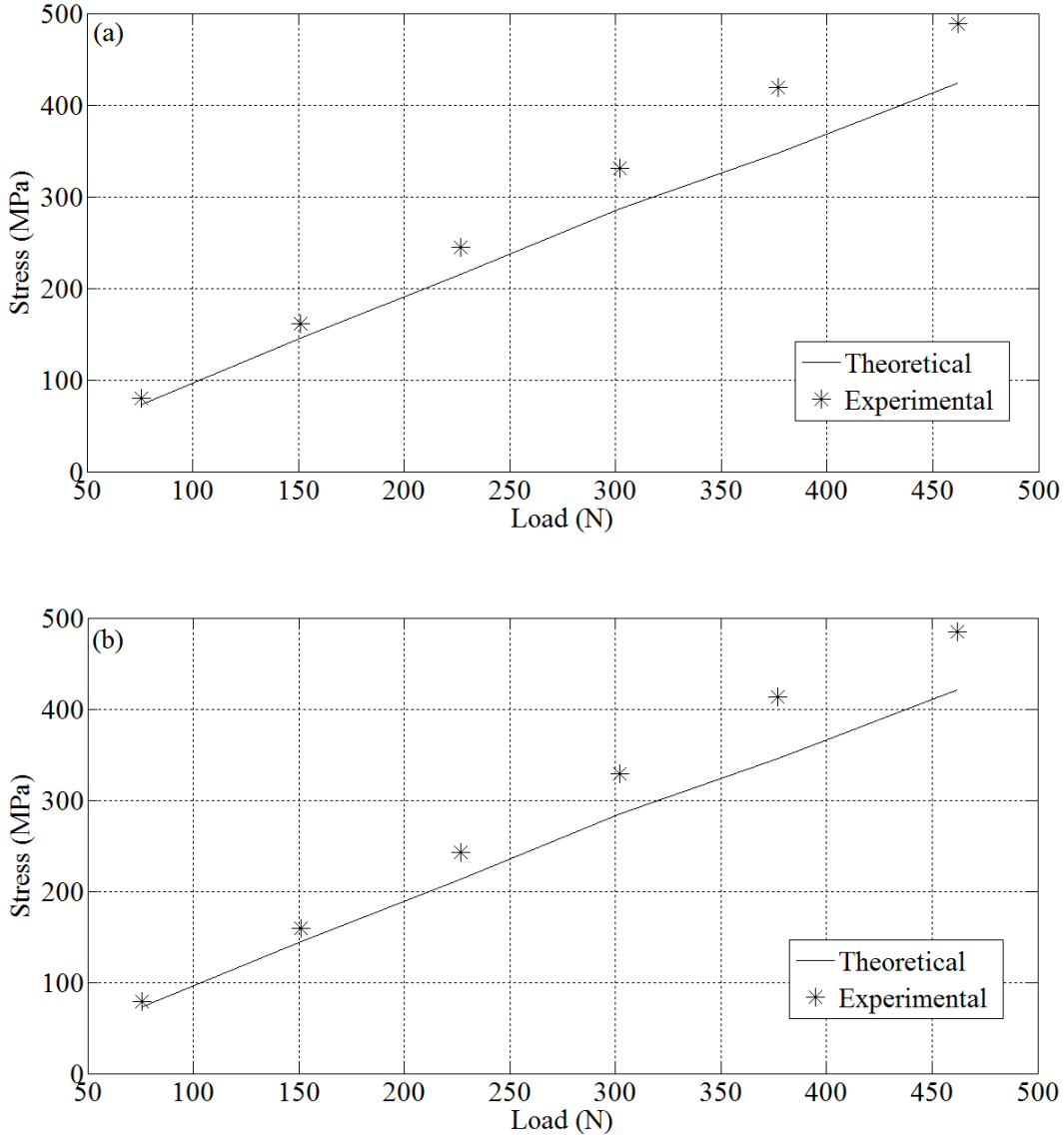

Fig. 4.14 Load vs. stress plots at (a) left and (b) right sides of the hole.

A correction in the cross-sectional area of the master leaf is done to capture the effect of hole in stress field developed in the master leaf. In this correction, it is assumed (Ryan and Fischer (1938)) that stress concentration is effective within the region five times the hole diameter (d) from centre of hole along x axis in both left and right sides. At centre of the hole, net cross-sectional area of the master leaf is $A_n = A - dh$. In both sides of the drill hole, cross-sectional area is varied linearly between A at boundaries of the stress concentration effected region and A_n at hole centre. Now with this correction, the theoretical stress results at locations of strain gauges are calculated under each load step and presented in Fig. 4.15. The figure also shows comparison between theoretical and experimental results and it is clearly seen that they are matching quite well. So it is obvious from these results that

presence of hole in master leaf spring produces stress concentration effect. In addition, the beam is not only subjected to bending but there is in plane tensile load as well. Effect of these factors in stress field is presented in the next section.

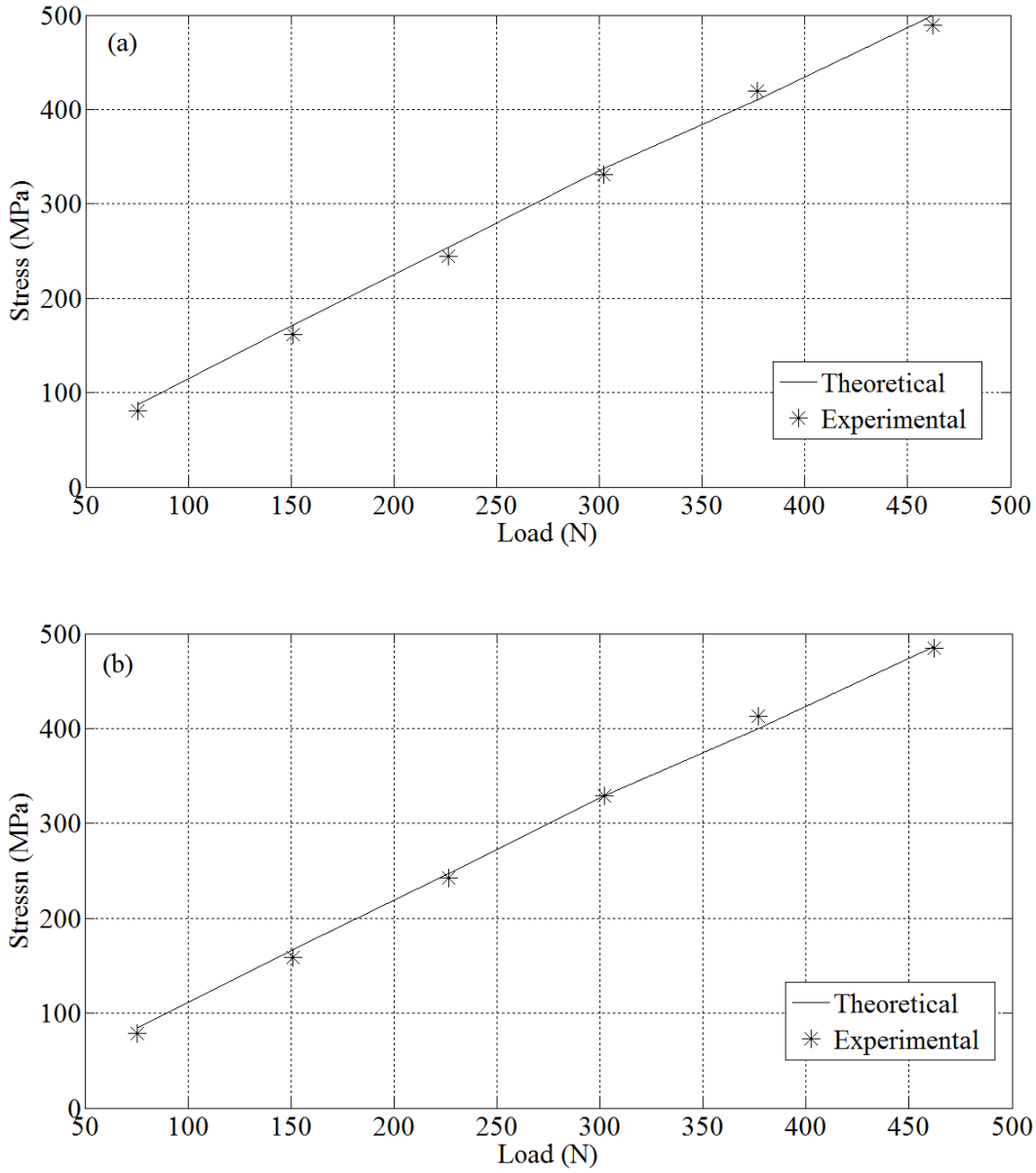

Fig. 4.15 Load vs. stress plots at (a) left and (b) right sides of the hole with correction.

4.5 Stress concentration effect

At location x $(0 \leq x \leq L)$ in plane load is given by $P_{tx} = P_{xL}\cos\varphi_x - V_x \sin\varphi_x$, where φ_x is slope of the beam profile at that location. This in plane load produces axial stress which is given by,

$$\sigma_{tx} = P_{tx}/b\,h \tag{4.4}$$

So at location x ($0 \leq x \leq L$), the beam is subjected to combined stress σ which is given by,

$$\sigma = \sigma_{bx} + \sigma_{tx} \tag{4.5}$$

Presence of circular hole in master leaf spring gives rise to stress concentration. Overall stress distributions around a circular hole in an infinite plate subjected to nominal stress σ, as given by Nagpal et al. (2011), are

$$\begin{aligned}\sigma_r &= (\sigma/2)[(1-\lambda^2) + (1+3\lambda^4 - 4\lambda^2)\cos(2\theta)] \\ \sigma_\theta &= (\sigma/2)[(1+\lambda^2) - (1+3\lambda^4)\cos(2\theta)] \\ \sigma_{r\theta} &= -(\sigma/2)[(1-3\lambda^4 + 2\lambda^2)\sin(2\theta)]\end{aligned} \tag{4.6}$$

In the above equations, $\lambda = a/r$, a is the radius of hole (refer Fig. 4.16). Due to the state of stress (σ_r, σ_θ, $\sigma_{r\theta}$) at point (r, θ), the induced stress along x axis is back calculated using the analytical form of Mohr's circle,

$$\sigma_x = \left[\frac{(\sigma_r+\sigma_\theta)}{2}\right] + \left[\frac{(\sigma_r-\sigma_\theta)}{2}\right]\cos 2(180-\theta) + \sigma_{r\theta}\sin 2(180-\theta) \tag{4.7}$$

4.5.1 Result and discussion

As discussed in the previous section, stress distribution around a hole in a loaded mechanical structure is highly sensitive to location (r, θ) with respect to the hole centre. Thus, actual locations of strain gauges around the drill hole in master leaf spring are required for stress calculation at strain gauge locations. To measure actual positions of strain gauges, photographs shown in Fig. 4.3 (b) are taken as background in the editor of AutoCAD® software. Then following the technique used for determining deflection profiles from photographs, actual positions $\{(x_i, y_i), i = 1, 2, \ldots, N_{sg}$(number of strain gauges)$\}$ of strain gauges are obtained and presented in Table 4.6. Positions of strain gauges are also shown in Fig. 4.16 through schematic diagram. Centre of the drill hole is considered as origin of the present coordinate system and scaling of drawing is done with width of the master leaf spring.

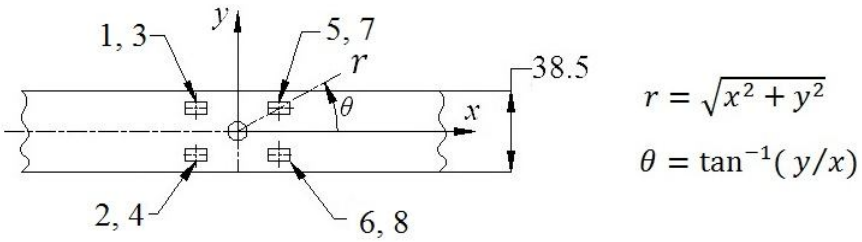

Fig. 4.16 Exact locations of strain gauges.

Table 4.6 Locations of strain gauges in Cartesian and polar coordinates

Strain gauge	x	y	r	θ (º)
1	-20.1227	12.7044	23.798	147.733
2	-21.6162	-11.9744	24.711	208.984
3	-21.0495	13.1993	24.846	147.910
4	-20.9790	-12.4150	24.377	210.616
5	20.7508	12.0027	23.972	30.046
6	21.4540	-12.3413	24.750	330.091
7	20.8382	13.7341	24.957	33.388
8	21.6691	-11.4341	24.500	332.181

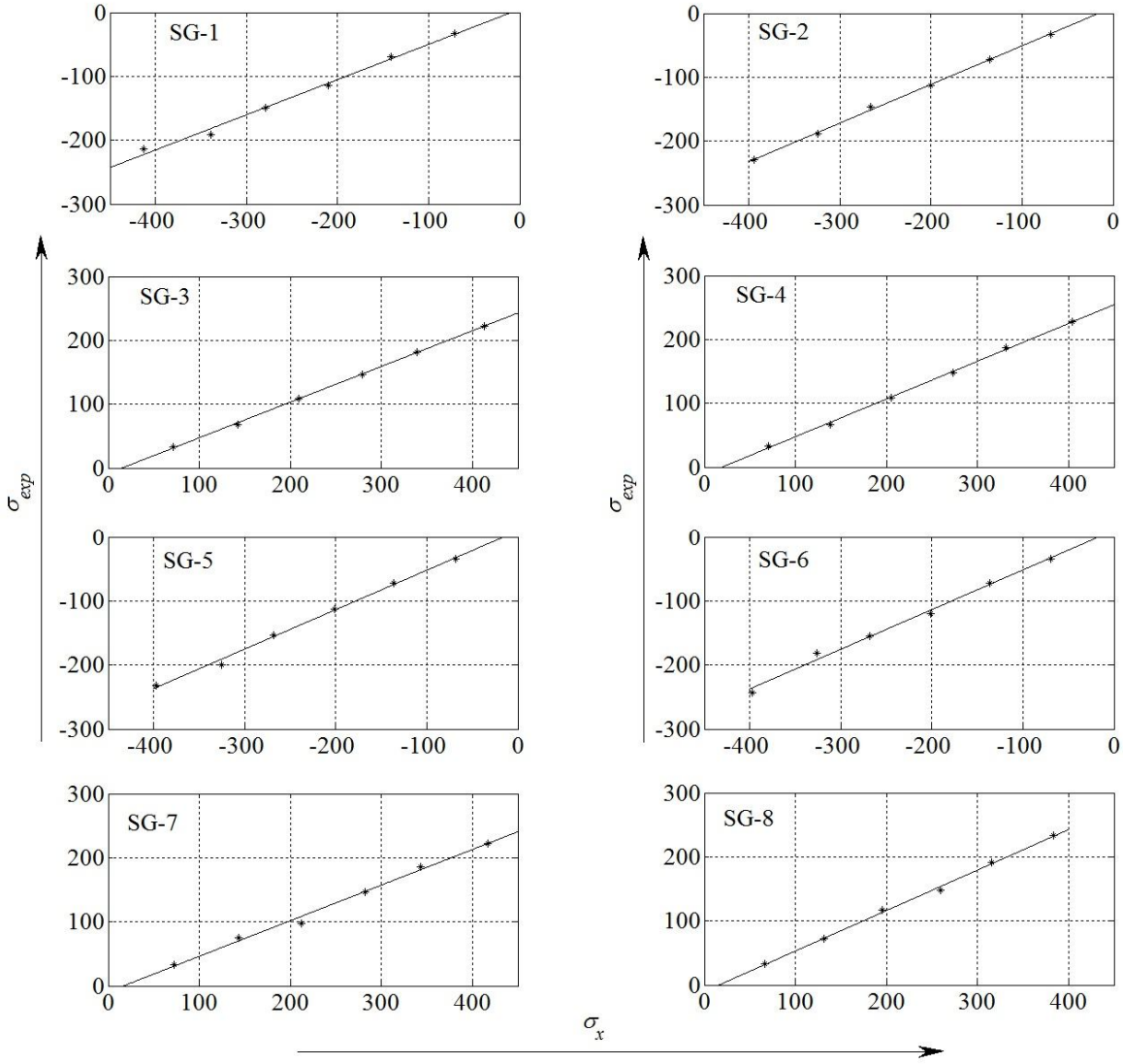

Fig. 4.17 Theoretical vs. experimental stresses for the eight strain gauges under load connector 1.

Once again, profiles of the master leaf spring at each load steps under load connector 1 are exported in MATLAB® computational platform. Now locations of strain gauges, as shown in Table 4.6, are taken on the leaf spring profile and at each of these N_{sg} points shear force and bending moment are calculated from Eqs. (4.1) and (4.2) respectively. Thereafter, combined stresses at locations of each strain gauge are calculated by calculating bending stress and in plane tensile stress from Eqs. (4.3) and (4.4) respectively. At each of these locations, induced stress along x axis due to presence of drill hole is calculated using Eq. (4.7). It is apparent that Eq. (4.7) has an in-built stress concentration factor, applicable for flat infinite plates with a circular hole under uniform uniaxial loading. Experimental stress values σ_{exp} at locations of strain gauges are obtained by multiplying experimental strain values presented in Table 4.5.1 with modulus of elasticity of spring material. Experimental stress values are plotted against theoretical stress values σ_x at each strain gauge location under load connector 1 and presented in Fig. 4.17.

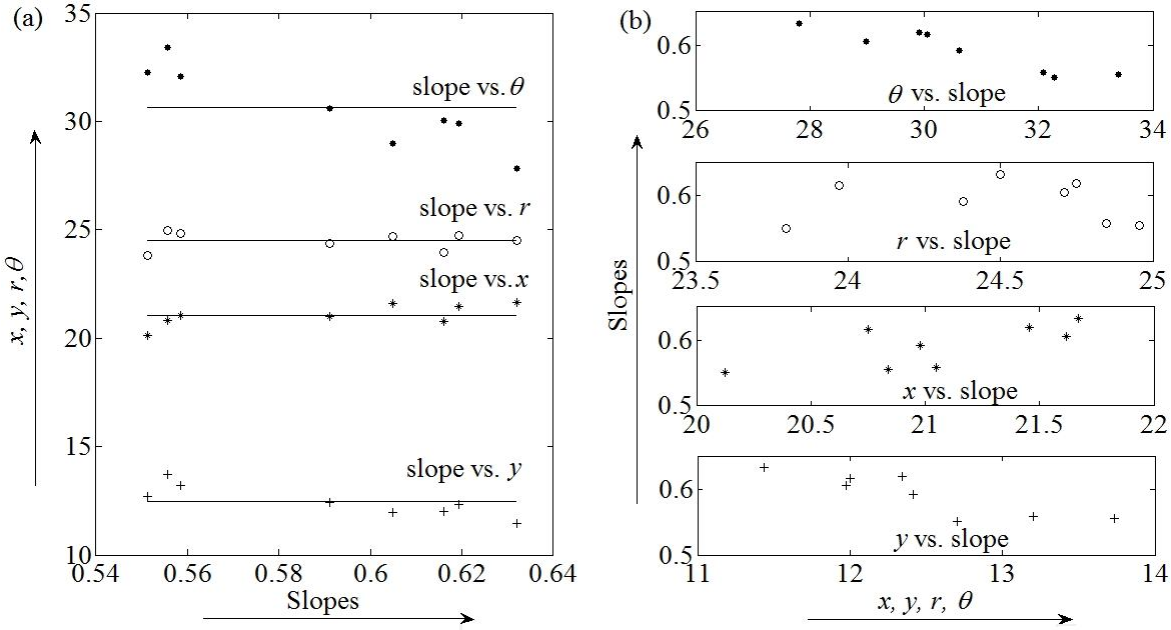

Fig. 4.18 Variations of slopes with strain gauge positions.

Best fitted lines are drawn from data points of plots presented in Fig. 4.17 and slopes of these lines are obtained. These slopes are function of strain gauge locations and their variations are presented in Fig. 4.18 (a). Figure 4.18 (b) plots the variations separately with x, y, r and θ coordinates of the strain gauge positions. From the plots of these slopes, it is

clearly seen that variations of slopes with positions have no definite trends. However, from Fig. 4.17, it is obvious that the slopes are dependent on nominal stress σ_x and hence on load W. This discrepancy may be due to the fact that the equations used for calculating stress field are not readily applicable in the present problem. The limitations of the theory lies in the assumptions that the hole present in the member is small compared to the width, so that stress distribution around a hole in flat infinite plate is applicable. But in actual case the ratio (a/b) is a parameter which need to be incorporated in the overall stress distribution equations. Moreover, the uniaxial stress field is produced through combined effect of bending and stretching, which is in deviation with theoretical assumption.

Chapter 5

CONCLUSION AND FUTURE SCOPE OF WORK

5.1 Conclusions

The conclusion of the research work contributed in the previous chapters is detailed here. The main objective of the research is to investigate stress and deflection behavior of master leaf spring under different loading conditions. Experimental and theoretical analyses of deflections and stresses are carried out by modeling master leaf spring as curved cantilever beam and curved beam under three point beam bending. The significant findings and various developments made during this thesis work are mentioned in the following paragraphs.

Firstly, large deflection analysis of leaf spring as cantilever beam is presented in chapter 3. In the experimental study, the master leaf spring is clamped centrally with the help of a hydraulic cylinder which divides the master leaf spring into two symmetric halves. In the present analysis, geometry of the master leaf is assumed as symmetric with respect to the central drill hole and thus experimental observation is made in one half of the spring only. Firstly, deflection profiles of master leaf are captured and recorded by using a digital camera. Then these observed data are post processed by using graph handling softwares (AutoCAD®, Microsoft Excel and MATLAB®) to get deflection profiles. Dynamic behavior of the master leaf under loaded conditions is also observed during experimentation. In theoretical analysis, master leaf is modeled as cantilever beam with initial curvature. Nonlinear differential equations are obtained for large deflection analysis of such beam. These equations are integrated directly which lead to solution in terms of elliptic integrals. Without using elliptic functions, elliptic integrals are evaluated by using numerical scheme in MATLAB® computational environment to deflection profiles. Experimental results are compared successfully with theoretical results in general. From the slight difference in trends of the comparison study, some relevant parameters of the physical system such as geometry variation in eye ends, non-uniform cross-section along length, clamping deficiency, etc. are identified. Further theoretical study on the large deflection behavior of a cantilever beam under distributed and combined load reveals that analytical solution based on elliptic integral is insufficient to predict the correct result. An iterative method with incremental loading has

been introduced additionally to study such problems. Here also results of other researchers have been compared successfully and new results have been furnished for initially curved cantilever beams.

On the other hand, stress and deflection analysis of leaf spring under three point bending is presented in chapter 4. Firstly, geometry of the master leaf spring is studied and found to be asymmetric with respect to the mounting drill hole. A special leaf spring testing rig is designed and set up in Machine Elements laboratory to study stress and deflection characteristics of leaf spring under three point bending. Due to asymmetric geometry of the master leaf, concentric and eccentric loading conditions are produced by using two different types of load connectors. At each of the loading condition, deflection profile is obtained by using two different techniques – direct measurement using scale, height gauge and indirect measurement through post processing photographs in graph handling softwares (AutoCAD®, Microsoft Excel and MATLAB®). The deflection profiles, obtained by indirect measurement technique, are compared successfully with directly measured ones. Development of bending stresses in the loaded master leaf spring is obtained by using full bridge strain gauge circuits and a portable strain indicator. Master leaf spring is modeled as curved beam under three point bending in mathematical formulation and stress calculation is carried out following Winkler-Bach curved beam theory. Stress field developed under each of the experimental loading conditions is obtained by importing deflection profiles in MATLAB® computational platform. From comparisons between experimental and theoretical results, effect of stress concentration due to presence of drill hole in master leaf spring is observed. In addition, it is also observed that the master leaf spring is not only subjected to bending, but it is subjected to combined bending-stretching stress field. To study effects of stress concentration and stretching stress field, individual strain gauge readings is observed using quarter bridge circuits with each strain gauge and a dummy gauge mounted on a piece of the same material as that of the master leaf. Actual locations of strain gauges around the drill hole of the master leaf are also measured using image processing technique. The theoretical study is further extended to incorporate effects of stress concentration due to combined bending-stretching stresses at strain gauge locations within the central region of master leaf spring. At each of the strain gauge location, experimental and theoretical stress results are compared and several observations are made which will facilitate rigorous stress analysis of leaf spring under different loading conditions.

5.2 Future scope of work

In the present thesis, stress and deflection behavior of master leaf spring is analyzed through two different models. In the first model, large deflection behavior of master leaf spring is analyzed as cantilever beam under tip concentrated load. Effect of geometry variations at eye ends, change of arc length with application of load, effect of locked up moment in clamping arrangement, etc., can be incorporated in mathematical formulation for further improvement. In the second set of experiment, stress and deflection analysis of master leaf spring is carried out following curved beam model under three point bending. In this analysis, proper modeling of roller supports should be incorporated employing the geometrically consistent kinematic and kinetic conditions. Apart from these, some of the other studies that can be taken up include,

- Large displacement response of leaf spring as roller supported curved beam in elastic regime.
- Static analysis of leaf spring as cantilever and roller supported beams in post-elastic regime.
- Dynamic analyses of leaf spring as cantilever and roller supported beams in elastic and post-elastic regimes.

References

- Ahmed, S. R., Mamun, A. A., & Modak, P. (2014). Analysis of stresses in a simply-supported composite beam with stiffened lateral ends using displacement-potential field. *International Journal of Mechanical Sciences, 78*, 140-153.
- Ahuett-Garza, H., Chaides, O., Garcia, P. N., & Urbina, P. (2014). Studies about the use of semicircular beams as hinges in large deflection planar compliant mechanisms. *Precision Engineering, 38*(4), 711-727.
- Almeida, C. A., Albino, J. C., Menezes, I. F., & Paulino, G. H. (2011). Geometric nonlinear analyses of functionally graded beams using a tailored Lagrangian formulation. *Mechanics Research Communications, 38*(8), 553-559.
- Al-Qureshi, H. A. (2001). Automobile leaf springs from composite materials. *Journal of materials processing technology, 118*(1), 58-61.
- Amon, R., Snell, J., & Widera, O. E. (1971). Reduction in stress concentration due to beam reinforcement of a circular hole in a sheet. *Nuclear Engineering and Design, 16*(3), 279-284.
- Aşık, M. Z., Dural, E., Yetmez, M., & Uzhan, T. (2014). A mathematical model for the behavior of laminated uniformly curved glass beams. *Composites Part B: Engineering, 58*, 593-604.
- Banerjee, A., Bhattacharya, B., & Mallik, A. K. (2008). Large deflection of cantilever beams with geometric non-linearity: Analytical and numerical approaches. *International Journal of Non-Linear Mechanics, 43*(5), 366-376.
- Batista, M. (2011). On the stress concentration around a hole in an infinite plate subject to a uniform load at infinity. *International Journal of Mechanical Sciences, 53*(4), 254-261.
- Batista, M. (2015). Large deflections of a beam subject to three-point bending. *International Journal of Non-Linear Mechanics, 69*, 84-92.
- Beléndez, T., Neipp, C., & Beléndez, A. (2002). Large and small deflections of a cantilever beam. *European Journal of Physics, 23*(3), 371-379.
- Beléndez Vázquez, T., Neipp López, C., & Beléndez Vázquez, A. (2003). Numerical and experimental analysis of a cantilever beam: a laboratory project to introduce geometric nonlinearity in mechanics of materials. *International Journal Engineering Education, 19*, 885-892.

- Bisshopp, K. E., & Drucker, D. C. (1945). Large deflection of cantilever beams. *Quarterly of Applied Mathematics*, *3*(1), 272-275.
- Cannarozzi, M., & Molari, L. (2013). Stress-based formulation for non-linear analysis of planar elastic curved beams. *International Journal of Non-Linear Mechanics*, *55*, 35-47.
- Castagnetti, D., & Dragoni, E. (2013). Stress concentrations in periodic notches: a critical investigation of Neuber's method. *Materialwissenschaft und Werkstofftechnik*, *44*(5), 364-371.
- Charde, R. B., & Bhope, B. V. (2012). Investigation of stresses in master leaf of leaf spring by FEM and its experimental verification. *International Journal Engineering Science and Technology*, *4*(2), 633-640.
- Chen, L. (2010). An integral approach for large deflection cantilever beams. *International Journal of Non-Linear Mechanics*, *45*(3), 301-305.
- Dado, M., & Al-Sadder, S. (2005). A new technique for large deflection analysis of non-prismatic cantilever beams. *Mechanics Research Communications*, *32*(6), 692-703.
- Eren, I. (2008). Determining large deflections in rectangular combined loaded cantilever beams made of non-linear Ludwick type material by means of different arc length assumptions. *Sadhana*, *33*(1), 45-55.
- Fraternali, F., & Bilotti, G. (1997). Nonlinear elastic stress analysis in curved composite beams. *Computers & structures*, *62*(5), 837-859.
- Ghodake, A. P., & Patil, K. N. (2013). Analysis of Steel and Composite Leaf Spring for Vehicle. *IOSR Journal of Mechanical and Civil Engineering (IOSR-JMCE) e-ISSN*, 2278-1684.
- He, X. T., Cao, L., Li, Z. Y., Hu, X. J., & Sun, J. Y. (2013). Nonlinear large deflection problems of beams with gradient: A biparametric perturbation method. *Applied Mathematics and Computation*, *219*(14), 7493-7513.
- Hou, J. P., Cherruault, J. Y., Nairne, I., Jeronimidis, G., & Mayer, R. M. (2007). Evolution of the eye-end design of a composite leaf spring for heavy axle loads. *Composite structures*, *78*(3), 351-358.
- Ko, W. L. (1985). *Stress Concentration Around a Small Circular Hole in the HiMAT Composite Plate* (No. NASA-H-1235). National Aeronautics and Space Administration Moffett Field Ca Ames Research Center.

- Kumar, Y. S., & Teja, M. V. (2012). Design and Analysis of Composite Leaf Spring. *International Journal of Mechanical and Industrial Engineering (IJMIE), ISSN*, (2231-6477).
- Kumar, R., Ramachandra, L. S., & Roy, D. (2004). Techniques based on genetic algorithms for large deflection analysis of beams. *Sadhana*, *29*(6), 589-604.
- Li, X. F., & Lee, K. Y. (2015). Effect of horizontal reaction force on the deflection of short simply-supported beams under transverse loading. *International Journal of Mechanical Sciences*, *99*, 121–129.
- Mahdi, E., & Hamouda, A. M. S. (2013). An experimental investigation into mechanical behavior of hybrid and nonhybrid composite semi-elliptical springs. *Materials & Design*, *52*, 504-513.
- Mohammadi, M., Dryden, J. R., & Jiang, L. (2011). Stress concentration around a hole in a radially inhomogeneous plate. *International Journal of Solids and Structures*, *48*(3), 483-491.
- Mohyeddin, A., & Fereidoon, A. (2014). An analytical solution for the large deflection problem of Timoshenko beams under three-point bending. *International Journal of Mechanical Sciences*, *78*, 135-139.
- Motra, H. B., Hildebrand, J., & Dimmig-Osburg, A. (2014). Assessment of strain measurement techniques to characterise mechanical properties of structural steel. *Engineering Science and Technology, an International Journal*, *17*(4), 260-269.
- Mujika, F. (2007). On the effect of shear and local deformation in three-point bending tests. *Polymer Testing*, *26*(7), 869-877.
- Mutyalarao, M., Bharathi, D., & Rao, B. N. (2010). On the uniqueness of large deflections of a uniform cantilever beam under a tip-concentrated rotational load. *International Journal of Non-Linear Mechanics*, *45*(4), 433-441.
- Mutyalarao, M., Bharathi, D., & Rao, B. N. (2010). Large deflections of a cantilever beam under an inclined end load. *Applied Mathematics and Computation*, *217*(7), 3607-3613.
- Nagpal, S., Jain, N., & Sanyal, S. (2011). Stress concentration and its mitigation techniques in flat plate with singularities-A critical review. *Engineering Journal*, *16*(1), 1-16.

- Nallathambi, A. K., Rao, C. L., & Srinivasan, S. M. (2010). Large deflection of constant curvature cantilever beam under follower load. *International Journal of Mechanical Sciences*, *52*(3), 440-445.
- Nguyen, D. K. (2014). Large displacement behaviour of tapered cantilever Euler–Bernoulli beams made of functionally graded material. *Applied Mathematics and Computation*, *237*, 340-355.
- Osipenko, M. A., Nyashin, Y. I., & Rudakov, R. N. (2003). A contact problem in the theory of leaf spring bending. *International journal of solids and structures*, *40*(12), 3129-3136.
- Ozmen, B., Altiok, B., Guzel, A., Kocyigit, I., & Atamer, S. (2015). A Novel Methodology with Testing and Simulation for the Durability of Leaf Springs Based on Measured Load Collectives. *Procedia Engineering*, *101*, 363-371.
- Pai, P. F., Anderson, T. J., & Wheater, E. A. (2000). Large-deformation tests and total-Lagrangian finite-element analyses of flexible beams. *International Journal of Solids and Structures*, *37*(21), 2951-2980.
- Parkhe, R., Raman, M., & Sanjay, B. (2014). Modeling and Analysis of Carbon Fiber Epoxy Based Leaf Spring under the Static Load Condition by Using FEA. *International Journal of Engineering Science and Engineering*, *2*(4), 39-42.
- Politch, J. (1985). Methods of strain measurement and their comparison. *Optics and lasers in engineering*, *6*(1), 55-66.
- Raghavedra, M., Hussain, S. A., Pandurangadu, V., & PalaniKumar, K. (2012). Modeling and analysis of laminated composite leaf spring under the static load condition by using FEA. *International Journal of Modern Engineering Research (IJMER) Vol*, *2*(4), 1875-1879.
- Rahman, M. A., Siddiqui, M. T., & Kowser, M. A. (2007). Design and non-linear analysis of a parabolic leaf spring. *Journal of Mechanical Engineering*, *37*, 47-51.
- Rajendran, I., & Vijayarangan, S. (2001). Optimal design of a composite leaf spring using genetic algorithms. *Computers & Structures*, *79*(11), 1121-1129.
- Rashmi, U. (2011). Stress analysis of crane hook and validation by photo-elasticity. *Engineering*, *3*, 935-941.
- Roy, D. K., & Saha, K. N. (2013). Nonlinear Analysis of Leaf Springs of Functionally Graded Materials. *Procedia Engineering*, *51*, 538-543.

- Ryan, J. J., & Fischer, L. J. (1938). Photoelastic analysis of stress concentration for beams in pure bending with a central hole. *Journal of the Franklin Institute*, *225*(5), 513-526.
- Shankar, G. S. S., & Vijayarangan, S. (2006). Mono composite leaf spring for light weight vehicle–design, end joint analysis and testing. *Materials science*, *12*(3), 220-225.
- Shenhua, Y., Shuqing, K., & Chunping, D. (1997). Research and application of precision roll-forging taper-leaf spring of vehicle. *Journal of materials processing technology*, *65*(1), 268-271.
- Shokrieh, M. M., & Rezaei, D. (2003). Analysis and optimization of a composite leaf spring. *Composite structures*, *60*(3), 317-325.
- Shvartsman, B. S. (2007). Large deflections of a cantilever beam subjected to a follower force. *Journal of Sound and Vibration*, *304*(3), 969-973.
- Shvartsman, B. S. (2013). Analysis of large deflections of a curved cantilever subjected to a tip-concentrated follower force. *International Journal of Non-Linear Mechanics*, *50*, 75-80.
- Sitar, M., Kosel, F., & Brojan, M. (2014). Large deflections of nonlinearly elastic functionally graded composite beams. *Archives of Civil and Mechanical Engineering*, *14*(4), 700-709.
- Sugiyama, H., Shabana, A. A., Omar, M. A., & Loh, W. Y. (2006). Development of nonlinear elastic leaf spring model for multibody vehicle systems. *Computer methods in applied mechanics and engineering*, *195*(50), 6925-6941.
- Tari, H. (2013). On the parametric large deflection study of Euler–Bernoulli cantilever beams subjected to combined tip point loading. *International Journal of Non-Linear Mechanics*, *49*, 90-99.
- Tolou, N., & Herder, J. L. (2009). A seminalytical approach to large deflections in compliant beams under point load. *Mathematical Problems in Engineering*, doi:10.1155/2009/910896.
- Troyani, N., Hernández, S. I., Villarroel, G., Pollonais, Y., & Gomes, C. (2004). Theoretical stress concentration factors for short flat bars with opposite U-shaped notches subjected to in-plane bending. *International journal of fatigue*, *26*(12), 1303-1310.
- Wang, C. M., Lam, K. Y., He, X. Q., & Chucheepsakul, S. (1997). Large deflections of an end supported beam subjected to a point load. *International Journal of Non-Linear Mechanics*, *32*(1), 63-72.

- Wang, T. M. (1968). Nonlinear bending of beams with concentrated loads. *Journal of the Franklin Institute*, *285*(5), 386-390.
- Wang, T. M. (1969). Non-linear bending of beams with uniformly distributed loads. *International Journal of Non-Linear Mechanics*, *4*(4), 389-395.

Bibliography

- Bhandari, V. B. (2010). *Design of machine elements.* Tata McGraw-Hill Education Private Limited.
- Doebelin, E. O., & Manik, D. N. (2011). *Measurement systems*. Tata McGraw-Hill Education Private Limited.
- Fertis, D. G. (2006). Basic Theories and Principles of Nonlinear Beam Deformations. *Nonlinear Structural Engineering: With Unique Theories and Methods to Solve Effectively Complex Nonlinear Problems.* Springer.
- Khurmi, R. S., & Gupta, J. K. (2005). *Machine design*. S. Chand.
- Nag, D., & Chanda, A. (2010). *Fundamentals of Strength of Materials*. Wiley India Private Limited.
- Spiegel, M. R., Lipschutz, S., & Liu J. (2009). *Mathematical handbook of formulas and tables*. Tata McGraw-Hill Education Private Limited.
- Timoshenko, S., & Goodier, J. N. (1951). *Theory of elasticity*. McGraw-Hill Book Company.
- Timoshenko, S., & Young, D. H. (2009). *Elements of Strength of Materials*. Affiliated east-west press private limited.

Publications from the Thesis

Journal

1. Ghuku, S., and Saha, K. N., A theoretical and experimental study on geometric nonlinearity of initially curved cantilever beams, *Engineering Science and Technology, an International Journal*, Vol.19, pp.135-146, 2016.
2. Ghuku, S., and Saha, K. N., An experimental study on stress concentration around a hole under combined bending and stretching stress field, *Procedia Technology*, Vol.23, pp.20-27, 2016.
3. Ghuku, S., and Saha, K. N., Design development and performance analysis of leaf spring testing set up in elastic domain, *The Association of Engineers, India*, 2016 (Communicated).

Conference

1. Ghuku, S., Karmakar, S., & Saha, K. N. An Experimental Study towards Geometric Nonlinearity of Leaf Springs. *Proceedings of 23rd IRF International Conference, Chennai, India*, pp.86-89, 2015.
2. Ghuku, S., & Saha, K. N. Experimental Analysis on Large Deflection of a Master Leaf under Three Point Bending Test. *Proceedings of International Conference on Trends in Industrial and Mechanical Engineering (IC TIME 2016), MANIT, Bhopal, India*, Vol.II, pp.393-402, 2016.
3. Ghuku, S., & Saha, K. N. Experimental stress and deformation analysis of an automobile master leaf spring. *Proceedings of International Conference on Materials, Design and Manufacturing Process (ICMDM 2016), Anna University, Chennai, India*, pp.135-141, 2016.
4. Ghuku, S., & Saha, K. N. An Experimental Study on Stress Concentration around a Hole under Combined Bending and Stretching Stress Field. *Proceedings of 3rd International Conference on Innovations in Automation and Mechatronics Engineering (ICIAME 2016), G H Patel College of Engineering & Technology, Gujarat, India*, pp.1, 2016.

ERRATA FOR THE PRESENT THESIS

(1) First photograph of Fig. 4.8.2 in page 87 should be replaced by

(2) Page 105, line 14 of the second paragraph: "…environment to deflection profiles…" should be read as "…environment to get deflection profiles…".